Karlsruhe Institute of Technology

UNIVERSITAT POLITÈCNICA DE CATALUNYA BARCELONATECH

3D Bunch-By-Bunch feedback system at ANKA to increase storable beam current

(3D Bunch-By-Bunch Feedback System in ANKA um speicherbare Strahlstromstärke zu steigern)

Master's Thesis
by

Núria Egidos Plaja

born in 08.07.1992 in Barcelona, Spain

Institut für Physik

Reviewer:	Prof. Dr. Anke-Susanne Müller (KIT – ANKA)
Second Reviewer:	Prof. Dr. Francesc Guinjoan (UPC)
Advisor:	Prof. Dr. Anke-Susanne Müller (KIT – ANKA)
Second Advisor:	Prof. Dr. Weber (KIT – ANKA)

Project frame: 08.02.2016 – 15.07.2016

Declaration of original work

I confirm that I have written this work independently and that no other than the specified sources and supports have been used, either for edition or contents, and that the Statute of KIT of 17.05.2010 to ensure good scientific practice in the applicable areas has been respected.

Karlsruhe, 15.07.2016, _____

Núria Egidos Plaja

Distribution copy approved by

Karlsruhe, 15.07.2016, _____

Prof. Dr. Anke-Susanne Müller (KIT – ANKA)

Abstract

In the ANKA storage ring, a digital state-of-the-art Bunch-by-Bunch (BBB) feedback system provides damping of Coupled-Bunch-Instabilities (CBI) in order to increase the maximum storable beam current and lifetime. Performance of this feedback strongly depends on the phase advance in the digital Finite Impulse Response (FIR) filter. Especially during energy ramping, retuning of FIR filter parameters is required as the electron beam's tune varies with changing machine optics. With this purpose, an algorithm for the automatic tuning of the filter is proposed. Tests performed during several energy rampings show an improvement in rejection of instabilities, which means the robustness of the feedback system against changes in machine settings is enhanced. Beam lifetime is also a critical parameter to evaluate performance of the storage ring. It is related to the bunch length in the longitudinal axis, which must be not too short to reduce beamloss. So as to increase the bunch length and thus enhance beam lifetime, beam modulation at the quadrupole resonance is applied in the longitudinal axis. An algorithm for the automatic configuration of this modulation has been implemented and tested during injection. Results show a significant enhancement of beam lifetime, but reproducibility of the obtained values will be discussed.

Acknowledgements

I would like to thank the entire THz group in the ANKA storage ring for their support and guidance, for encouraging the participation in the group meetings and for the very nice conversations in the coffee break. Special thanks to my supervisors Prof. Dr. Anke-Susanne Müller and Prof. Dr. Marc Weber for their guidance regarding physics, but also for the key learnings about research dynamics and procedures. My gratitude to Dr. Manuel Schedler, with whom I had the chance to work closer, for his readiness to help, constant availability and flexibility. My most sincere gratitude for your patience and for helping me to improve my German.
Many thanks in addition to Dr. Erik Bruendermann for an indispensable introduction to the real world of research; to Edmund Blomley and Christian Fehlinger, amongst others, for making possible the experimental part of this thesis; to Dr. Stefan Funkner, Dr. Markus Schwarz, Miriam Brosi and Florian Rämisch for their advice when preparing the presentation and writing the thesis. Thanks in addition to Nigel Smale and Bennie Smit, for being so nice with me and giving me advice in areas I would not have expected to - I guess they were not aware either.
I must also praise the efficiency and kindness of the DB and SBB/CFF employees, thanks to whom my laptop and me crossed our paths again on a long and intensive journey form Karlsruhe to Barcelona, thus making possible that this work was finished in time.
Thanks to my family and friends, for your advice, your support and for making the distance vanish every Friday evening. The smallest things make life incredibly better with such a gang.

Disclaimer

Experimental results presented in this document were obtained on 20/5/2016 in ANKA storage ring, right after a shutdown due to the replacement of a damaged component. Vacuum pressure and beam current (about a dozen of mA) were not the nominal operation conditions, which may have significantly biased the obtained values. Discussion on results and evaluation of performance of algorithms presented are based on obtained values, so measurements should be repeated under nominal operation conditions in order to verify improvements claimed here.

Contents

Abstract v

Acknowledgements vii

Disclaimer ix

1. Introduction 1

2. On characterization of a storage ring 5
- 2.1. Fundamental physics of a storage ring . . . 5
- 2.2. Beam dynamics of a single, charged particle . . . 7
  - 2.2.1. Effects of magnetic fields on particle motion and emission of synchrotron light . . . 8
  - 2.2.2. Effects of electric fields on particle motion . . . 8
- 2.3. Beam dynamics in the multibunch scenario . . . 10
- 2.4. Methods for correction of CBI to increase storable beam current . . . 11
  - 2.4.1. Frequency control of the Higher Order Modes (HOM) of the RF cavities 12
  - 2.4.2. Active feedback . . . 12
- 2.5. Methods to enhance the beam lifetime . . . 13

3. Bunch-by-Bunch control system 15
- 3.1. Fundamentals of feedback loops . . . 15
- 3.2. Feedback loop of a BBB control system . . . 15
- 3.3. Heterodyne demodulation of the readout of the Beam Position Monitor . . . 19
- 3.4. Spectra of the temporal changes of a single bunch's positions . . . 21
  - 3.4.1. Synchrotron sidebands observed in the transverse spectrum in ANKA 24
  - 3.4.2. Spectra of the temporal changes of a single bunch's positions observed in ANKA . . . 25
- 3.5. Generation of the control action . . . 26

4. Algorithm for automatic FIR filter tuning in the transverse BBB feedback 33
- 4.1. System behaviour during energy ramping in terms of fractional tune . . . 34
- 4.2. Effects of transverse BBB control detuning due to betatron tune shift during energy ramping . . . 35
  - 4.2.1. Excitation of betatron CBI . . . 37
  - 4.2.2. Excitation of synchrotron sidebands in the transverse spectrum . . . 39
  - 4.2.3. Asymmetry of the dip at the betatron fractional tune in the transverse spectrum magnitude . . . 42
  - 4.2.4. Partial beamloss during energy ramping . . . 43
- 4.3. Algorithm for the automatic FIR filter tuning in the transverse BBB control system . . . 44
  - 4.3.1. Configurable parameters and criteria to dimension the digital FIR filter 45

4.3.2. Algorithm for automatic FIR filter tuning 47
4.4. Discussion on results obtained with automatic FIR filter tuning 50
4.4.1. Effect of the automatic FIR filter tuning on the damping of betatron CBI and synchrotron sidebands 50
4.4.2. Effect of the automatic FIR filter tuning on the asymmetry of the dip at the betatron fractional tune 53
4.4.3. Effect of the automatic FIR filter tuning on the partial beamloss during energy ramping 54

5. Algorithm for the automatic tuning of the DAC Drive arbitrary signal generator in the longitudinal feedback **57**
5.1. Algorithm for the automatic tuning of the DAC Drive generator parameters to enhance beam lifetime 59
5.2. Methods to evaluate the performance of the automatic DAC Drive generator tuning algorithm and discussion on the obtained results 60

6. Summary **63**

Appendix **65**
A. Figures of ANKA storage ring 65
B. C++ source code corresponding to algorithms presented in this thesis . . . 65
C. Matlab code for processing of signals acquired from EPICS interface 65

Bibliography **67**

List of Figures

2.1. Overview of the ANKA storage ring 6

2.2. Coordinate system to which particle motion is referred: X, Y and Z stand for horizontal, vertical and longitudinal axes respectively. Particles revolving about the storage ring describe oscillations in respect of the nominal trajectory (that of the synchronous particle) in the transverse plane (the so-called betatron oscillations) and in the longitudinal plane (synchrotron oscillations) 7

2.3. Electric field in the RF cavity as a function of time and its effect on longitudinal particle motion: synchronous particles gain an energy associated to this field which is exactly that lost in one turn due to synchrotron radiation. Particles with higher energy arrive later, thus gaining less energy, and the reverse for particles with lower energy. Thanks to this difference, longitudinal focusing is achieved 9

3.1. Overview of a feedback system: the response of the system (feedback pickup acquired with sensors) is to be matched to a reference or set point, but this might not be achieved due to disturbances at the input of the system. So as to counteract them, a control action is computed with a controller; and then it is applied to the system to be stabilised (plant) by means of an actuator. This control action becomes the new input to the system, thus steering it towards the desired performance 16

3.2. Overview of a BBB control system: the response of the system (amplitude and phase of the oscillations of the beam around its nominal trajectory) is to be matched to a reference or set point, i.e. the stable motion in the transverse and longitudinal planes (in the case of BBB, there is no external reference, but the stable motion is achieved inherently). This might not be achieved due to disturbances at the input of the system (CBI). So as to counteract them, a control action is computed with a controller; and then it is applied to the beam by means of an actuator (kicker). This control action becomes the new input to the system, thus steering the beam towards a stable motion 17

3.3. Implementation of the BBB control system in ANKA 19

3.4. Sketch of signals involved in the heterodyne demodulation, which is performed by the frequency mixer (shaded area). BPM readout in the longitudinal axis is demodulated in phase by mixing its third harmonic with the third harmonic of the reference clock shifted by $\pi/2$. This provides a signal proportional to the amplitude of the synchrotron oscillations. The readout in the transverse plane is demodulated in amplitude by mixing its third harmonic with the third harmonic of the reference clock, which provides a signal proportional to the amplitude of the betatron oscillations. The frequency content beyond $\omega_{RF}/2$ is discarded with a lowpass filter. The demodulated signals are acquired with an ADC, which samples them at ω_{RF}. The signal corresponding to each individual bunch is obtained by triggering the ADC at ω_o 22
3.5. Sketch to illustrate the frequencies involved in the digitalization of the BPM readout. Each line represents the BPM readout corresponding to a given bunch, which is acquired with the ADC: the motion of this bunch is sampled once every turn (it is acquired with ω_o). The total of bunches are acquired individually in one turn, thus the ADC samples at ω_{RF}. The selection of a given bunch is achieved by downsampling the reference clock (ω_{RF}) by a factor corresponding to the harmonic number 22
3.6. Spectra associated to the BPM readout in the single bunch scenario 24
3.7. Spectrum of the transverse signal acquired with the BPM for one single bunch under the effect of the coupling between transverse and longitudinal planes, which is due to the sensitivity of the mixer to the fluctuations in phase of the BPM readout 25
3.8. Magnitude of the spectrum obtained from the BRAM acquisition module. It corresponds to the average of all FFTs calculated from the temporal changes of the individual bunches' positions 30
3.9. Impulse and frequency responses of the digital FIR filter with parameters corresponding to the horizontal axis in Table A.2 31

4.1. Evolution of fractional tunes with energy during ramping 36
4.2. Scheme to evaluate the excitation of CBI due to the shift in betatron tune during energy ramping. Amplitude of the superposition of feedback signal and betatron oscillation ($s'(t)+s(t)$) is compared to the amplitude of betatron oscillation (if there were no feedback, $0 + s(t)$), at the time instant when the last would have a peak. Phase shift introduced by the FIR filter for several values of betatron fractional tune is considered, showing that for frequencies such that the phase shift is larger than 90°, betatron oscillation is excited instead of being damped - the superposition $s'(t) + s(t)$ has a larger amplitude at the aforemetioned instant than the signal without feedback 38
4.3. "Peak" amplitude of superposition signal $s(t) + s'(t)$ (amplitude in the time instant when it would have a peak if there were no feedback, $s(t)+0$) divided by the peak amplitude of $s(t)$, as a function of the phase advance introduced by the FIR filter at the frequency of $s(t)$ in respect of the phase at the filter's central frequency (phase shift in respect of 180°). Three phase values are highlighted: 0° corresponds to the filter properly tuned to the betatron oscillation, which is ideally damped; damping is worse (resulting "peak" amplitude is higher) as the phase shift increases; a phase shift beyond 90° leads to the excitation instead of damping of CBI 39
4.4. Method to detect the synchrotron sidebands in the transverse BRAM spectrum magnitude 41

4.5. Scheme to evaluate the excitation of synchrotron sidebands regarding the phase advance introduced by the FIR filter. Amplitude of the superposition of feedback signal at the synchrotron sideband frequency and the sideband itself ($s'(t) + s(t)$) is compared to the amplitude of the synchrotron sideband (if there were no feedback, $0 + s(t)$), at the time instant when the last would have a peak. Several phase advance values introduced by the FIR filter are considered, showing that for phase shifts larger than 90°, synchrotron sidebands are excited instead of being damped: the superposition has a larger amplitude at the aforemetioned instant than the signal without feedback) 42
4.6. Method to quantify the asymmetry of the dip in the transverse spectrum magnitude in terms of its average value 44
4.7. Frequency response of the FIR filter calculated as the FFT of equation 3.10 for coefficients in Table A.2. The central frequency is marked as a green spot 45
4.8. Phase shift introduced by the FIR filter (phase advance at its bandwidth in respect of the phase at its central frequency) as a function of the number of taps. The theoretical maximum phase shift allowed in order to avoid exciting the synchrotron sidebands is indicated with a red, dashed line; the maximum phase shift allowed considered in the presented algorithm corresponds to the green, dashed line 47
4.9. Bandwidth of the FIR filter and as a function of the number of taps. The distance between the synchrotron sidebands and the betatron fractional tune, which corresponds to the synchrotron fractional tune, is indicated with a red, dashed line 48
4.10. Steps of the algorithm for automatic FIR filter tuning which are executed periodically during energy ramping 49
4.11. Optimal number of taps as a function of the FIR central frequency (betatron fractional tune expressed in kHz) for central gain = shift gain = 1 51
4.12. Evolution of the magnitude of the transverse spectrum (obtained from the BRAM acquisition module) at the synchrotron sideband and at the betatron fractional tune frequencies as a function of energy during ramping. The range of energy displayed is that in which the effect of the automatic FIR filter tuning algorithm is most significant 52
4.13. Evolution of the mean asymmetry of the dip in the betatron spectrum magnitude with energy during ramping. The range of energy displayed is that in which the effect of the automatic tuning algorithm is most significant 54
4.14. Beam current decay during energy ramping; three rampings without automatic FIR filter tuning, two with automatic tuning applied in the horizontal axis and two with automatic tuning applied in the vertical axis are shown. In the cases when automatic FIR filter tuning is applied, the partial beamloss and the slope of beam current decay are computed from the red, dashed line (the steep initial decay is not considered because is not related to the BBB control system) 55

5.1. Panel of the EPICS graphic interface corresponding to the DAC Drive arbitrary signal generator. Fields marked in red are modified by the automatic tuning algorithm 58
5.2. Algorithm for phase modulation using the DAC Drive generator in the longitudinal BBB control system 60
5.3. Effect of the phase modulation at the quadrupole resonance of the beam on the beam lifetime 61

List of Tables

A.1. Compilation of parameters of the ANKA storage ring 66
A.2. Predetermined FIR filter parameters for the transverse BBB feedback (horizontal/vertical/longitudinal) 66

1. Introduction

Particle accelerators are based on the principle that a charged particle in a potential difference (voltage) is accelerated across it [Tia]. They are used in a wide range of applications, including scientific research, applied physics, chemistry, biology, medicine, industrial processing and power engineering.
Some examples of industrial applications are ion implantation in the semiconductor industry or modification of surface properties of many materials. Radiation that can be generated is used to preserve food, sterilize toxic waste or polymerize plastics.
In medicine, they are used for diagnosis and therapy, as well as cancer treatment with gamma rays, neutrons and heavy charged particles.
Regarding power engineering, accelerators can provide the additional heating needed for plasma ignition for producing controlled thermonuclear fusion power. Research is also carried out in the line of incineration of long-life nuclear waste [Bar94].

Particle accelerators can be classified regarding several criteria, for instance the type of particles which are accelerated (electrons, protons, etc.) or the shape of the accelerator (linear or circular). A synchrotron is a type of circular particle accelerator in which charged particles are accelerated by means of electromagnetic fields until they approach the speed of light. In this process, radiation is emitted in the form of synchrotron light.
In 1947 researchers at the General Electric Research Laboratory (GERL) first observed synchrotron radiation, which was initially considered a nuisance because it provided an energy loss to the revolving particles. By the late 1950's, it was found that this type of radiation could be used for diffraction and spectroscopy. Since the 1960's, accelerator facilities devoted to producing synchrotron radiation have been built all over the world [lso16] and they have become a thriving line of research in the aforementioned fields [Tia].

Two examples of synchrotrons are high energy physics machines (particle colliders), for instance the Large Hadron Collider at CERN; and sources of synchrotron light, which exploit the generated synchrotron light [Dia14]. ANKA Synchrotron Radiation Facility at the Karlsruhe Institute of Technology [ANKb] is one of the second kind.
Starting in 1999, ANKA is an electron storage ring which operates at a maximum energy of 2.5 GeV. Its synchrotron radiation allows conducting research in the fields of life science, environmental research, nanosciences and microtechnologies, amongst others ([ANKb]; [Her13], p.1).

Regarding its operation, the highest beam intensity is desired in order to maximise the brightness of the generated radiation. However, due to the electromagnetic coupling that appears among the bunches (groups of particles that compose the beam) via the resonant structures of the machine, coherent instabilities can occur at high beam currents. In order to increase the storable beam current, control of such unstable motion is required ([Tey04], p.iii). With this purpose, a Bunch-By-Bunch (BBB) control system is implemented.

ANKA is a multipurpose machine: it can operate at several energy levels and it can support a low-alpha operation mode dedicated to the production of short bunches [ANKa]. It is a ramping facility: injection energy (0.505GeV) is different from the energy at which most experiments are performed (2.5GeV), so energy ramping is performed from the first to the second level.
These conditions pose a changing and challeging environment for the BBB control system. Its setting depend strongly on the electron beam's eigenfrequencies, which change regarding the conditions of operation.

This work deals with the enhancement of performance of the BBB control system in two regimes: on the one hand, robustness of control in the horizontal and vertical axes is to be achieved during energy ramping to increase the storable beam current. On the other hand, beam lifetime is to be increased by applying a modulation at the quadrupole resonance of the beam in the longitudinal axis when operating at injection energy.

In chapter 2, fundamentals of operation of a storage ring are introduced, thus setting the bases for understanding the following sections. Equations of particle motion are presented, starting with the case of one single bunch stored in the accelerator and expanding it to the multibunch scenario. In the second case, effects of the interaction of bunches with the environment and among them (the so-called Coupled-Bunch Instabilities, CBI) are presented. The effects of CBI and also methods to correct them are introduced.

Chapter 3 deals with one of these methods, the Bunch-By-Bunch (BBB) control system, which is implemented in the ANKA storage ring. The main purpose of this method is to damp CBI in order to increase the storable beam current. Its architecture and principles of operation are explained, and its limitations are introduced.

Among these limitations, the BBB control system is detuned when the energy varies during energy ramping, which deteriorates its performance. A strategy to avoid this detuning is presented in chapter 4. The main contribution of the present work in this section is an algorithm for the automatic adjustment of the controller of the BBB system, a digital Finite Impulse Response (FIR) filter, which enables retuning the system as the energy changes during ramping and thus enhances the performance of the control system. Other contributions are the algorithms to detect the involved frequency components (betatron tune, synchrotron sidebands).

Another parameter which determines the performance of the storage ring is the bunch length. A short bunch length in the longitudinal axis is required for the proper operation of the undulators, periodic structures of dipole magnets that stimulate the emission of highly brilliant synchrotron radiation. However, too short a bunch length gives rise to particle collisions (intrabeam scattering, IBS), which reduces the beam lifetime. In chapter 5, a strategy to increase the bunch length and thus enhance the beam lifetime is presented, which consists in modulating the beam at its quadrupole resonance in the longitudinal axis. This modulation is applied by means of the longitudinal BBB control system. The main contribution of the present work in this section is an algorithm for the automatic configuration of the signal generator in the BBB control system which provides the aforementioned modulation.

The algorithms for the automatic FIR filter tuning in the transverse BBB control and the automatic tuning of the signal generator in the longitudinal BBB control have been implemented and tested in the ANKA storage ring. The obtained results are discussed and further lines of improvement are presented. These tests were performed after a shutdown forced by the replacement of a damaged component and neither the vacuum conditions nor the level of beam current were the nominal ones. This might have influenced the results, which are discussed in chapters 4 and 5.

Finally, the main features of the performed work and the obtained results are compiled in chapter 6. Specific information on the parameters of the ANKA storage ring is provided in Appendix A.
The algorithms which are the contributions of this thesis are provided in Appendix B for codes implemented in C++ and Appendix C for Matlab codes.

2. On characterization of a storage ring

In order to achieve a high brightness of the generated synchrotron light, a beam intensity as high as possible is required . This gives rise to instabilities that can provoke beamloss, thus limiting the maximum storable current. So as to counteract these instabilities and increase the storable beam current, correction techniques are implemented to enhance the accelerator performance ([Lon08], p.1). The present project focuses on these techniques, in particular on their application in the ANKA storage ring.
This section deals with the basic principles of accelerator physics that will be used for the implementation of the control techniques. The state of the art of these techniques is presented and the challenges to be addressed are introduced, thus defining the motivations for this work.

2.1. Fundamental physics of a storage ring

The general structure of ANKA storage ring is depicted at Figure 2.1 [ANKc]. Charged particles (electrons in this case) are generated in the electron gun and clumped in bunches in the microton. The total of all bunches compose the beam. Bunches are considered in terms of their centre of mass for analysis purposes.
Particles reach their final speed (close to the speed of light) after the microton; however, their level of energy is still lower than that required for being injected into the storage ring. Therefore, the energy of particles is incremented following a ramp profile: in the case of ANKA storage ring, energy is ramped from 0.505 GeV to 2.5 GeV in 49500 steps at an increment rate of 180 Hz.

Once injected into the storage ring, bunches are exposed to electric and magnetic fields in order to shape their trajectory and generate synchrotron radiation, which is the final purpose of the ring. Particles remain orbiting for several hours emitting synchrotron light, which is channeled through beamlines to the stations where the experiments take place [NSR10].
A beam current (electrical charge passing by a current monitor per unit time, regarding [Wie07], p.290) as high as possible is required to maximise the brightness or intensity of the generated radiation; it decays with time with an exponential trend.
Another figure to characterize a storage ring is beam lifetime, that is, the time interval after which the intensity of the beam has reached 1/e of its initial value. In the case of ANKA, beam lifetime is 16 hours for a 150 mA current level [ANKc].

Particle trajectory is referred to the coordinate system depicted at Figure 2.2 ([Sch15], p.7). In this figure, the green line represents the nominal trajectory, which is described by the so-called "synchronous particle" - a particle orbiting with the ideal trajectory, speed (close to the speed of light) and energy level.

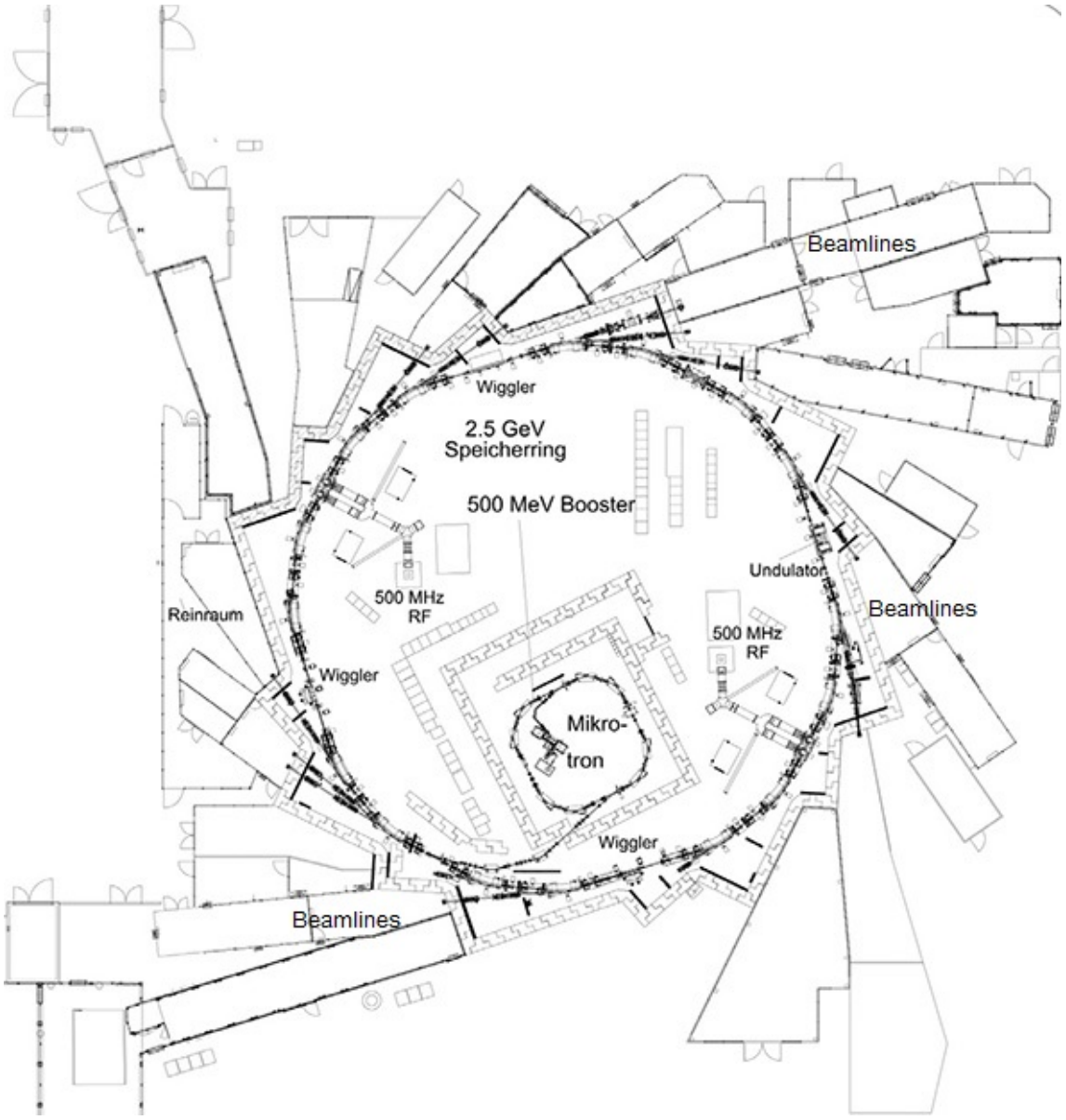

Figure 2.1.: Overview of the ANKA storage ring

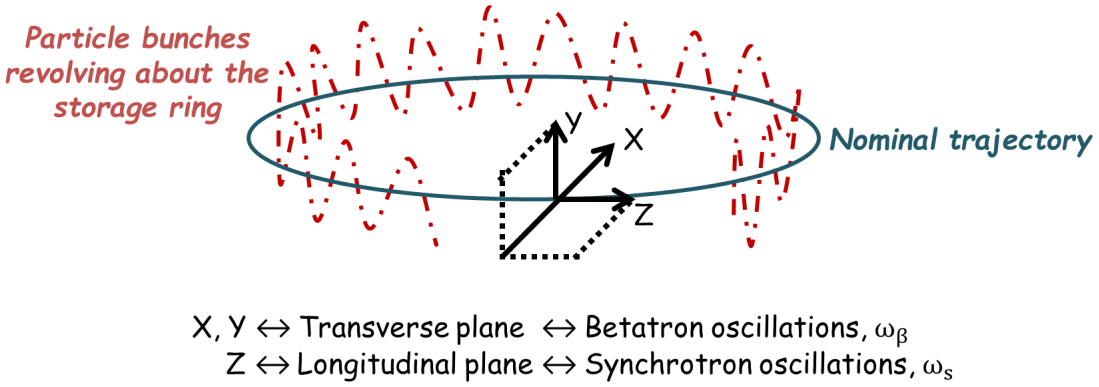

Figure 2.2.: Coordinate system to which particle motion is referred: X, Y and Z stand for horizontal, vertical and longitudinal axes respectively. Particles revolving about the storage ring describe oscillations in respect of the nominal trajectory (that of the synchronous particle) in the transverse plane (the so-called betatron oscillations) and in the longitudinal plane (synchrotron oscillations)

Deviations from the nominal trajectory can occur in the transverse plane (horizontal and vertical axes), which are called betatron oscillations; and in the longitudinal axis, the so-called synchrotron oscillations.
In the coming sections, beam dynamics, which describe the aformentioned oscillations, are presented: first, the equations to define the trajectory of a single bunch are introduced and the effects caused by the electromagnetic fields on its motion are explained. After this, beam dynamics are expanded to the multibunch (multiple-bunches) scenario, which is the case for ANKA.

2.2. Beam dynamics of a single, charged particle

Particles revolving about the storage ring do not describe the ideal, circular trajectory indicated in green at Figure 2.2, but they oscillate around of it both in the transverse and longitudinal planes. These oscillations or, in general terms, the motion of a charged particle in a storage ring can be described with the harmonic oscillator analogy by means of the Hill's equation ([Wie07], p.250):

$$\ddot{s}(t) + 2D\dot{s}(t) + \omega^2 s(t) = 0 \tag{2.1}$$

$s(t)$ stands for the oscillation coordinate: x for horizontal or y for vertical displacements; z for longitudinal oscillations. D is the natural damping or radiation damping: the power radiated by a particle in the form of synchrotron light is proportional to the fourth power of its energy; the higher the energy, oscillations can become unstable, but also the more power is radiated, thus compensating for the excess in energy and leading towards a stable motion ([Wie07], p.299).
ω is the natural frequency of the oscillation, which can be expressed as:

$$\omega = \upsilon\omega_o \tag{2.2}$$

where υ is defined as the betatron tune for oscillations in the transverse plane or synchrotron tune for the longitudinal plane. It corresponds to the number of oscillations executed by a particle or by a bunch of particles while travelling one turn around the ring.
The tune has an integer part and a fractional part, the fractional tune, which is denoted

by Q_x, y, s for the horixontal, vertical and longitudinal axes respectively. If the beam is observed at one single point around the ring, only the fractional tune can be determined ([JYA+], p.3).
ω_o is the revolution frequency, that is, the rate at which each bunch completes one turn around the ring. The bunch repetition frequency (the inverse of the time separation between two bunches) is expressed as $h\omega_o$, with h the harmonic number (number of RF buckets, which is the theoretical maximum number of bunches that can be stored). The particular values of these magnitudes in the ANKA storage ring are listed in Table A.1.

In the transverse plane, oscillations are periodic horizontal or vertical displacements from the nominal, centered trajectory. In the longitudinal plane, they are periodic differences of time of arrival of the bunch with respect to that of the synchronous bunch. This means that the particles will see a different phase of the RF electric field which accelerates them as that phase corresponding to the synchronous particle. For this reason, longitudinal oscillations are also known as "phase oscillations".
If $\omega >> D$, an approximated solution to equation 2.1 is the following damped sinusoidal oscillation:

$$s(t) = ke^{-\frac{t}{\tau_D}} sin(\omega t + \psi) \tag{2.3}$$

where $s(t)$ are the oscillations in the transverse plane or longitudinal axis; k is the amplitude of those oscillations in the corresponding axis and ψ is an arbitrary phase; $\tau_D = 1/D$ is the damping time and D is the damping rate. This solution shows that the oscillations of a single bunch are damped in a natural way, converging to the nominal trajectory.

The particle trajectory and energy are determined by means of electromagnetic fields, as it will be seen next.

2.2.1. Effects of magnetic fields on particle motion and emission of synchrotron light

In the ANKA storage ring, magnetic fields are generated by dipole, quadrupole and sextupole magnets ([Her13] p.10). Dipole fields bend the beam, thus steering it towards a circular trajectory; in addition, when the accelerated electrons are deflected by the magnetic field (they move on a curved path), they radiate synchrotron light [NSR10].
Similar to light rays, particle beams have a tendency to spread out due to an inherent beam divergence. To keep the particle bunch together and thus maintain the desired beam properties, quadrupole magnets act like lenses and focus the bunch in the transverse plane ([Wie07], p.42).
Finally, sextupole magnets are used to correct for chromatic errors, that is, the change of focal length (a measure of focusing strength) of quadrupole magnets when energy varies ([Wie03], p.82).
In conclusion, magnetic fields enable the generation of synchrotron light and correct deviations from the nominal trajectory in the transverse plane.

2.2.2. Effects of electric fields on particle motion

Once electrons are injected into the ring, they revolve at a constant speed and they are intended to have a constant energy too, thus describing orbits of the same radius [Tia]. However, due to radiation of synchronous light, particles lose some of their energy in each turn, and this affects the radius of the orbit they describe. This energy loss is compensated by means of a time-varying longitudinal electric field provided by radio frequency (RF) cavities.
These are resonant structures of a high quality factor (high-Q cavities). They are shaped to

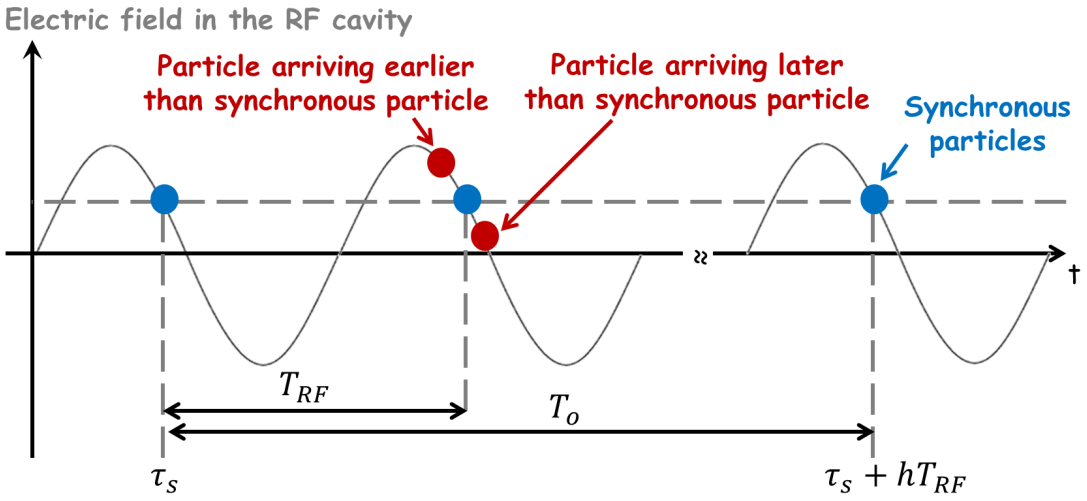

Figure 2.3.: Electric field in the RF cavity as a function of time and its effect on longitudinal particle motion: synchronous particles gain an energy associated to this field which is exactly that lost in one turn due to synchrotron radiation. Particles with higher energy arrive later, thus gaining less energy, and the reverse for particles with lower energy. Thanks to this difference, longitudinal focusing is achieved

resonate at the frequency of the electric field (RF), so as to transfer the energy they receive from a RF power source to the electrons as they pass through the cavity, and thus restore the energy lost during one turn. With this, the radius of their orbit is to be maintained constant [uWo01]. The frequency of the RF electric field is also the theoretical maximum bunch repetition frequency ω_{RF} ($500MHz$ in the case of ANKA, as shown in Table A.1). Energy gained by a bunch with crossing the cavity is proportional to the amplitude of the voltage in the cavity and this, in turn, is proportional to the RF electric field strength [WBX], as illustrated with expression 2.4. In a time instant τ, the energy transferred to a particle crossing the cavity can be expressed as:

$$E(\tau) = eV(\tau) \propto \int_0^{\tau} \epsilon(\omega_{RF} t)dt \tag{2.4}$$

with e the electron charge; $V(\tau)$ the RF voltage in the cavity in the time instant τ; and ε the electric field of frequency ω_{RF}.
This equation shows that energy is related to the integral of the RF electric field. Since this is sinusoidal, energy and electric field are shifted by $\pi/2$. Therefore, the relation between the particle longitudinal motion and the energy gained when crossing the cavity can be expressed in terms of the RF electric field, taking into account this phase shift.
In this line, Figure 2.3 shows the RF electric field in the cavity and the instants of arrival of the different bunches. Synchronous bunches, those describing the nominal trajectory (their rotation is synchronous with the RF field), are depicted in blue. It can be seen that there are two phases of arrival in which the synchronous bunch can gain the energy lost due to synchrotron radiation in one turn (this level of energy is indicated by the dashed horizontal line); but only the one with descending slope of the electric field corresponds to a phase of stable equilibrium ([San79], p.83).
There is an integer number of RF periods T_{RF} in one revolution period T_o: h is the harmonic number and it corresponds to the maximum of synchronous particles or bunches represented by its centre of mass orbiting the ring. As a consequence, h is also the maximum number of storable bunches ([San79], p.81).

In addition to restoring the energy lost in one turn, the RF electric field provides longitudinal

focusing, that is, it forces that all particles tend to arrive in the instant corresponding to a synchronous particle. So is represented in Figure 2.3 and it can be understood as follows ([Hol12], p.12):

- Particles orbit at a constant speed, but the orbit radius depends on dispersion effects that take place in the magnets regarding particle's energy: particles with a higher energy are less deflected and thus describe a longer orbit, and particles with a lower energy are more deflected and thus follow a shorter orbit.
- In the case of the particle describing the longer orbit, it will arrive later to the cavity, and thus will see a phase of the RF field which is advanced in respect of the synchronous phase. In turn, it will see a lower amplitude of the field or, in other terms, it will gain a lower energy. Due to this, it will describe a shorter orbit in the following turns, thus adjusting its motion to the nominal one.
- The reverse occurs for the particle describing the shorter orbit: it will arrive earlier to the cavity, it will see a higher level of the RF field and thus will gain more energy than the nominal one. This excess of energy will lead to a longer orbit, approaching the synchronous timing in the following turns.

Beyond adjusting the longitudinal motion to the synchronous one, longitudinal focusing groups particles around the corresponding multiple of the synchronous time, thus generating the bunches and defining their length.

At this point, beam dynamics for the single bunch scenario have been presented and it has been seen how bunches can be steered using magnetic fields and how they are generated and accelerated with electric fields. It has also been explained that dynamics of a single bunch are intrinsically stable due to natural or radiation damping.
However, there are multiple bunches orbiting the storage ring (a maximum of h bunches). The motion of each bunch has an effect on that of the other bunches, as presented in the next section.

2.3. Beam dynamics in the multibunch scenario

In the multibunch scenario, dynamics of a given bunch are affected by those of the surrounding bunches, they are coupled by an electromagnetic field. With a weak (low intensity) beam, individual bunches behave essentially like single bunches and their motion is inherently stable - as seen with equation 2.3, oscillations are naturally damped. But with an intense beam as that required for modern synchrotron light sources, the large number of moving charges leads to the generation of an additional "self-induced electromagnetic field" or "wakefield" when crossing the RF cavities ([Lac92], p.368); or by interacting with the walls of the vacuum chamber through which they circulate ([Wol09a], p.45).
The wakefield excited by a given bunch is sampled by the following bunches, thus coupling the dynamics of bunches revolving about the ring ([FCM+], p.7; [Wie07], p.674).

Similar to the single bunch case, particle motion corresponding to one bunch in the multibunch scenario can be described as a harmonic oscillator. In this case, effects of coupling to the other bunches adds a "driving force" or perturbation denoted by F to the equation of motion ([Lon08],p.4):

$$\ddot{s}(t) + 2D\dot{s}(t) + \omega^2 s(t) = F(t) \tag{2.5}$$

Instabilities can occur when bunches oscillate in a coherent way (coupled-bunch oscillations), that is, when the centre of mass of the different bunches oscillate in phase and at the same

frequency either in the transverse or longitudinal planes ([Wei03]). Under this condition, the equation of motion for one bunch in the multibunch case can be rewritten as:

$$\ddot{s}(t) + 2(D - G)\dot{s}(t) + \omega^2 s(t) = 0 \tag{2.6}$$

where $\tau_G = 1/G$ is the growth time constant and G is the growth rate. The growth time is usually in the order of hundreds or tens of turns ([Wol09a], p.29).
Analogous to equation 2.3, if $\omega >> (D - G)$, an approximated solution of equation 2.6 is:

$$s(t) = ke^{-\frac{t}{\tau}} sin(\omega t + \psi) \tag{2.7}$$

where $s(t)$ are the oscillations in the transverse plane or longitudinal axis; k is the amplitude of those oscillations in the corresponding axis and ψ is an arbitrary phase; and $1\ \tau = 1/\tau_D - 1/\tau_G$. If $D > G$, $1/\tau > 0$, the amplitude of the oscillation decays. G is proportional to the stored beam current: for low beam currents, damping prevails and the beam remains stable. But for levels beyond the limit current, and also depending on other factors (characteristics of the wakefields, beam energy, synchrotron radiation damping rates, etc.), it can occur that $D < G$, and thus oscillations grow exponentially in amplitude. In this way, coupled dynamics become unstable, which means Coupled-Bunch-Instabilities (CBI) arise ([Wol09a], p.45).

In the multibunch scenario, each bunch oscillates at the betatron and synchrotron frequencies and, in addition, there can be different modes of oscillation (multi-bunch modes), which depend on how each bunch oscillates with respect to the other bunches ([Lon08], p.4). For h identical bunches equally spaced around the ring, there can be up to h different modes of oscillation characterized by the phase difference between adjacent bunches:

$$\Delta\psi = m\frac{2\pi}{h} \quad ; \quad m \in [0, h-1] \tag{2.8}$$

with m the mode number. CBI arise when one or more of these modes become unstable. In order to avoid that, the storage ring could operate at low currents, but this is opposite to the purpose of the machine. In practical terms, these instabilities set the upper limit for the storable beam current ([Wol09a], pp.29-37). Particle beam intensity is critically important, as the brightness of the synchrotron light produced is directly proportional to the stored electron beam current ([Wie07], pp.671-672).
If the amplitude of the bunch oscillations becomes too large, that is, beam dynamics becomes unstable due to coupled-bunch effects, beam quality is degradated. In the worst case, beam can be lost; otherwise, instabilities provoke that the brightness and the spectral purity of the synchrotron light source are reduced ([Lon08], p.1; [Tey04], p.17).
So as to avoid the uncontrolled growth of oscillation amplitude, i.e. to damp CBI to increase the storable beam current, several control techniques are available. The next section reviews some of these techniques.

2.4. Methods for correction of CBI to increase storable beam current

The need for high brightness in synchrotron light sources implies storing beam currents as high as possible, and this gives rise to Couple-Bunch-Instabilities that can deteriorate the performance of the storage ring. These instabilities manifest as oscillations that grow exponentially in amplitude in the transverse plane (related to deviations in the bunch trajectory in respect of the nominal one) and in the longitudinal plane (related to deviations in the bunch energy).
In order to avoid the deterioration in performance caused by CBI and thus enhance the storable beam current, correction techniques are required. This section presents some of these techniques: frequency control of High Order Modes (HOMs) of RF cavities; and active feedback ([Mos99], [Mos]).

2.4.1. Frequency control of the Higher Order Modes (HOM) of the RF cavities

RF cavities are resonant structures, metallic empty volumes inside of which the electromagnetic field resonates at certain given frequencies or modes that are determined by the geometry of the cavity. The modes beyond the first are Higher Order Modes (HOMs) ([SES], pp.2-4).
As it has been seen, coupled-bunch dynamics can also resonate at several modes. If some of them excite the corresponding mode of the cavity, CBI arise ([DCH+03], p.15).
So as to avoid this, RF cavities can be designed to damp the HOMs ([Wie07], p.674); or tuned during operation (for instance, with an accurate regulation of the temperature of operation) so that HOMs do not match the eigenfrequencies of the beam, in order to avoid exciting those frequencies ([KHP+03], [VKK+95]). The second is the case of ANKA.
Tuning RF cavities in order to shift their resonances has mechanical limits and a slow response, which means it is not a suitable method if frequent and numerous adjustments of machine parameters (for instance, magnet aligments) are required.

2.4.2. Active feedback

Stabilization of CBI can also be achieved by means of control systems or feedback systems. These can be understood in frequency domain (Mode-by-Mode feedback) or in time domain (Bunch-by-Bunch feedback) ([FEH+93], p.1).
In the multibunch scenario, although each bunch oscillates at the betatron and synchrotron tune frequencies, there can be different modes of oscillation, called multibunch modes, which are characterized by the phase shift at which each bunch oscillates with respect to the other bunches ([Lon08], p.4). In a ring filled with h bunches, there are h possible multibunch modes; if the amplitude of the oscillation corresponding to some of them grows exponentially, it is said that those modes become unstable, i.e. CBI arise.
Regarding Mode-by-Mode feedback, a single narrow-band feedback channel is provided for every unstable of those modes. It consists of a frequency-selective filter to detect the unstable mode, a power amplifier and a kicker which applies the control action to counteract the unstable mode. Multiple unstable modes are treated with parallel feedback systems [FEH+93].
With time, the number of bunches stored in synchrotron light sources and the operation current have increased, and with this, the number of potential unstable multibunch modes ([Tey04], p.17). As a consequence, Mode-by-Mode control might be unfeasible.
The alternative to this type of control is the time-domain approach: in Bunch-By-Bunch (BBB) control systems, each bunch is treated as an individual oscillator driven by a disturbance (which is the result of the coupled-bunch motion). The deviation from the ideal dynamics, those of the synchronous particle, is detected in the transverse and longitudinal planes, and a particular feedback signal is generated for every bunch. This feedback signal is applied as an electromagnetic "kick" or correction to the trajectory of each bunch individually, which keeps its oscillations within the stability boundaries ([Wol09a], pp.29-37).
BBB control systems can be analog or digital. The second offer the advantages of more flexibility, scalability and reproducibility, as well as the additional feature of providing accelerator diagnostic tools ([Lon08], pp.1,15), such as the measurement of complex HOM impedances ([FCM+], p.47).
In ANKA, a BBB control system provided by Dimtel, Inc. [dim] is implemented. In the coming chapters, this control system is explained in detail and some limitations of its performance are presented.

2.5. Methods to enhance the beam lifetime

CBI can limit the storable beam current and reduce the brightness of the synchrotron light source. Another figure to evaluate the performance of the storage ring is the beam lifetime, that is, the time interval after which the intensity of the beam has reached 1/e of its initial value. It can be obtained from the beam current using the expression:

$$I(t) \approx I(0)e^{-t/\tau_L} \tag{2.9}$$

with $I(t)$ the current stored at time t, $I(0)$ the initial value of the current and τ_L the lifetime of the beam, typically measured in hours ([Pea12], p.19). In the case of ANKA, the beam lifetime is 16 hours for a 150 mA current level [ANKc].
The highest possible beam lifetime is desired. However, it is limited by several effects; particles can be lost due to: gas scattering effects (collisions with the residual gas and ions inside the vacuum system of the storage ring); intrabeam scattering (IBS, collisions among particles within the bunch, which is also known as Touschek effect); quantum effects for electron machines (it is related to the discrete or quantized nature of the emission of synchrotron radiation [Wal92], p.481); or as a result of CBI, amongst others ([Bru66], chapters 26, 30 and 31). The contribution of these factors to the total beam lifetime can be expressed as follows:

$$\frac{1}{\tau_L} = \frac{1}{\tau_T} + \frac{1}{\tau_q} + \frac{1}{\tau_g} + \frac{1}{\tau_{CBI}} \tag{2.10}$$

with τ_T the Touschek lifetime, τ_q the quantum lifetime, τ_g the gas scattering lifetime and τ_{CBI} the contribution of CBI to lifetime, each of them associated to the corresponding effect.
When CBI are not the dominant effect (for instance, because they are damped by the BBB control system), the limiting factors are the gas scattering effect and the Touschek effect. Residual gas scattering is the dominant effect in the case of poor vacuum pressure. As a numeric example, the poor vacuum scenario in the Cornell Electron Storage Ring would be a pressure higher than a residual gas pressure of 3.4×10^{-9} $Torr$ ([USP01], p.17).
When CBI are not limiting and the vacuum pressure is below the residual gas pressure, the Touschek effect becomes the dominant factor.

The longitudinal bunch length is defined as twice the maximum excursion of particles from the bunch center in the direction of this axis ([Wie07], p.216, p.751). The Touschek lifetime is directly proportional to the RMS bunch length in the horizontal, vertical and longitudinal axis (σ_x , σ_y and σ_z respectively) and inversely proportional to the density of particles in the bunch, regarding the relation ([JHKM14], p.222):

$$\frac{1}{\tau_T} \propto \frac{N}{\sigma_x \sigma_y \sigma_z} \tag{2.11}$$

The density of particles is calculated as:

$$\rho = \frac{N}{\sigma_x \sigma_y \sigma_z} \tag{2.12}$$

with N the the number of electrons per bunch and $\sigma_x \sigma_y \sigma_z$ the RMS volume of the bunch. The effects of intrabeam scattering derived from the betatron and longitudinal motions are projected into the longitudinal plane ([Piw98], p.2), so an enhancement of Touschek lifetime can be achieved by acting on the longitudinal bunch length.

On the one hand, a short bunch length in the longitudinal axis is required for the proper operation of the undulators, periodic structures of dipole magnets that stimulate the emission of highly brilliant synchrotron radiation. Usual values for longitudinal bunch length are a few hundreds of μm (compare [KPPL08], [MTH+07], [KKJ+16]). However, the Touschek effect is more significant with short bunches, because the particle density is higher.
If the beam lifetime is limited due to the Touschek effect, expression 2.11 shows that the Touschek lifetime could be elongated in the same amount as the bunch length in the longitudinal axis ([SIMT], p.11). This is explained because with a higher bunch length, the particle density is reduced (which is shown with expression 2.12) and, with this, the probability of collisions among particles within the bunch is also lower. That is, the IBS or the Touschek effect are reduced and thus the Touschek lifetime is enhanced ([WN13], p.25; [Wie07], p.573).

A technique to increase the bunch length is RF voltage modulation: if such a modulation is applied at about twice the synchrotron frequency (that is, the longitudinal quadrupole resonance), a redistribution of particles in the longitudinal plane is produced. This redistribution can be understood as a quadrupole modulation of the longitudinal motion ([SIM+00], p.692; [SHL+98], p.1339), which leads to an increment of the longitudinal bunch length. As a consequence, a lower density of particles is achieved in the bunch core ([Ng15], p.108; [WCC+99], p.1), which reduces the probability of particle collision inside the beam. This leads to a reduction of the Touschek effect and thus the beam lifetime is enhanced ([WN13], p.25; [SIMT], pp.1,3,11; [KFH+10], p.2755).

RF voltage modulation is applied by means of the Low-Level-RF (LLRF) control system of the storage ring. It reaches the beam at the RF cavities, which have a high quality factor and thus a narrow bandwidth - a maximum bandwidth of a few dozens of kHz [SCG+] is the usual value, so it can well be that the applied modulation exceeds the cavity bandwidth (in [SIM+00], 46.7 kHz is used as frequency for the modulation). In order to achieve the desired effect while operating outside of the cavity bandwidth, a large RF power is required. This leads to high reflected powers which are beyond the design levels, so an RF interlock can occur to prevent the damage of components, which would lead to beamloss.
In chapter 5, an alternative solution to overcome the limitation of the narrow bandwidth of the RF cavities will be presented. This solution, which has been implemented in the ANKA storage ring, is based on the BBB control system.

3. Bunch-by-Bunch control system

In practice, the beam can be stable at low currents in the multibunch scenario, as seen in section 2.3. As more current is injected into the ring, at some point a mode of the coupled-bunch oscillations can become unstable and lead to an exponential growth of the oscillation amplitude, which will provoke beamloss.
Some methods to correct CBI have been presented in section 2.4. Among these methods, the Bunch-By-Bunch (BBB) digital feedback is the alternative implemented in the ANKA storage ring. The main goal of this control system is to add damping to the motion of particles or, in other words, complement the natural damping of CBI ([FEH+93], p.4; [Wol09a], p.29).
This enables restraining the amplitude of beam oscillations within the stability boundaries, thus enhancing the beam quality and lifetime, which in turn increases the storable beam current ([Sch15], p.62).

In this chapter, the general structure of a BBB control system is introduced and its main components are explained. The chapter is structured as follows: first, general concepts of control systems and its applications to beam dynamics are explained. Then the explanation focuses on the components of the BBB control system, particularizing for the case of ANKA. Finally, limitations of BBB control systems are presented, thus defining the challenges to deal with in the present work.

3.1. Fundamentals of feedback loops

A general overview of a feedback control system is depicted at Figure 3.1 [FEH+93]. The control aims to change the output of a dynamic system to behave as desired by acting on the input of that system.
System output (obtained from the corresponding sensors) becomes the feedback pickup, which is to be matched to a reference value or set point. To minimize the difference or error between them, a controller provides the new, corrected input to the system or control action, which will be applied by means of actuators.
The plant or system to be controlled is subject to external disturbances which affect its output. As in the case of the BBB feedback, a performance criteria of the control system can be the reduction of the transfer gain from external disturbance input to plant output or, in other terms, the measurement of attenuation of these disturbances as seen from the output.

3.2. Feedback loop of a BBB control system

In the BBB control approach, each bunch is treated individually. As an analogy to Figure 3.1, a generic BBB feedback loop is depicted at Figure 3.2. System output, that is, the

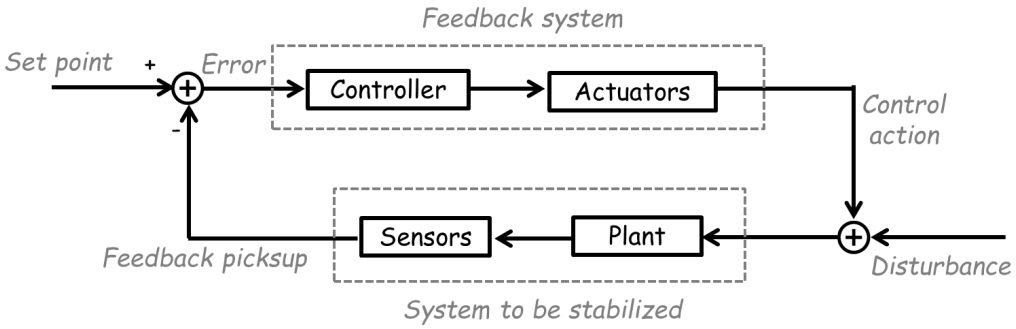

Figure 3.1.: Overview of a feedback system: the response of the system (feedback pickup acquired with sensors) is to be matched to a reference or set point, but this might not be achieved due to disturbances at the input of the system. So as to counteract them, a control action is computed with a controller; and then it is applied to the system to be stabilised (plant) by means of an actuator. This control action becomes the new input to the system, thus steering it towards the desired performance

motion of a particular bunch (beam position and phase), is obtained from one or more beam pickups (in ANKA, one beam pickup is installed for the BBB control system).

CBI act as a disturbance to be attenuated by the control system. In Figure 3.1, an external set point was considered, that is, a signal provided in order to force a given behaviour in steady state of the system to be controlled. In the case of BBB control, there is no external set point: with a proper operation of the control system, the desired motion is inherently achieved. On the one hand, if the feedback loop has the suitable gain and phase responses at the betatron tune, oscillations in the transverse plane are damped, and the transverse motion tends to match the synchronous trajectory. On the other hand, if the proper configuration of the control system in the longitudinal plane is achieved, the synchrotron oscillations are damped and bunches tend to arrive at the synchronous phase. Therefore, the control action which is generated for each particular bunch aims to approach its motion to that defined by the reference or synchronous particle. In the case of a digital control system, the controller (the block in charge of computing the control action) can be a Digital Signal Processor (DSP) or a Field-Programmable-Gate-Array (FPGA, as in the case of ANKA).
The calculated control signal is sent to a RF power amplifier, which provides the following stage in the loop (the kicker) with the necessary RF power by amplifying this signal. The kicker is the feedback actuator, it aims to counteract the effects of CBI, which are represented as a disturbance to be attenuated by the control system. The kicker generates an electromagnetic field in the corresponding plane that steers the bunches with small "kicks" as they pass through it, which corrects their trajectory and keeps oscillations within stability boundaries ([Lon08], p.23). The "kick" is proportional to the deviation of the bunch from the beam centre in the transverse plane, and proportional to the energy offset relative to the synchronous energy in the longitudinal plane. The overall effect is the damping of the oscillations in the corresponding plane ([DCH+03], p.21).
Ideally, the kick should correct the bunch trajectory instantaneously; however, due to limitations on the technical components, a series of small kicks are applied over several turns to achieve this correction. Modern digital control systems can achieve the desired damping in several turns ([Wol09a], pp.29-37).

The architecture corresponding to the BBB control system of the ANKA storage ring is

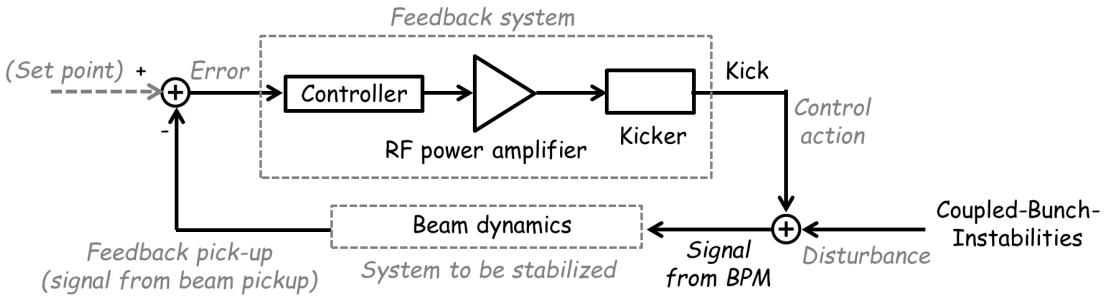

Figure 3.2.: Overview of a BBB control system: the response of the system (amplitude and phase of the oscillations of the beam around its nominal trajectory) is to be matched to a reference or set point, i.e. the stable motion in the transverse and longitudinal planes (in the case of BBB, there is no external reference, but the stable motion is achieved inherently). This might not be achieved due to disturbances at the input of the system (CBI). So as to counteract them, a control action is computed with a controller; and then it is applied to the beam by means of an actuator (kicker). This control action becomes the new input to the system, thus steering the beam towards a stable motion

depicted at Figure 3.3 ([Sch15], pp.52,55; [Wol09a], p.28). The BBB system in this facility has been implemented by Dimtel, Inc. [dim].
The numbers in this figure correspond to the aforementioned stages in the feedback loop, namely:

1. **Beam pickup to obtain the bunch dynamics**
   The Beam Position Monitor provides the changes in the position of the different bunches in respect of the centered, nominal trajectory.
   In the transverse plane, the deviation in respect of the centre of the beam is related to the amplitude of betatron oscillations. This amplitude is the envelope of a carrier signal of the bunch repetition frequency ω_{RF}. In order to obtain the information corresponding to the amplitude of betatron oscillations, amplitude demodulation is applied to the BPM readout in this plane.
   In the longitudinal axis, the value of the BPM readout is related to the time of arrival of the bunch, in particular to the difference of its time of arrival in respect of that of the synchronous particle. As a consequence, the BPM signal in this axis is modulated in phase.
   Analogously to the transverse plane, this modulation is the envelope of a carrier signal of the bunch repetition frequency ω_{RF}. In order to obtain the information corresponding to the amplitude of synchrotron oscillations, phase demodulation is applied to the BPM readout in the longitudinal axis ([Lon08], p.10).
   Amplitude and phase demodulation can be performed with the heterodyne scheme, which will be explained in section 3.3. The frequency content of interest of the demodulated signal is comprised in the range DC to $\omega_{RF}/2$, so a lowpass filter (LPF in the figure) discards frequencies higher than these.

2. **Digitalization of the demodulated BPM readout, acquisition of each bunch individually**
   Once the amplitudes corresponding to betatron and synchrotron oscillations are available, they are digitilized and stored in up to three acquisition modules, regarding on which of them are selected.
   The digitalization of the BPM readout is performed with an ADC sampling at ω_{RF}; the frequency content to be acquired is limited to $\omega_{RF}/2$, so the Nyquist theorem is respected with this acquisition rate. The numbering of the bunches is achieved by

downconverting the reference clock times the harmonic number.

The available acquisition modules are the following:

- Block Random Acquisition Memory (BRAM): it is integrated in the FPGA and it has a maximum acquisition window of 0.5656 ms, which corresponds to about 1536 turns described by the $h = 184$ bunches. It supports a maximum acquisition rate of 5 Hz.
- Static Random Access Memory (SRAM): it is an external module with an acquisition window of 25.2 ms, which corresponds to about 68384 turns described by the $h = 184$ bunches. It supports a maximum acquisition rate of 2 Hz.
- Single Bunch (SB): it stores the temporal changes in the positions of one single bunch, supporting an acquisition window of 32.6 ms (98304 turns described by the specified bunch).

The SB acquisition module provides the highest resolution, but the slowest update rate. In this work, the BRAM module is used.

The FFT of the signal acquired for each bunch (corresponding to the temporal changes in its positions) is computed, and then the average of these spectra is calculated. In this work, the control signal is computed in the frequency domain based on this averaged spectrum, which will be explained in detail in section 3.4.

3. **Computation of the control action for each bunch individually**
The control signal for a particular bunch is computed with an FPGA. The operation consists in filtering the signal acquired for each bunch individually with a digital Finite Impulse Response (FIR) filter, whose phase advance and gain and the betatron or synchrotron tunes are such, that when the control signal is translated to the beam as an electromagnetic kick, it provides the damping of these oscillations in the required amount.
The specification of the parameters of this filter is performed in the frequency domain, as it will be seen in section 3.5.
In the longitudinal axis, an additional signal is superimposed to the control action provided by the filter. The additional signal modulates the beam in the longitudinal axis at its quadrupole resonance, which aims to enhance beam lifetime. Chapter 5 is focused on the generation and the effects of this additional signal. In terms of software, the BBB control is implemented using the EPICS platform [epi], which consists of a set of open source software tools, libraries and applications that enable implementing a distributed soft real-time control system. The filter parameters and the signals required for control, diagnostics, etc. can be acquired and processed in the form of "Process Variables" (PVs). In this work, these variables are accessed by means of an API developed in C++ by Dr. Manuel Schedler.
4. **Application of the control action as an electromagnetic "kick"**

The calculated feedback signal is then sent to the RF power amplifier and the kicker, which applies the electromagnetic steering action to the beam.
In the transverse plane, the kicker is a stripline which can operate in the range of frequencies of the control signal (DC to $\omega_{RF}/2$). In the longitudinal plane, it consists of a cavity which operates at a higher frequency (and which can support the control $\omega_{RF}/2$ bandwidth), so correction signal is upconverted in frequency by mixing it with

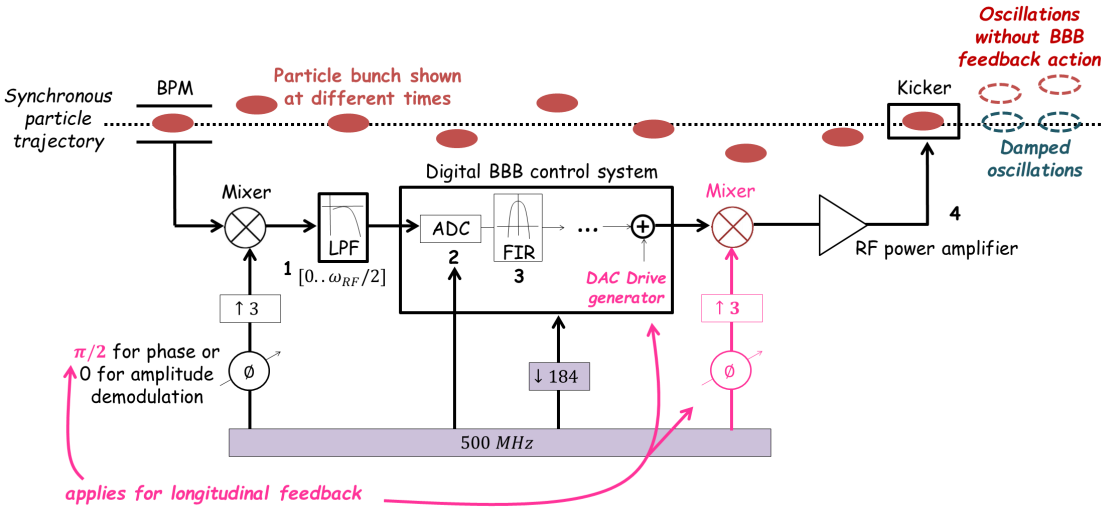

Figure 3.3.: Implementation of the BBB control system in ANKA

the third harmonic of the reference clock in order to match the cavity's operation frequency. An additional phase shift may be added to compensate for delays due to electronics and to maximize the output signal.

In the following sections, points 1, 2 and 3 in Figure 3.3 will be explained in detail. This comprises the demodulation of BPM readout in order to obtain the amplitude and phase signals associated to the betatron and synchrotron oscillations respectively; the obtention and interpretation of the spectrum corresponding to the temporal changes of each bunch's positions; and the explanation of the characteristics of the controller, the digital FIR filter.

3.3. Heterodyne demodulation of the readout of the Beam Position Monitor

A beam pickup or Beam Position Monitor (BPM) consists of a transducer, transmission lines, electronics and software which provide the signal to be processed by the BBB controller ([Fox16], pp.8-16). One BPM is implemented for the BBB control system in ANKA, which captures the temporal changes of the bunches' positions in the transverse and longitudinal planes.

In the transverse plane, the amplitude of the acquired signal is related to the deviation of the bunch from the nominal trajectory. In the case of h stored bunches arriving in the BPM with the theoretical maximum bunch repetition frequency ω_{RF}, the resulting signal is a train of samples of this frequency, modulated by the amplitude of the betatron oscillation. In other words, ω_{RF} is the carrier frequency of the modulation.
In order to extract the information corresponding to the amplitude of betatron oscillations, amplitude demodulation is applied using the heterodyne technique.
Heterodyne demodulation is a method for detecting a signal of a given frequency by applying a non-linear mixing with a signal of a reference frequency. The resulting signal's spectrum includes the difference of the aforementioned components, which carries the information to be detected (amplitude modulation in this case) of the original higher frequency signal, but oscillating at a lower frequency, which is more easily processable [VB]. It is a common technique in telecommunications.
The operation corresponding to heterodyne demodulation is depicted at Figure 3.4: the

third harmonic of the BPM readout is mixed with a the third harmonic of the reference clock. This provides components at the sum and at the difference of frequencies of the signals at the input of the mixer. The higher frequencies are discarded with a lowpass filter (LPF) with a cutoff frequency of $\omega_{RF}/2$. The remaining, low-frequency content is the envelope of the betatron oscillations, that is, the amplitude of the deviation from the nominal trajectory.

In the longitudinal plane, the time of arrival of the bunches is related to the amplitude of the synchrotron oscillations. In the case of h stored bunches arriving in the BPM with the theoretical maximum bunch repetition frequency ω_{RF}, the resulting signal is a train of samples of this frequency, whose time of arrival depends on the amplitude of the synchrotron oscillation. In other words, a phase modulation is produced and ω_{RF} is the carrier frequency of this modulation.
In order to translate the information of the time of arrival into an amplitude which can be acquired and processed by the controller, a phase demodulation by means of the heterodyne technique is applied.
This operation is depicted at Figure 3.4: the third harmonic of the reference clock is mixed with the third harmonic of the BPM readout in the longitudinal plane. This shifts the involved frequency components to higher frequencies (corresponding to the addition of the phases of the input signals of the mixer) and to lower frequencies (those associated to the subtraction of the phases of the input signals of the mixer). The first are discarded with a lowpass filter (LPF) with a cutoff frequency of $\omega_{RF}/2$. The low frequency component in the range DC to $\omega_{RF}/2$ corresponds to the demodulated envelope of the synchrotron oscillations (since these have a small amplitude, $sin(\phi(t))$ can be approximated to $\phi(t)$, which is the amplitude corresponding to the synchrotron oscillations).

Figure 3.5 aims to explain the reason why the third harmonic of the reference clock is selected for the frequency mixing. Three signals are depicted: the sinewaves correspond to the first and third harmonic of the reference clock; the "arrows" are the BPM readout in two instants of time which illustrate the maximum range of variation of this readout due to betatron and synchrotron oscillations.
On the one hand, the amplitude of the "arrows" indicates the maximum deviation from the centre of the beam in the transverse plane (regardless the sign of this deviation), which is related to the amplitude of the betatron oscillations. On the other hand, the time of arrival of the "arrows" corresponds to the peak-to-peak excursion of the synchrotron oscillation, i.e. the maximum possible phase delay and phase advance.
The output of the mixer at the instants in which the "arrows" arrive corresponds roughly to the product of their amplitude times the amplitude of the mixing signal at those instants of time.
If there were no synchrotron oscillations, the "arrows" should arrive at the time instant corresponding to the peak of the mixing signal, so as to produce the maximum value at the output of the mixer. The highest possible output is desired in order to maximize the dynamic range used at the input of the ADC, because this will provide a better resolution of the acquired signal.
The output of the mixer will be larger for a higher amplitude of the considered "arrow", that is, for a more intense deviation from the centre of the beam. This is the result of amplitude demodulation.
In the longitudinal axis, however, the reverse result is desired. In this case, if the "arrow" appears at exactly the peak of the mixing signal, it means the time of arrival of the bunch

is matched to the synchronous phase. Therefore, the output of the mixer should be zero (the values greater than zero will indicate the deviation from the synchronous phase). So as to achieve a zero output when the time of arrival corresponds to the synchronous phase, the reference clock is shifted by $\pi/2$ for this axis, which provides phase demodulation.
As a result, the presence of synchrotron oscillations is detected in the longitudinal axis as a fluctuation of the time of appearance of the "arrows" in the linear regime of the mixing signal (the itme instants around its zero crossing).
In order to maximize the output of the mixer in this axis, a high slope of the mixing signal is desired in its linear range. As indicated in Figure 3.5, the dynamic range corresponding to the maximum deviations in the time of arrival of the bunch increases with the slope of the mixing signal in its linear regime. This is the reason why the reference clock is upconverted to its third harmonic to obtain the mixing signal: with a higher frequency of this signal, a larger dynamic range is obtained at the output of the mixer, which will provide a better resolution of the acquired signal.
Note that the benefit of the slope of the mixing signal in its linear regime only affects in the longitudinal axis. In the transverse plane, since the peak of the mixing signal is used for the demodulation, the slope in this region is almost flat and the higher frequency of the signal does not increase the dynamic range at the output of the mixer.

As it has been explained before, amplitude demodulation provides a value at the output of the mixer which is related to the fluctuation in the amplitude of the BPM readout in the transverse plane (and thus to the amplitude of the betatron oscillations). This fluctuation provides a different result of the product of the BPM readout times the peak value of the mixing signal.
However, the result of this product is also affected by the time of arrival of the bunch. In the transverse plane, the presence of synchrotron oscillations is detected as a fluctuation of the time of appearance of the aforementioned "arrows" around the peak of the mixing signal, which affects the output of the mixer.
As a result, the output of the mixer in the transverse plane depends both on the amplitude of the betatron oscillations and also upon the time of arrival of the bunch (which is related to the amplitude of the synchrotron oscillations). Therefore, there is a coupling between the transverse and longitudinal planes due to the sensitivity of the mixer to the fluctuations in the phase of the BPM readout, as indicated in Figure 3.4.
The coupling between both planes can be detected in the spectrum corresponding to the temporal changes of a single bunch's positions in the transverse plane, as it will be seen in the next section.

3.4. Spectra of the temporal changes of a single bunch's positions

The FIR filter which provides the control signal to be applied to the beam in order to damp the betatron or synchrotron oscillations is configured in the frequency domain. The demodulated, digitilized BPM readout obtained for each bunch individually is thus translated to the frequency domain to perform the proper dimension of the filter. In this section, the expression of the spectra corresponding to the temporal changes of each bunch's positions acquired individually is presented and the spectra observed in the ANKA storage ring are shown.

As explained in sections 2.2 and 2.3, bunch oscillations are sinusoidal, so the turn-by-turn position of a bunch measured at the BPM is a sampled sinusoid. Since each bunch is treated individually, the signal obtained and its corresponding spectrum correspond to the

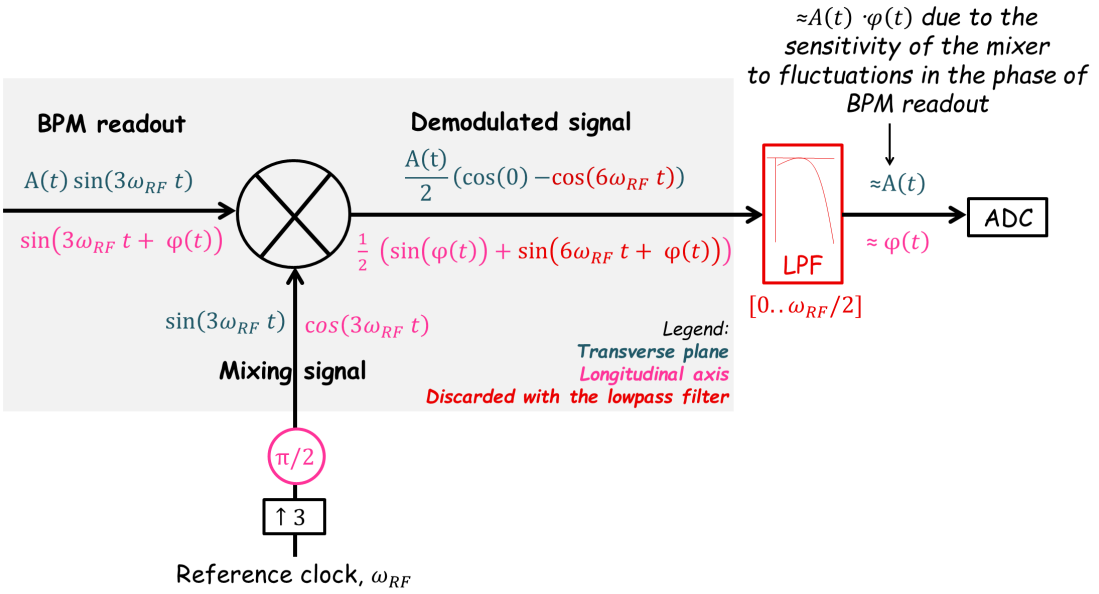

Figure 3.4.: Sketch of signals involved in the heterodyne demodulation, which is performed by the frequency mixer (shaded area). BPM readout in the longitudinal axis is demodulated in phase by mixing its third harmonic with the third harmonic of the reference clock shifted by $\pi/2$. This provides a signal proportional to the amplitude of the synchrotron oscillations. The readout in the transverse plane is demodulated in amplitude by mixing its third harmonic with the third harmonic of the reference clock, which provides a signal proportional to the amplitude of the betatron oscillations. The frequency content beyond $\omega_{RF}/2$ is discarded with a lowpass filter. The demodulated signals are acquired with an ADC, which samples them at ω_{RF}. The signal corresponding to each individual bunch is obtained by triggering the ADC at ω_o

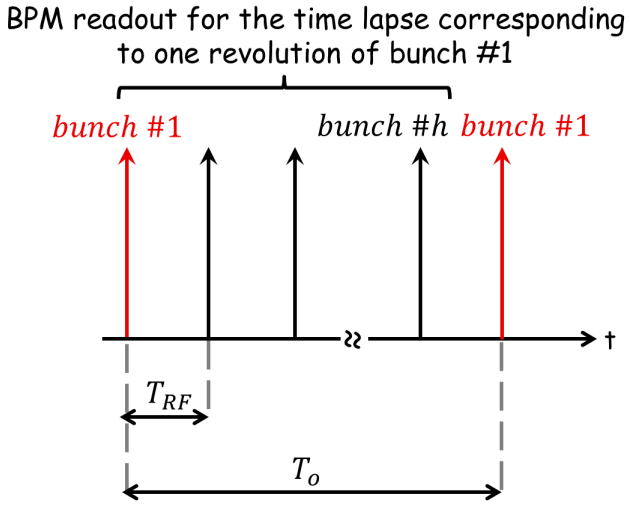

Figure 3.5.: Sketch to illustrate the frequencies involved in the digitalization of the BPM readout. Each line represents the BPM readout corresponding to a given bunch, which is acquired with the ADC: the motion of this bunch is sampled once every turn (it is acquired with ω_o). The total of bunches are acquired individually in one turn, thus the ADC samples at ω_{RF}. The selection of a given bunch is achieved by downsampling the reference clock (ω_{RF}) by a factor corresponding to the harmonic number

single bunch scenario. Transverse and longitudinal planes will be explained separately in the following.

The demodulated BPM readout acquired for each bunch individually corresponds to a sinusoid sampled at multiples of the revolution period (one sample is acquired per turn). In the transverse plane, the amplitude of this sinusoid is proportional to the deviation of the bunch from the nominal, centered trajectory. Signal acquired in this plane can be expressed as:

$$s(t) = A_\beta cos(\omega_\beta t) \sum_{k=-\infty}^{\infty} \delta(t - kT_o) \tag{3.1}$$

with ω_β the betatron tune and $T_o = 1/\omega_o$ the revolution period. A_β is the amplitude proportional to the deviation from nominal trajectory.

In the longitudinal plane, the phase of the acquired sinusoid is proportional to the deviation in arrival time in respect of the synchronous particle. Therefore, it can be expressed as a phase modulation of magnitude τ at the synchrotron frequency ω_s:

$$s(t) = \sum_{k=-\infty}^{\infty} \delta(t + \tau sin(\omega_s t + \phi_s) - kT_o) \tag{3.2}$$

with τ the amplitude of the phase modulation, ω_s the synchrotron tune, ϕ_s the synchronous phase and $T_o = 1/\omega_o$ the revolution period.

As it has been commented before, feedback processing is performed in the frequency domain. So as to understand which signals are involved, the spectrum associated to the time domain readout obtained from the BPM is presented.
In the transverse plane, frequency equivalent to expression 3.1 is the convolution of the cosine modulating function with the bunch spectrum:

$$S(\omega) = \frac{A_\beta \omega_o}{2} \sum_{k=-\infty}^{\infty} \delta(\omega - k\omega_o \pm \omega_\beta) \tag{3.3}$$

This means that the acquired spectrum is a series of harmonics of the revolution frequency with sidebands at a distance corresponding to the betatron tune, as it can be seen in Figure 3.6a. These harmonics correspond to frequencies defined by:

$$\omega = k\omega_o \pm \omega_\beta \quad ; \quad k \in (-\infty, \infty) \tag{3.4}$$

For the longitudinal plane, the spectrum is a series of harmonics of the revolution frequency with sidebands following a Bessel distribution: they are located at a distance corresponding to multiples of the synchrotron tune in respect of the corresponding harmonic of the revolution frequency, as it can be seen in Figure 3.6b. These harmonics correspond to frequencies defined by:

$$\omega = k\omega_o \pm l\omega_s \quad ; \quad k, l \in (-\infty, \infty) \tag{3.5}$$

For small oscillation amplitudes, the lowest order terms of the Bessel function (l = 0 and l = ± 1) are enough to describe the phase modulation. The amplitude of these components shows the magnitude of the phase modulation (τ in expression 3.2).

Due to the periodicity of the transverse and longitudinal spectra in the single bunch scenario and the symmetry of sidebands around the harmonics of the revolution frequency, the information required to compute the control action can be obtained from the first harmonic. Therefore, only the frequency content between DC and $\omega_o/2$ is considered. As it has been mentioned before, the sampling frequency of the ADC to acquire each bunch individually is ω_o, so the Nyquist theorem is respected.

In the case of ANKA, the spectra obtained from the BPM readout acquired for each bunch individually are averaged. The observed waveforms, which are considered in the range DC to $\omega_o/2$, are presented next.

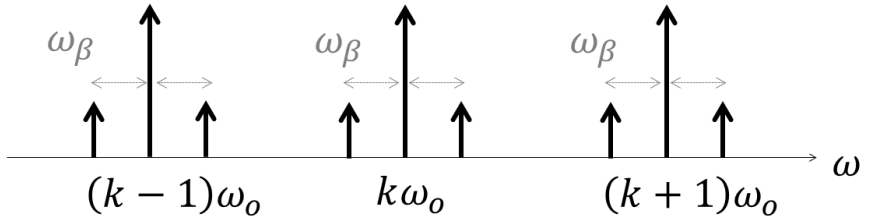

(a) Components of the spectrum of the transverse signal acquired with the BPM for one single bunch

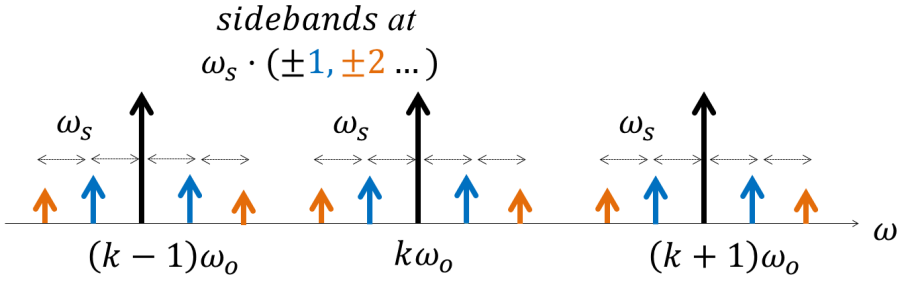

(b) Components of the spectrum of the longitudinal signal acquired with the BPM for one single bunch

Figure 3.6.: Spectra associated to the BPM readout in the single bunch scenario

3.4.1. Synchrotron sidebands observed in the transverse spectrum in ANKA

The theoretical spectra in the transverse and synchrotron planes for the single bunch scenario are depicted at Figure 3.6. However, additional frequency components might appear due to non-idealities of the electronics. This is the case of the synchrotron sidebands observed in the transverse spectra in ANKA.
Regarding expression 3.4 and taking into account that only the range from DC to $\omega_o/2$ is considered, the expected frequency content in the transverse plane would be located at the betatron tune ω_β, that is, the upper sideband of the fundamental harmonic of the revolution frequency. Since in ANKA only one BPM is installed for the BBB control system, the observed component in the transverse plane corresponds to the fractional betatron tune

Q_β.
However, it will be seen in the next section that an additional pair of sidebands appear around Q_β at a distance corresponding to the fractional synchrotron tune Q_s. Therefore, the components observed in the transverse spectra are those depicted at Figure 3.7 instead of the ideal ones in Figure 3.6a.
The additional sidebands located at a distance from Q_β corresponding to Q_s appear due to the sensitivity of the mixer (which performs the amplitude demodulation of the BPM readout for the transverse plane) to the fluctuations in the phase of the BPM readout for the transverse plane.

As it has been seen with Figure **??** the amplitude of the BPM readout in the transverse plane is related to the amplitude of the betatron oscillations. The spectrum associated to this amplitude modulation are the sidebands around the harmonics of the revolution frequency, located at a distance corresponding to the betatron tune.
However, the detected amplitude also depends upon the time of arrival of the bunch: the product of the amplitude of the readout with the mixing signal will be larger or smaller regarding the phase of the second, that is, depending on the instant in which the demodulation takes place. This introduces a dependance between the synchrotron oscillations and the readout corresponding to betatron oscillations.
The coupling between transverse and longitudinal planes due to the sensitivity of the mixer to these fluctuations in the phase of the BPM readout can be expressed as indicated in Figure 3.4. As a result of this coupling, the output of the mixer is no longer the envelope $A(t)$ (i.e. $A_\beta cos(\omega_\beta t)$ in expression 3.1), but the product of this envelope times the envelope corresponding to the phase oscillations $\phi(t)$ (i.e. $\tau sin(\omega_s t + \phi_s)$ in expression 3.2).
When this product is translated to the frequency domain, the convolution of both spectra is obtained. The resulting spectrum which is observed in the range from DC to $\omega_o/2$ contains a component at Q_β and the first of the sidebands associated to the Bessel distribution in Figure 3.6b (which are located at each side of Q_β at a distance corresponding to Q_s). The rest of sidebands of the Bessel distribution are not observed at these frequencies in ANKA because their amplitude is below the noise floor.

The next section presents the spectra observed in ANKA corresponding to the temporal changes of each bunch's positions. In the transverse plane, the synchrotron sidebands will be identified.

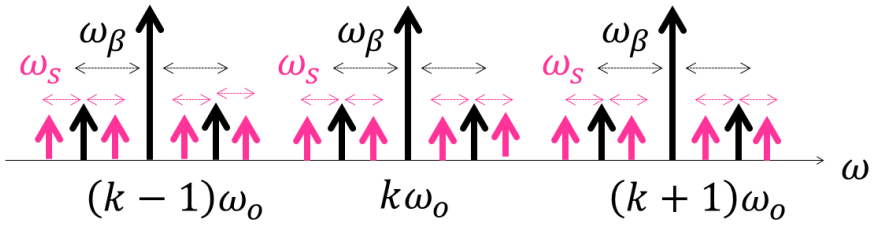

Figure 3.7.: Spectrum of the transverse signal acquired with the BPM for one single bunch under the effect of the coupling between transverse and longitudinal planes, which is due to the sensitivity of the mixer to the fluctuations in phase of the BPM readout

3.4.2. Spectra of the temporal changes of a single bunch's positions observed in ANKA

Regarding section 3.4, the spectrum corresponding to the temporal changes of a single bunch's positions is a series of harmonics of the revolution frequency with sidebands at the

betatron or synchrotron tunes, depending on the plane. Due to the periodicity of these spectra, they can be cropped in the range from DC to $\omega_o/2$, thus considering the upper sideband of the fundamental harmonic of the revolution frequency. In the case of ANKA, since one BPM is installed for the BBB control system, the observed sidebands correspond to Q_β or Q_s.
The magnitude of the spectrum corresponding to the average of spectra obtained from the temporal changes in each bunch's positions is represented in Figures 3.8a, 3.8b and 3.8c for the horizontal, vertical and longitudinal axes respectively. It has been obtained from the BRAM acquisition module by acquiring the the correspoding signal or PV of the control software interface. A zoom is shown around the position of the corresponding tune. Since only one BPM is implemented for the BBB control system, this corresponds to the fractional tune.

The spectral representation of the temporal changes of a single bunch's positions is visualized as a well pronounced peak at the frequency of this oscillation. With a proper operation of the BBB control system (when oscillations are damped), this peak turns into a dip. The depth of the notch, that is, the distance from magnitude at the dip to the noise floor, is related to the damping strength of the BBB control system. The higher the attenuation (the deeper the dip), the more robust is the system against CBI. However, this also implies a larger gain of the feedback loop, and this leads to amplifying the noise in the loop (mainly the noise introduced by the ADC) and can eventually provoke feedback instability. Therefore, a deep notch is desired as long as gain of the feedback loop is not as large as to provoke feedback instability ([Sch15], Kapitel 7 and Kapitel 8).
In addition to this dip, further frequency content is observed in DC in Figure 3.8, which might be due to non-idealities of the machine electronics. In the case of longitudinal spectrum, an additional peak is observed at twice the synchrotron fractional tune (labelled as quadrupole resonance). This corresponds to a control strategy to enhance performance of longitudinal BBB feedback at injection energy, which will be explained in Chapter 5.

In the transverse spectra, a pair of sidebands are observed around the betatron tune at a distance corresponding to the synchrotron fractional tune. As it has been explained in section 3.4.1, they are due to the sensitivity of the mixer to the fluctuations in the phase of the BPM readout.
These sidebands are visualized as a dip (see 3.8a,3.8b), because they are damped by the feedback (if it is correctly tuned) as in the case of betatron oscillations. This notch is less deep than that of the tune because these sidebands are a consequence of small variations in the amplitude of the BPM readout corresponding in the transverse plane.
In this plane, the result of the frequency mixing is higher when the bunch arrives at the instant corresponding to the peak of the mixing signal or around of it. Therefore, the effect of the fluctuations in the time of arrival will be most significant when the bunch arrives at times around the peak of the mixing signal.
The slope of the mixing signal around its peak is almost flat, which leads to small amplitude variations with the fluctuation in the time of arrival of the bunch. This, in turn, explains that the notch at the sidebands is less deep than the notch at the betatron fractional tune.

In the following section, the characteristics of the controller of the BBB feedback loop are presented. It consists of a digital FIR filter, which provides the required control action to damp the aforementioned frequency components.

3.5. Generation of the control action

The multibunch scenario can be understood as a Multiple-Input-Multiple-Output (MIMO) scheme in which each bunch is treated as a harmonic oscillator coupled to all other bunches.

Individual bunch positions are the plant outputs and correction kicks are the plant inputs referring to Figure 3.1.
In the BBB control approach, position of all bunches is obtained from the same pickup and correction signal is applied with a single kicker, which can be achieved by time multiplexing (one bunch is treated at a time). This simplifies the problem to the Single-Input-Single-Output (SISO) case: each bunch is treated as an individual oscillator driven by a disturbance, which is the result of coupling to the other bunches ([Tey03], p.1; [Tey04], p.42).
As the control system acts equally on every bunch, it also acts equally on every eigenmode, which means the BBB feedback can stabilize all oscillation modes simultaneously ([Tey03], p.4).

Bunch-to-bunch coupling occurs due to the wakefield produced when particles circulate through RF cavities or interact with the walls of the vacuum chamber, because the wakefield generated by one bunch is sampled by the following bunches ([Wol09a], p.45). Under certain combinations of wakefield amplitudes and frequencies, the overall system becomes unstable. In this case, wakefields can be considered as a perturbation to particle motion, which can be described regarding equation 2.6. From this expression, the effect of feedback can be described as:

$$\ddot{s}(t) + 2(D - G + D_{FB})\dot{s}(t) + \omega^2 s(t) = 0 \tag{3.6}$$

where $\tau_G = 1/G$ is the growth time constant and G is the growth rate; $\tau_D = 1/D$ is the damping time constant and D is the damping rate; and D_{FB} is the damping term that feedback adds to the particle motion.
Bunch oscillations are sinusoidal, so the turn-by-turn position of a bunch measured at a given location (acquired with a Beam Position Monitor) is a sampled sinusoid. Regarding expression 3.6, the feedback action ($D_{FB}\dot{s}(t)$) must be proportional to the first derivative of bunch motion. This means that feedback action will have the shape of the oscillation of the particular bunch which is to be corrected (a sampled sinusoid), with some amplitude gain and a phase shift of $\pi/2$ or multiples of this ([Lon08], p.4). Next, further requirements for the feedback signal are presented and its generation is explained.

The control block in charge of providing the feedback action must fulfill the following specifications ([Lon08], p.33; [FEH+93], p.2077; [Wu12], p.81; [DGG+03], p.5; [DCH+03], p.27):

- Provide enough gain in the frequency range of interest so that CBI are damped.
- Provide the suitable phase response at the oscillation frequency, which is a multiple of $\pi/2$. This corresponds approximately to a differentiator (as it has been seen, the feedback signal must be proportional to the derivative of the oscillation).
  The nominal phase at the central frequency of the filter should be a multiple of $\pi/2$, but its actual value may vary due to delays associated to electronics (among them, the most significant is that introduced by cables). In ANKA, a nominal phase shift of 180° between detector and kicker is desired so as to ensure a) negative feedback, otherwise it would be instable; and b) purely resistive feedback, which means no shift will be provoked in those variables sensitive to imaginary impedance components, e.g. the betatron or synchrotron tunes.
- Reject DC component (closed orbit or stable beam motion) so as to avoid saturating the ADC/DAC in the feedback loop and, in a later stage, the amplifier. This means that after processing, the closed orbit signal sent to the kicker must be much smaller than the feedback signal at betatron or synchrotron frequency.

- Minimize high frequency components: the coupled-bunch motion has a periodic spectrum at multiples of the theoretical maximum bunch repetition frequency, which can saturate the RF power amplifier in the feedback loop or mask the oscillation to be damped if these harmonics are large enough. In addition, a narrow frequency response helps in rejecting detector noise and focuses control action at the frequency of the oscillation to be damped ([FCM+], p.14).

Taking advantage from the inherent sampling at revolution frequency (BPM samples bunch motion once every turn), these specifications can be fulfilled with a digital filter implementing a differentiator or a bandpass filter centered at the oscillation frequency. Either a finite impulse response (FIR) or infinite impulse response (IIR) filter are suitable ([FEH+93], p.2077).
In general, IIR filters offer a more flexible performance than FIR filters. However, their design is more delicate and their implementation is more complex. On the other hand, FIR filters are inherently stable, since the output to a bounded input is also bounded, regardless the filter coefficients ([Mit01], p.364). FIR filters are the preferred option for this application ([Lon08], p.31).

FIR filters can be defined in terms of finite difference equations, as shown in expression 3.7;

$$y[n] = \sum_{k=0}^{N_{taps}-1} b_k x[n-k] \tag{3.7}$$

with n the indexes of the samples of signals involved (discretized time), b_k the filter coefficients, N_{taps} the number of taps or number of coefficients of the filter ($N_{taps}-1$ is the order of the filter), $x[n]$ the input to the filter and $y[n]$ the filtered signal. FIR filters are non-recursive, which means output signal depends only on a finite number of input samples and not on past values of the filtered signal, as in the case of the IIR filters. As a result, the length of its impulse response and the delay it introduces in terms of number of samples is determined by the number of coefficients. In order to provide DC rejection, the sum of all coefficients must be zero.
A differentiator can provide the required $\pi/2$ (or multiples) phase response at oscillation frequency. This type of filter has a frequency response in the form of: $H(\omega) = -iK\omega$, with $i = \sqrt{-1}$ and K a constant value. Ideal differentiators have the inconvenience that they amplify high frequency noise, which contradicts the requirements for BBB feedback. So as to overcome this limitation, an approximation of a differentiator over a finite frequency range can be used. This is achieved with a frequency response in the form of:

$$H(\omega) = -K \sum_{k=1}^{N_{taps}} h_k e^{-j\omega T_s k} \tag{3.8}$$

with K a constant value, N_{taps} the number of taps and T_s the sampling rate for discretization ([HEF+93], p.2).
Equation 3.8 particularized for ANKA leads to the set of time domain coefficients ([KHK+], p.117):

$$c[k] = 2^g G sin(2\pi Q_{frac}(k+1) + 2\pi\phi) \tag{3.9}$$

$$h[k] = c[k] - \frac{1}{N_{taps}} \sum_{l=0}^{N_{taps}-1} c[l] \tag{3.10}$$

$$k \in [0, N_{taps}-1]; \quad Q_{frac} \in (0,1); \quad \phi \in [-180°, 180°]$$

$h[k]$ are the coefficients to perform the convolution with input signal (b_k in equation 3.7). They are computed in two steps: first, central frequency (Q_{frac}), phase (ϕ) and gain ($2^g G$) at this frequency are determined, providing the interim coefficients $c[k]$. Central frequency is set to the tune to be damped (in the case of systems with one single BPM, such as ANKA, the fractional tune is used). The phase is chose in a way that it provides the required $\pi/2$ offset or a multiple of it between detector and kicker, so as to implement the differentiator functionality. Gain provides the required damping without provoking control system instability; in the case of ANKA, it is determined by means of two parameters: shift gain g and central gain G, as it will be described in more detail in section 4.3.1.
In a second step, the mean value of the obtained coefficients is removed in order to force zero gain at baseband, thus providing DC rejection.

These are called selective filters. Their impulse response (the filter coefficients) is a sampled sinusoid with a frequency equal to the central frequency, as it can be seen in Figure 3.9a (filter coefficients have been computed regarding parameters of horizontal axis in Table A.2). Its frequency response is depicted at Figure 3.9b: amplitude response has a maximum at central frequency, thus focusing damping by the control system at this frequency.
Phase response is linear within the filter bandwidth, which means the phase of the filter can be expressed as a linear function of the frequency in this margin: $\psi = K\omega$, with K the slope of the phase or phase delay. For a sinusoidal, discrete input signal $x[n] = sin(\omega n)$, filter's output can be expressed as: $y[n] = H_\omega sin(\omega(n + K))$, with H_ω the amplitude response of the filter at frequency ω. This shows that with a linear phase, all frequency components are delayed in the same amount, corresponding to the phase delay of the filter.
Bandwidth of the control system is limited by the largest delay in the feedback loop. Since all frequencies are delayed in the same amount, such a filter does not change the limiting frequency component. Therefore, feedback bandwidth is maintained and with this the closed-loop stability margins ([Mat]).
The higher the number of taps, the more selective the filter - the narrower its bandwidth.

The aforementioned requirements must be fulfilled in order to achieve the desired functionality of the BBB control system. However, it might not be possible to match some of them during operation. This is the case of centering the action of the BBB control system at the frequency of the oscillation to be attenuated.
This frequency varies with energy during ramping, especially in the transverse plane, as it will be seen in section 4.1. This means that the feedback action might not be applied at the right frequency for certain levels of energy. The detuning of the BBB control system deteriorates its performance and can even lead to beamloss. In the next chapter, a strategy is proposed to avoid the aforementioned detuning, namely an automatic readjustment of the FIR filter parameters.

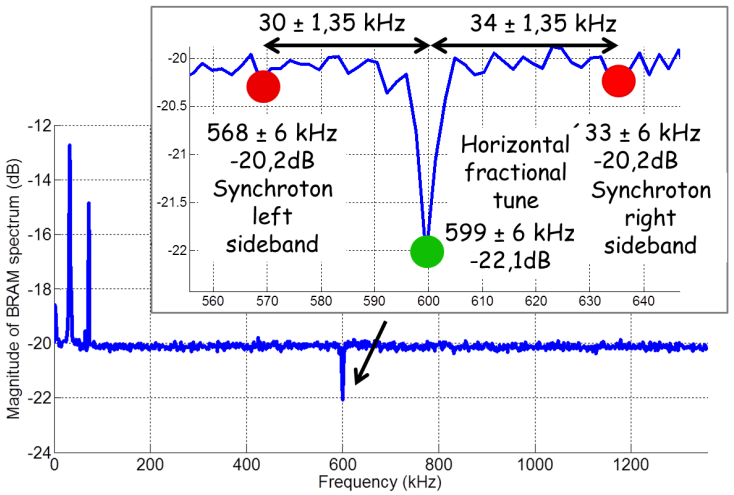

(a) Magnitude of the BRAM spectrum, horizontal axis (2.5 GeV)

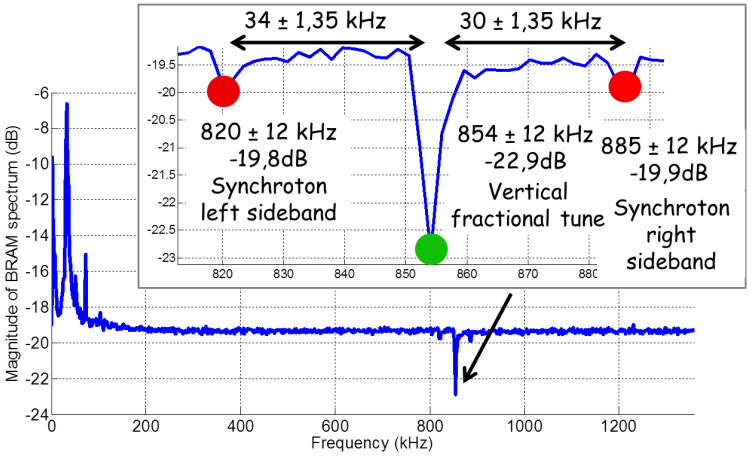

(b) Magnitude of the BRAM spectrum, vertical axis (2.5 GeV)

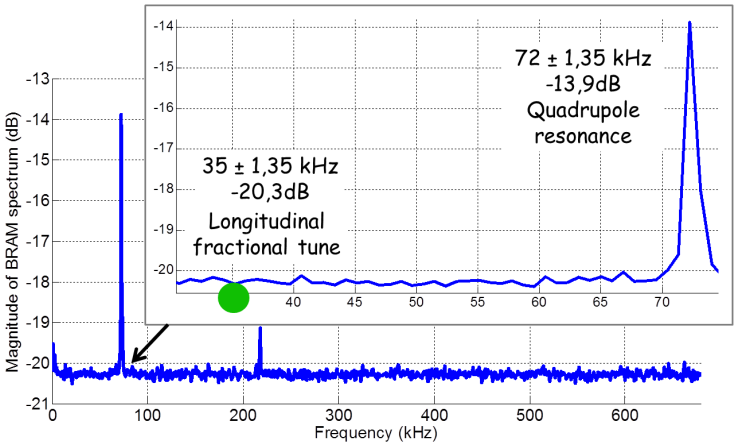

(c) Magnitude of the BRAM spectrum, longitudinal axis (0.505 GeV)

Figure 3.8.: Magnitude of the spectrum obtained from the BRAM acquisition module. It corresponds to the average of all FFTs calculated from the temporal changes of the individual bunches' positions

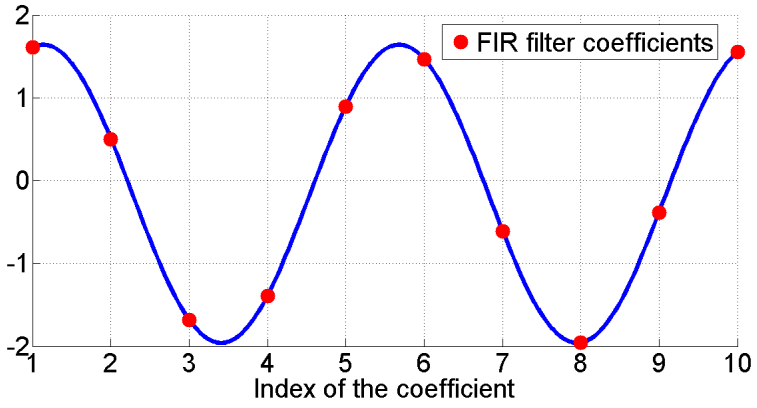

(a) Impulse response of the digital, selective FIR filter

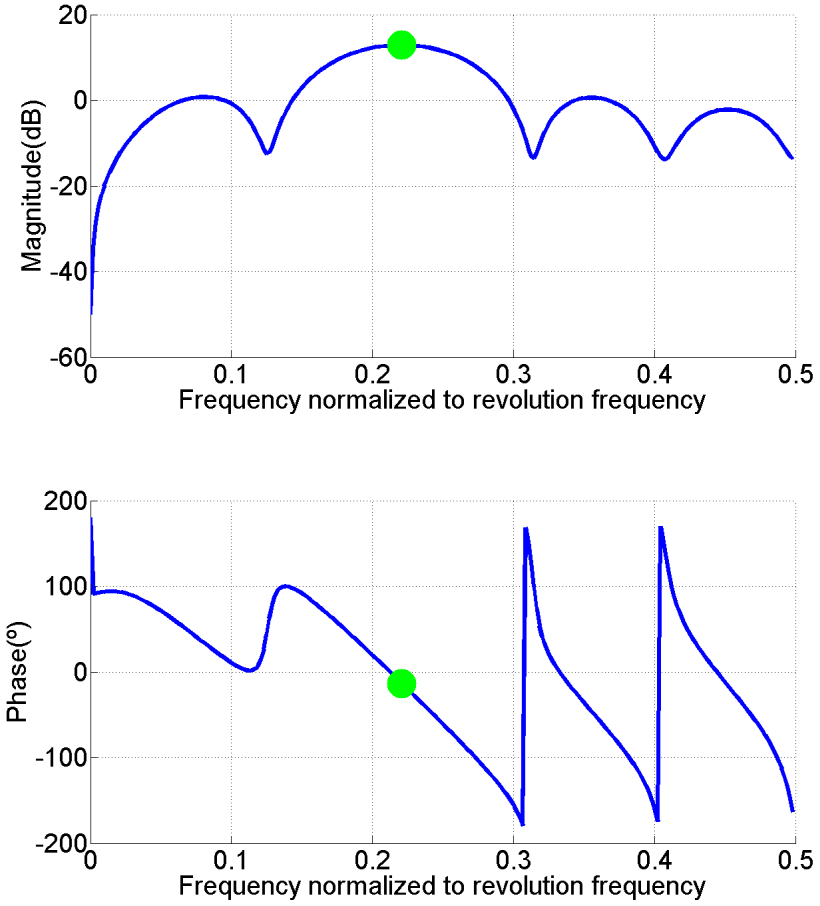

(b) Amplitude and phase responses of the digital, selective FIR filter

Figure 3.9.: Impulse and frequency responses of the digital FIR filter with parameters corresponding to the horizontal axis in Table A.2

4. Algorithm for automatic FIR filter tuning in the transverse BBB feedback

Purpose and action of the transverse BBB control system were introduced in chapter 3. In short terms, the main goal of this system is to provide a feedback signal which has such phase and amplitude characteristics that, when applied to the beam, the betatron oscillations are damped. So as to achieve this, a digital FIR filter located in the feedback loop (as depicted at Figure 3.3) applies the suitable phase and amplitude corrections to the signal picked up with the Beam Position Monitor in the transverse plane.
In the ANKA storage ring, the adjustment of this FIR filter's parameters is currently performed manually. This requires the constant presence of a responsible person with a deep expertise not only in accelerator physics, but specifically in this particular synchrotron. A predetermined filter configuration is available (see Table A.2); it has been determined based pm the performance observed during operation, but still this has severe limitations:

- System behaviour and thus the effectiveness of the control system depend strongly on the configuration of quadrupole magnets, beam energy, beam current, etc. ([Ste08], p.320). The preset parameters have not been optimized for the conditions of one particular operation, so they might not provide the required performance of the control system.
- The preset parameters are such that the action of the FIR filter can be valid for as broad a range of operation energies as possible. As it will be explained in this section, this implies using a broadband filter, which makes the control system vulnerable to noise and does not provide the optimal damping of CBI. As a consequence, instabilities can still provoke beamloss during energy ramping.
- The responsible person may need to reconfigure the filter manually when some system parameter is changed, for instance, when accelerator optics are readjusted. It cannot be ensured that the new configuration of the filter enhances control performance, the contrary could occur.

In the present chapter, it will be seen that these limitations apply specially during energy ramping, for the change of betatron tune with energy requires a readjustment of FIR filter parameters with every new level of energy. The consequences of having a mismatched FIR filter will also be shown.
So as to overcome the aforementioned limitations and thus enhance the performance of the transverse BBB control system during energy ramping, an algorithm for the automatic adjustment of FIR filter parameters in this plane is presented. The algorithm tracks the betatron tune as it changes with energy and readjusts the filter accordingly.
In addition to enhancing the performance of the transverse BBB control system, automatic FIR filter tuning opens the door to custom optics settings, e.g. for the generation of THz radiation in the so-called low-alpha mode.

The contribution of the present work to the transverse BBB feedback control in ANKA consists of the algorithm for automatic FIR filter tuning, as well as the methods for detecting the involved frequency components (betatron tune and synchrotron sidebands).
In order to assess the functionality of the automatic FIR filter tuning algorithm, several tests have been performed during energy ramping. The results when the algorithm is applied are compared to those obtained when it is disabled, so as to evaluate the enhancement in the BBB control performance.

4.1. System behaviour during energy ramping in terms of fractional tune

The BBB control system is adjusted for the control action to take place centered at the CBI eigenfrequency, that is, either the betatron or synchrotron tunes. During energy ramping, longitudinal and transverse dynamics (the betatron and synchrotron tunes in particular) vary with energy due to the change in quadrupole field's strengths.
In this section, the procedure to calculate the betatron and synchrotron fractional tunes is presented and applied to detect the variation of these frequencies during energy ramping in ANKA. Since one BPM is implemented for the BBB control system, all comments regarding the aforementioned eigenfrequencies are referred to fractional tunes.

Detection of betatron and synchrotron fractional tunes using the magnitude of BRAM spectrum

First step for adjusting the BBB control system to be centered at the corresponding fractional tune is detecting its frequency. CBI of both transverse and longitudinal planes can be visualized as a well pronounced peak at the respective frequency in the magnitude of the spectrum obtained from the BRAM acquisition module. This spectrum is the average of all FFTs performed from the raw data acquired for every bunch individually, i.e. the temporal changes of a single bunch's position.
With a proper operation of the BBB control system (when oscillations are damped), this peak converts into a dip in the spectrum of the corresponding axis (see Figures 3.8a,3.8b,3.8c). The depth of the notch, that is, the distance from the magnitude at the dip to the noise floor, is related to the damping strength of the BBB control system, as explained in section 3.4.2 ([Sch15], Kapitel 7 and Kapitel 8).
The method used in this work to detect the betatron and synchrotron fractional tunes consists of locating the corresponding dip in the BRAM spectrum magnitude.
The dip appears usually around the nominal value to which these tunes have been configured; in the case of the measurements performed in this work, these values are 600 kHz for the horizontal axis; 800 kHz for the vertical axis; and 36 kHz for the longitudinal axis. Taking profit of this information, the method to determine CBI fractional tunes is the following:

- The spectrum magnitude is cropped around aforementioned reference frequencies. Initially, a span of 50 kHz at each side of the reference frequency was considered. After the firsts tests, measurements showed that the largest deviation of measured tune with respect to the reference value occurs in vertical axis and it is lower than 15 kHz, as it will be explained with Figures 4.1a,4.1b and 4.1c. Considering a safety margin, the final value of frequency range considered for cropping around the reference frequency is 20 kHz.

- The most pronounced dip in the magnitude of the cropped spectrum is detected, which corresponds to the fractional tune.

In the present chapter, the transverse spectrum is used to determine the betatron fractional tunes. In chapter 5, the londitudinal spectrum is used to determine the synchrotron fractional tune. The variation of both with energy during ramping is evaluated next.

Variation of betatron and synchrotron fractional tunes with energy during ramping

Using the aforementioned method, betatron and synchrotron fractional tunes were recorded during the energy ramp in ANKA. The evolution of these frequencies as a function of energy is represented in Figure 4.1a, Figure 4.1b and Figure 4.1c for horizontal, vertical and longitudinal axes respectively. Their average value and margin of error are indicated in the legend.

These figures characterize the behaviour of the system during energy ramping. On the one hand, it can be seen that the betatron fractional tune varies significantly with energy: a deviation of about $\pm 8\,\mathrm{kHz}$ is observed in the horizontal axis and $\pm 12\,\mathrm{kHz}$ in the vertical axis. This can well exceed the bandwidth of the digital FIR filter in the BBB control loop, which is aimed to focus the control action at the tune frequency. Therefore, the transverse control system will be detuned during energy ramping and the control performance will be deteriorated, even provoking beamloss.
Later in this chapter, a strategy to enhance the performance of the transverse BBB control system during energy ramping is proposed, which consists of an algorithm for the automatic FIR filter tuning.

On the other hand, Figure 4.1c shows the synchrotron fractional tune in respect of energy during the ramp. The observed quantization steps are due to the limited acquisition rate of the ADC which digitalizes the BPM readout. It can be seen that the synchrotron fractional tune varies an amount of $\pm 2\,\mathrm{kHz}$ around its average value, a margin which is safely comprised within the FIR filter bandwidth in the longitudinal BBB control. Therefore, no enhancement strategy is required in this axis.

The next section explains in detail what are the consequences of a detuned BBB control system in the transverse plane due to the variation in the betatron tune, thus defining the need for an automatic tuning solution.

4.2. Effects of transverse BBB control detuning due to betatron tune shift during energy ramping

The shift in the fractional tune during energy ramping is critical for the transverse plane. Transverse BBB control is adjusted so that control action takes place centered at the betatron tune; when its value varies, the feedback action provides a phase advance which is no longer the nominal one. This leads to a deterioration of control performance and even the excitation (instead of damping) of instabilities, which can cause beamloss. In this section, the effects of feedback detuning due to the shift in the betatron tune with energy are explained, comprising the excitation of instabilities, the asymmetry of spectrum magnitude at the betatron tune and the decay in beam current.

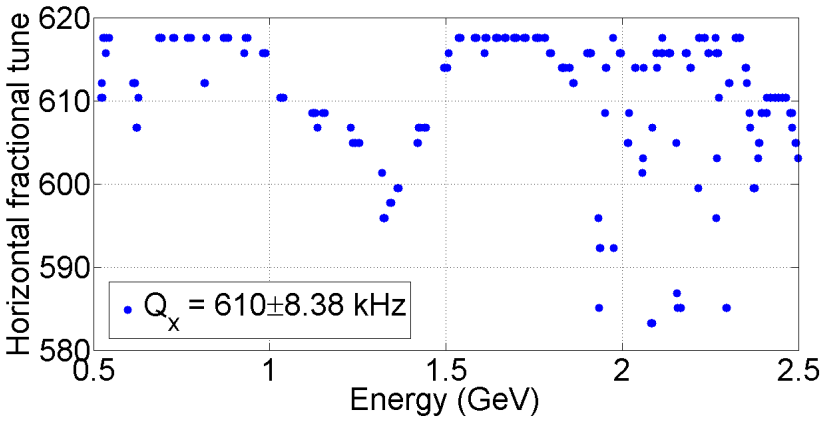

(a) Evolution of horizontal fractional tune with energy during ramping. One ramping without automatic FIR filter tuning and two with automatic tuning are superimposed, showing no difference in the evolution of this frequency because automatic tuning does not change it

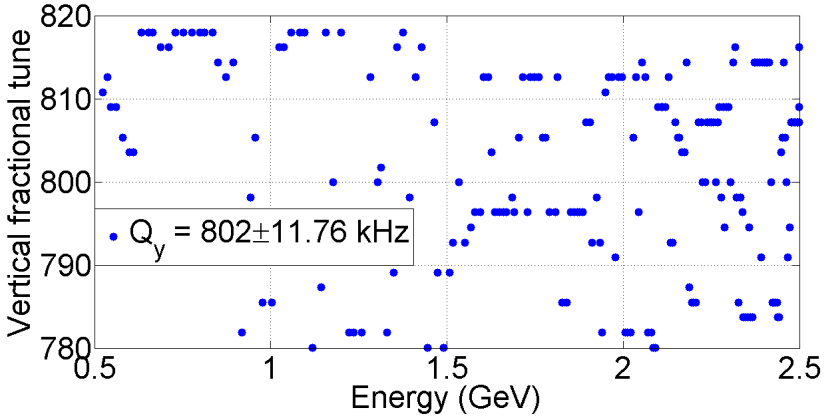

(b) Evolution of vertical fractional tune with energy during ramping. One ramping without automatic FIR filter tuning and two with automatic tuning are superimposed, showing no difference in the evolution of this frequency because automatic tuning does not change it

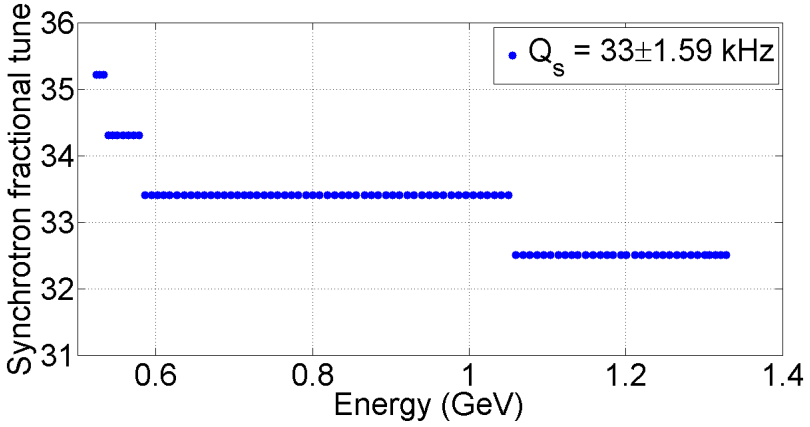

(c) Evolution of synchroton fractional tune with energy during ramping. No automatic tuning is applied in this axis: it is not necessary because of the little variability of its fractional tune with energy (almost ten times smaller than in the transverse plane). Quantization steps are observed due to the limited acquisition rate to digitilize BPM readout

Figure 4.1.: Evolution of fractional tunes with energy during ramping

4.2.1. Excitation of betatron CBI

The detuning of the transverse BBB control system is mainly due to the digital FIR filter implemented in the feedback loop. The central frequency of this filter should match the fractional tune, so that phase and amplitude corrections have the required effect at this frequency and thus damp the oscillations associated to CBI.
When the tune is shifted from its nominal value during energy ramping and the filter configuration is maintained, the phase and amplitude which are applied as a control action are different from the nominal ones.

Figure 3.9b shows the transfer function corresponding to the filter in the BBB control loop. On the one hand, the amplitude introduced by the filter is maximum at its central frequency. This means that the strongest damping of CBI will be applied when the betatron tune matches the filter's central frequency.
When the betatron fractional tune deviates from this central frequency, the control action has a lower amplitude. This situation provides a worse attenuation of CBI, but it does not provoke feedback instability. Such instability occurs for high feedback gains, and since the amplitude gained in the case of mismatched frequencies is lower than the nominal one, this risk does not come into play.

A different scenario is that of the phase advance of the filter. Depending on the phase added by the FIR filter to the pickup signal in order to obtain the control action, when the last is applied to the beam at the kicker, the resulting signal may be smaller or greater than without BBB control. The first is the desired scenario, for CBI would be attenuated; but if the second occurs, CBI would be excited and this could lead to beamloss.

Figure 4.2 will be used to explain the effect of having a phase advance of the filter different from the nominal one: *s(t)* is the oscillation of betatron tune frequency obtained from the BPM. This signal is acquired and processed by the BBB control system, resulting in a feedback signal sent to the kicker, *s'(t)*, which is shifted in phase and amplitude in respect of *s(t)* regarding the control action to be applied. So as to simplify the explanation, in this figure no amplitude modification takes place and the phase added by the control system is exclusively provided by the digital FIR filter.
In order to evaluate the effect of this phase advance, the amplitude of the superposition of *s(t)* and feedback signal *s'(t)* is considered. Worst case is found at the "peak" of this resulting signal, that is, the instant when *s(t)* would have a peak if no feedback was applied. The amplitude of the superposition signal at this instant will be compared to the peak amplitude of *s(t)* to quantify the damping achieved with the feedback.
Filter's central frequency is set to the nominal betatron tune and phase at this frequency is such, that when *s(t)* has this frequency, there is a phase shift of 180° between the detector and the kicker, thus achieving the required negative, resistive feedback.

If the frequency of *s(t)* matches the nominal tune (situation in green in the figure), when superimposed to the feedback action *s'(t)*, the filter introduces no phase shift in respect of the nominal phase advance, that is, feedback signal and pickup signal have a phase difference of 180°. As a consequence, they cancel when superimposed and thus the oscillation is ideally damped.
However, if the tune is shifted from the nominal value, the phase difference between

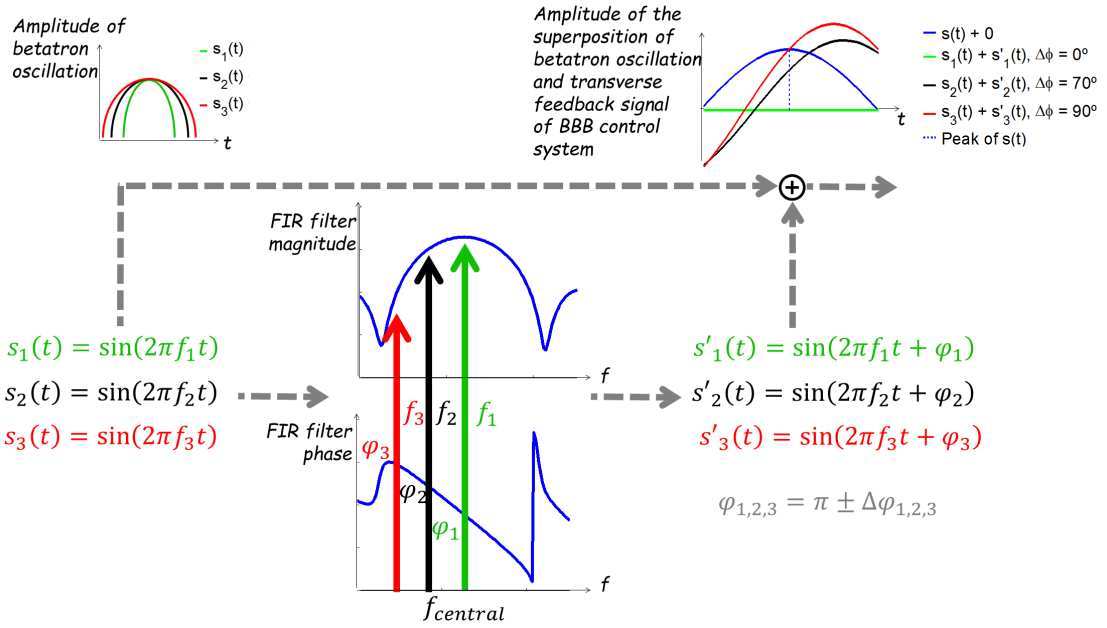

Figure 4.2.: Scheme to evaluate the excitation of CBI due to the shift in betatron tune during energy ramping. Amplitude of the superposition of feedback signal and betatron oscillation ($s'(t) + s(t)$) is compared to the amplitude of betatron oscillation (if there were no feedback, $0 + s(t)$), at the time instant when the last would have a peak. Phase shift introduced by the FIR filter for several values of betatron fractional tune is considered, showing that for frequencies such that the phase shift is larger than 90°, betatron oscillation is excited instead of being damped - the superposition $s'(t) + s(t)$ has a larger amplitude at the aforemetioned instant than the signal without feedback

feedback and pickup signals is no longer 180°, and thus the superposition of the both has an amplitude greater than zero. The larger the change in tune, the greater the phase shift in respect of the required 180°, and thus the higher can be the amplitude of signal superposition. As a consequence, damping of the betatron oscillation is deteriorated.
When the frequency of *s(t)* is such that the feedback phase is $180° \pm 90°$ or, in other words, the phase shift in respect of the nominal situation is ±90° (case in red in the figure), the amplitude of superimposed signals is the same of *s(t)*, i.e. the feedback has no effect.
This is a critical point: if the phase shift (difference of phase advance with respect to the nominal one, 180°) is larger than ±90°, the resulting amplitude of superimposing pickup and feedback signals is greater than without feedback, which means the beatron oscillation is excited instead of being damped.

The relation between the phase shift in respect of the nominal 180° and the corresponding "peak" amplitude of superposition signal (that is, the amplitude of *s(t) + s'(t)* in the instant when *s(t)* would have a maximum if there were no feedback) is represented in Figure 4.3. As explained before, phase shifts beyond ±90° lead to a resulting amplitude of the superposition signal which is greater than without feedback. Thefore, betatron oscillation is excited instead of being damped.

In order to provide the optimal damping of betatron oscillations, the central frequency of the FIR digital filter must track the betatron tune in every value it can have during energy ramping. This is the main goal of the solution proposed later in this chapter to enhance the performance of the transverse BBB control.

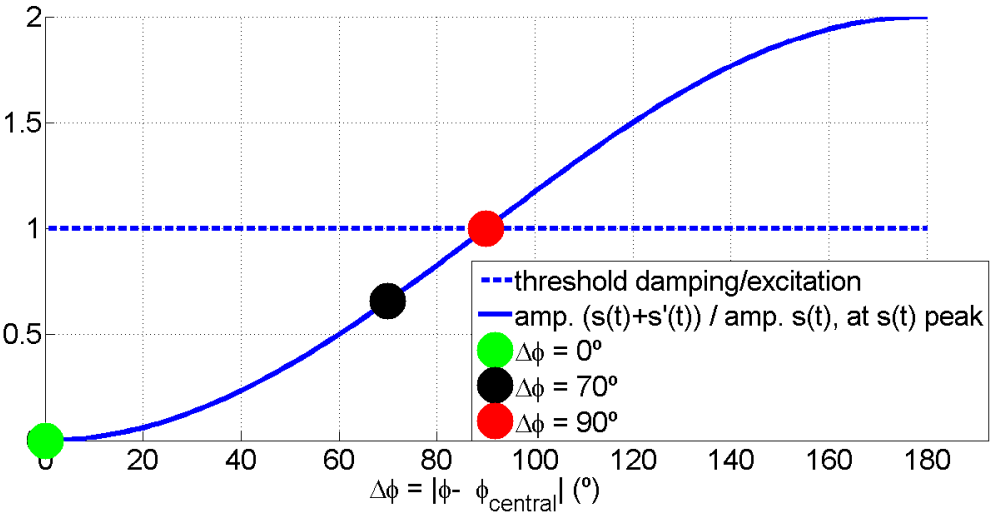

Figure 4.3.: "Peak" amplitude of superposition signal $s(t) + s'(t)$ (amplitude in the time instant when it would have a peak if there were no feedback, $s(t) + 0$) divided by the peak amplitude of $s(t)$, as a function of the phase advance introduced by the FIR filter at the frequency of $s(t)$ in respect of the phase at the filter's central frequency (phase shift in respect of 180°). Three phase values are highlighted: 0° corresponds to the filter properly tuned to the betatron oscillation, which is ideally damped; damping is worse (resulting "peak" amplitude is higher) as the phase shift increases; a phase shift beyond 90° leads to the excitation instead of damping of CBI

4.2.2. Excitation of synchrotron sidebands in the transverse spectrum

As it has been seen in section 4.2.1, the phase advance introduced by the FIR filter in the transverse BBB feedback loop can provoke that CBI comprised within its bandwidth are excited instead of being damped. This is the case of the betatron oscillation when its frequency changes with energy during ramping; and it also applies to the synchrotron sidebands introduced in section 3.4.1.
A pair of sidebands are observed around the betatron fractional tune located at a distance corresponding to the synchrotron fractional tune (see Figures 3.8a, 3.8b). They are due to the sensitivity of the mixer to the fluctuations in the phase of the BPM readout.
Since they are associated to synchrotron oscillations (which can become unstable) and reflect a coupling between longitudinal and transverse planes, they should be damped by the transverse BBB feedback.
Analogously to the explanation provided for Figure 4.5, these sidebands could be excited instead of being damped depending on the phase advance introduced by the digital FIR filter.

In this section, the method used to detect the synchrotron sidebands in the transverse spectrum is explained. After that, the conditions under which they are damped or excited will be evaluated based on the FIR filter's configuration.

An important remark on the excitation of synchrotron sidebands is the following: these sidebands are observed regardless if the transverse BBB control system is detuned or if the filter central frequency is properly matched to the fractional betatron tune, and for every level of energy during ramping. The damping or excitation of these sidebands depends on

the phase advance introduced by the FIR filter at their frequency.

Detection of synchrotron sidebands in the transverse spectrum

As presented in section 3.4.1, there are a left and a right sidebands around betatron fractional tune, located at a distance corresponding to the synchrotron fractional tune. With the proper configuration of the FIR filter in the BBB transverse control system, these sidebands are attenuated analogously to the betatron fractional tune, so they can be detected as two small dips in the transverse spectrum magnitude around a bigger dip corresponding to the tune. The magnitude of these three dips is an indication of the feedback strength, that is, how well the CBI are damped.
In order to detect the dips corresponding to synchrotron sidebands, the method sketched in Figure 4.4 is applied. The magnitude of the spectrum obtained from the BRAM acquisition module in the vertical axis is used as an example. This spectrum is the average of all spectra corresponding to the temporal changes of a single bunch's positions.
This method has been implemented with Matlab and the associated code is provided in Appendix C).
The procedure consists of the following steps:

- First, the magnitude of the transverse spectrum is cropped around the betatron fractional tune. Sidebands are expected at a distance corresponding to the synchrotron fractional tune, which is in the order of 36kHz during energy ramping. As a safety margin, twice this value is considered at each side of the betatron fractional tune in order to detect the corresponding sideband.
- Second, peaks and dips are detected in the cropped spectrum. Sidebands will be located in one of these dips, but the distance in respect of the peaks is required to determine which of the dips corresponds to the synchrotron sideband.
- Third, the envelope of the peaks is calculated. The betatron fractional tune is included in the envelope; otherwise, the algorithm would always yield the result that this frequency corresponds to the sideband, because the tune would be located at the greatest distance from the envelope.
- Finally, those dips at the greatest distance from the envelope (excluding the tune) are detected as the synchrotron sidebands.

Once the synchrotron sidebands are detected, their magnitude is used to evaluate in which amount they are damped by the transverse BBB feedback or, in the worst case, to detect when they are excited. This last situation can occur for certain values of the phase advance introduced by the digital FIR filter at the frequency of the synchrotron sidebands, as it will be seen next.

Excitation of synchrotron sidebands depending on the FIR filter configuration

Synchrotron sidebands are comprised within the bandwidth of the digital FIR filter in the transverse BBB feedback. As a consequence, they are sensitive to the phase advance introduced by the filter, which can lead to their excitation instead of damping, and this detriments the performance of the BBB control system.

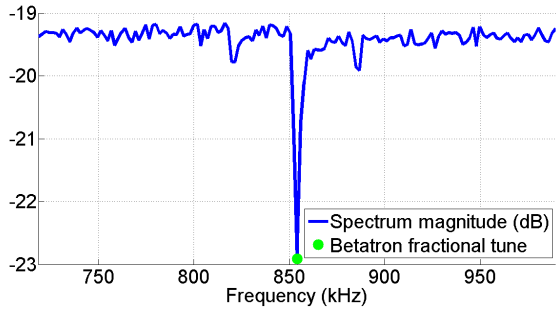

(a) Step 1: crop spectrum magnitude around fractional tune

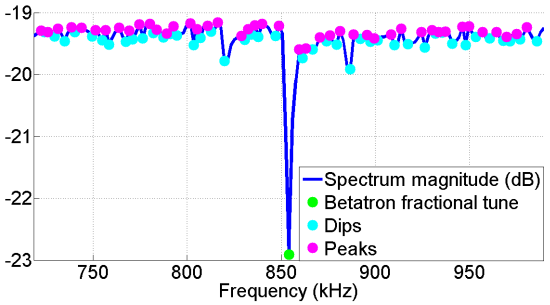

(b) Step 2: detect dips and peaks in the cropped spectrum

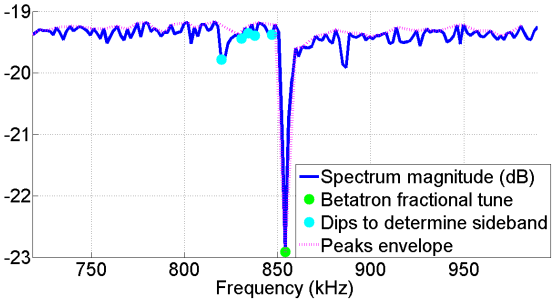

(c) Step 3: consider dips within nominal sideband bandwidth; compute peaks envelope

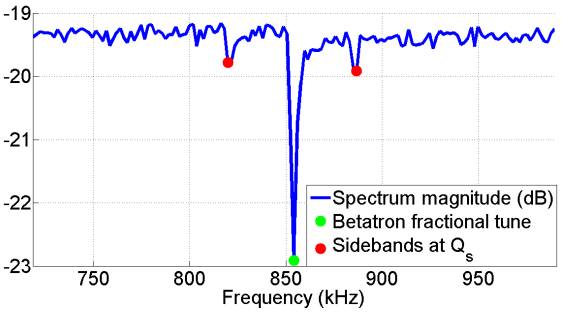

(d) Step 4: determine sideband as the dip furthest from peak envelope

Figure 4.4.: Method to detect the synchrotron sidebands in the transverse BRAM spectrum magnitude

The effect of the phase advance of the filter on the damping or excitation of a certain frequency component has already been introduced in section 4.2.1. This explanation can be readapted to the case of synchrotron sidebands, as depicted at Figure 4.5.
In this case, *s(t)* is the left synchrotron sideband (the explanation is analogous for the right sideband). Its phase will be shifted by the amount defined by the phase response of the filter at its frequency. *s'(t)* represents the signal with this phase advance introduced by the filter.
Since the phase response of the filter is linear (see Figure 3.9b) and neglecting all components outside of the filter's bandwidth, the maximum phase advance takes place at the filter's bandwidth. So as to consider the worst case scenario, it is assumed that the frequency of the sideband $s(t)$ corresponds to the filter's bandwidth.
In order to simplify the explanation, it is also assumed that the central frequency of the filter is matched to the betatron fractional tune and that the phase advance at the central frequency is exactly 180° so as to provide negative and purely resistive feeback.
As indicated in Figure 4.5, the phase advance at the sideband's frequency can be expressed as a phase shift in respect of the 180° phase at the central frequency. Under the aforementioned assumptions, the phase shift will always be greater than 0° (the filter has a bandwidth greater than 0Hz) or, in other words, the sideband $s(t)$ cannot be completely cancelled with the filtered signal $s'(t)$.
The strength of the feedback action (the damping effect on synchrotron sidebands) can be evaluated in terms of the "peak" amplitude of the superposition of the signal pickup and the feedback signal $(s(t) + s'(t))$, that is, the amplitude of $s(t) + s'(t)$ in the instant when $s(t)$ would have a peak if there were no feedback. The relation between the phase shift in respect of the central phase of the filter and the corresponding "peak" amplitude of superposition signal is represented in Figure 4.3.

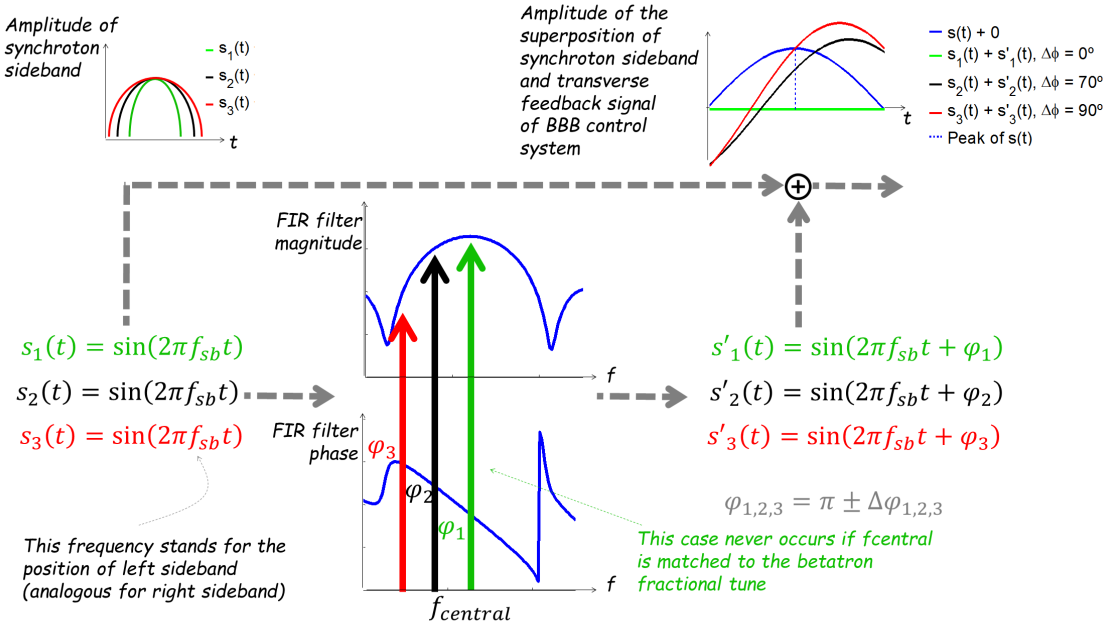

Figure 4.5.: Scheme to evaluate the excitation of synchrotron sidebands regarding the phase advance introduced by the FIR filter. Amplitude of the superposition of feedback signal at the synchrotron sideband frequency and the sideband itself ($s'(t) + s(t)$) is compared to the amplitude of the synchrotron sideband (if there were no feedback, $0 + s(t)$), at the time instant when the last would have a peak. Several phase advance values introduced by the FIR filter are considered, showing that for phase shifts larger than 90°, synchrotron sidebands are excited instead of being damped: the superposition has a larger amplitude at the aforemetioned instant than the signal without feedback)

It can be seen that phase shifts beyond ±90° lead to a resulting amplitude of the superposition signal which is greater than withouth feedback, that is, the synchrotron sideband is excited instead of being damped.
Therefore, it is required a phase shift lower than 90° at the FIR filter's bandwidth in respect of the phase at its central frequency in order to avoid the excitation of synchrotron sidebands.

In section 4.3.1, it will be seen that the aforementioned phase shift depends upon the number of coefficients or number of taps of the filter. Therefore, this parameter will be dimensioned to achieve a phase shift at the filter's bandwidth lower than 90° in order to avoid the excitation of synchrotron sidebands.

4.2.3. Asymmetry of the dip at the betatron fractional tune in the transverse spectrum magnitude

When the betatron oscillations are damped, they can be detected as a dip located at the betatron fractional tune in the magnitude of the spectrum in the transverse plane corresponding to the temporal changes of a single bunch's positions. The depth of the notch, that is, the distance from magnitude at the dip to the noise floor, is related to the damping strength of the BBB control system, as explained in section 3.4.2 ([Sch15], Kapitel 7 and Kapitel 8). In addition to damping the betatron oscillations, the BBB control system also attenuates those signals comprised within the bandwidth of the digital FIR filter in the feedback loop.
It has been seen that the magnitude of the transfer function of this filter is symmetric around its central frequency (see section 3.5). Therefore, the same attenuation factor is

expected for signals located at the same distance from the central frequency, regardless if they are below or above it, as long as they are comprised within the filter bandwidth.
As a consequence of this symmetric attenuation, if the filter's central frequency is matched to the betatron tune, signals located around of it (within the filter bandwidth) will be damped in the same amount. Therefore, a symmetric dip is expected in the spectrum magnitude when the BBB control is correctly tuned to the betatron fractional tune. In other words, when the betatron tune is shifted during energy ramping, the dip in the spectrum will become asymmetric; the greater the shift in the tune, the more severe the asymmetry.

The assymetry of the dip reveals a detuning of the BBB control system, which has the effects presented in the former section (it can lead to excitation of CBI instead of damping). This asymmetry can be used to measure the detuning of the control system during energy ramping, and thus it enables rating the effectiveness of the automatic FIR filter tuning algorithm proposed in this work.
Asymmetry of the dip at betatron tune can be quantified in terms of its mean value at every level of energy during ramping. The method used for its calculation for a given energy value is depicted at Figure 4.6 (the associated Matlab code is provided in Appendix C); it consists of the following steps:

- First, the magnitude of the spectrum of the horizontal or vertical axes is cropped in the frequency range in which the asymmetry will be calculated. This range comprises frequencies between left and right synchrotron sidebands.
  As it has been seen in section 4.2.2, these sidebands are located above and below the betatron fractional tune at a distance corresponding to the synchrotron fractional tune. Since the last has a change with energy almost ten times smaller than the variation in the betatron tune (see 4.1c), the position of the synchrotron sidebands is considered as a constant distance, which enables comparing the asymmetry obtained for the different energy levels and among several rampings.
- Next, the cropped signal is split in halves around the betatron fractional tune. The difference between these halves is obtained by subtracting the magnitude of samples opposite in each side of the fractional betatron tune (the tune itself is not considered). With this, a vector of half the length of the original, cropped spectrum magnitude is obtained.
- Finally, the average of this vector is computed, providing one single value to quantify the notch asymmetry at a given energy level.

This process is repeated for the several stages during energy ramping, thus providing a set of values which quantify the detuning of the BBB transverse feedback system during the ramp.

4.2.4. Partial beamloss during energy ramping

The rise of CBI can provoke partial or total beamloss. In order to avoid these effects, a BBB control system properly matched to the betatron tune is required, for this provides the appropriate damping of CBI.
Before reaching the point of total beamloss, the evaluation of the partial beamloss is an indirect measurement of the transverse BBB control mismatch - the lower the loss, the better the tuning of the feedback system.
Beamloss is evaluated in terms of the beam current, which is measured using a DC current transformer (DCCT, [CVCMb]) and it can be obtained by reading the corresponding signal

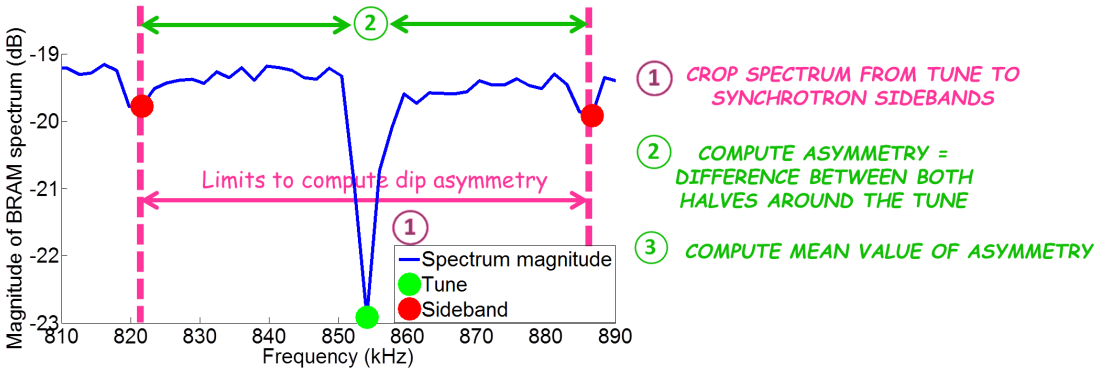

Figure 4.6.: Method to quantify the asymmetry of the dip in the transverse spectrum magnitude in terms of its average value

or PV on the EPICS interface. Partial beamloss is computed as defined in expression 4.1, with *I(t)* the beam current, t_{start} and t_{end} the initial and final points of the ramp respectively.

$$Loss = \frac{I(t_{start}) - I(t_{end})}{I(t_{start})} \tag{4.1}$$

4.3. Algorithm for the automatic FIR filter tuning in the transverse BBB control system

The action of transverse BBB control system is aimed to take place centered at the betatron fractional tune, in order to damp the oscillations of the beam in the transverse plane. Due to the variation of betatron tune with energy, the transverse BBB control becomes detuned during energy ramping, which deteriorates its performance: damping of CBI is reduced and the excitation of instabilities can occur instead, which can even provoke beamloss.
The digital FIR filter which provides this control action must fulfill the requirements introduced in section 3.5. Among them, the filter should have a narrow frequency response in order to reject detector noise and focus the control action at the frequency of the oscillation to be damped ([FCM+], p.14).
A narrow frequency response has the limitation that the central frequency of the filter must be accurately adjusted to the betatron tune, which varies during energy ramping. So as to overcome this limitation, the present configuration of the filter in transverse BBB feedback in ANKA (see Table A.2) provides a broadband, flat transfer function, especially for the vertical case, as it can be seen in Figure 4.7. This enables applying the feedback action over a wider range of frequencies, at the expense of reducing the efectiveness of CBI damping. And yet even with a broadband filter, feedback must be switched off some times during energy ramping to avoid beamloss.

In order to avoid feedback detuning and, at the same time, be able to operate with a narrowband filter, this work proposes an algorithm for the automatic tuning of the FIR filter in the transverse BBB control loop, which a) tracks the betatron tune during energy ramping and readjusts the central frequency of the filter accordingly; and b) configures the filter gain and number of coefficients to optimize its frequency response regarding the requirements presented in section 3.5.

In addition to enhancing the performance of the transverse BBB control during energy ramping, automatic FIR filter tuning opens the door to custom optics settings, e.g. for the generation of THz radiation in the so-called low-alpha mode.
In this section, the algorithm for the automatic FIR filter tuning is presented, explaining which parameters are configured, which criteria is used for their adjustment and the steps that compose the algorithm.

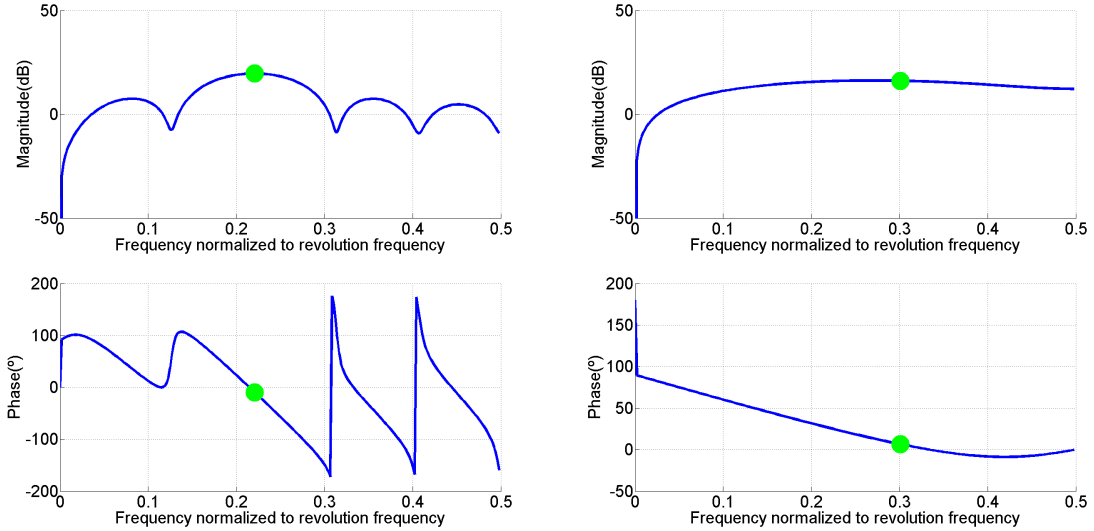

(a) Frequency response of the horizontal FIR filter

(b) Frequency response of the vertical FIR filter

Figure 4.7.: Frequency response of the FIR filter calculated as the FFT of equation 3.10 for coefficients in Table A.2. The central frequency is marked as a green spot

4.3.1. Configurable parameters and criteria to dimension the digital FIR filter

The filter in the transverse BBB feedback is a digital, bandpass, selective FIR filter whose impulse response (filter coefficients) is a sampled sinusoid with frequency equal to its central frequency - in the nominal case, the betatron fractional tune. Its main characteristics were already presented in section 3.5; in the present section, its features are particularized for the filter in ANKA.
The coefficients of this filter are computed regarding expression 3.10 ([Sch15], pp.57-58). Parameters available for its configuration are the following:

- Central frequency normalized to revolution frequency: $Q_{frac} \in [0, 1]$. It is set to match the betatron fractional tune (normalized to ω_o), so that the control action takes place centered at this frequency.
- Central phase: $\phi \in [-180°, 180°]$. It is is determined once (callibrated during machine setup) and it is not affected by the energy variation. Its nominal value is 180° (so as to provide negative and purely resistive feedback), but its actual dimension may be different so as to compensate for delays introduced by the electronics. This parameter is not adjusted with the algorithm presented in this work, but manually tuned.
- Shift gain ($g \in [0, 7]$, coarse magnitude tuning) and central gain ($G \in [0, 1]$, fine magnitude tuning) should be big, so as to provide the required feedback gain to damp CBI; however, the BBB feedback system using a FIR filter as a controller is conditionally stable, which means it is stable only over a finite range of loop gains. If the shift and central gains are too big, feedback instability is provoked, which can

lead to beamloss. Therefore, feedback damping will be limited to the maximum gain and shift gain that do not provoke feedback instability ([HEF+93], p.2).
These gains are set at the beginning of the energy ramp to the maximum value which does not provoke beamloss.

- Number of taps ($N_{taps} \in [1, 32]$, the number of coefficients of the filter). It is related to the filter bandwidth (the -3dB bandwidth is considered in this work): the higher the number of taps, the narrower the bandwidth achieved, and the reverse - $N_{taps} = 1$ provides a flat frequency response. In addition, N_{taps} also defines the slope of the phase response of the filter and, as a consequence, the phase shift between the bandwidth and the central frequency.

As explained in section 4.2.2, the number of taps should provide a phase shift between the bandwidth and the central frequency lower than 90° in order to avoid exciting the synchrotron sidebands that appear in the transverse spectrum. This phase limit corresponds to the ideal case when the phase advance in the feedback loop is provided exclusively by the FIR filter.
However, additional delays might be introduced by the electronics, for instance due to parasitic losses of the coaxial cables. Coaxial cables in the order of 30m connect the detector and the processor, which regarding [AL97], p.11 will introduce a delay lower than a hundred of nanoseconds. In turn, this time lapse can be expressed in terms of a phase delay by multiplying it times the frequency of operation.
In section 4.1, it was explained that betatron fractional tunes observed during energy ramping are in the order of 600kHz for the horizontal axis and 800kHz for the vertical axis; and the synchrotron fractional tune is in the order of 36kHz. Taking this into account, synchrotron sidebands will appear approximately at frequencies (600.0 ± 3.6) kHz in the horizontal axis and (800.0 ± 3.6) kHz in the vertical axis.
The greatest delay in terms of phase due to the electronics will occur with the highest of the aforementioned frequencies, that is, 836kHz. If the effect due to coaxial cables is considered the dominant contribution to the delays, the phase delay associated to electronics can be calculated as $2 \cdot \pi \cdot 836\,\text{kHz} 70\,\text{ns} \cdot 180/\pi \approx 20°$.
This rough estimate of the additional delay introduced by the electronics is considered as a safety margin to define the maximum phase shift allowed between the bandwidth and the central frequency: 70° maximum phase shift instead of the nominal 90° is considered.

Figure 4.8 shows the effect of the number of taps of the filter on the phase shift between the bandwidth and the phase at the central frequency. These values have been obtained from the phase response of the filter defined by parameters in Table A.2 and with coefficients calculated applying the equation 3.10, when a sweep in the number of taps is performed. Horizontal and vertical cases are superimposed.
The red, dashed line in this figure stands for the nominal, maximum phase shift allowed between the bandwidth and the central frequency; and the green, dashed line corresponds to the actual limit considered, i.e. 70°. The biggest circles indicate which numbers of taps provide a phase shift below the maximum of 70° allowed.
It can be seen that there is more than one possible configuration for the number of taps which complies with the maximum phase shift allowed. In order to determine which of these will be used to configure the filter, the obtained bandwidth is used: as explained in section 3.5, a narrow bandwidth is required to reject detector noise and focus the control action at the frequency of the oscillation to be damped ([FCM+], p.14).

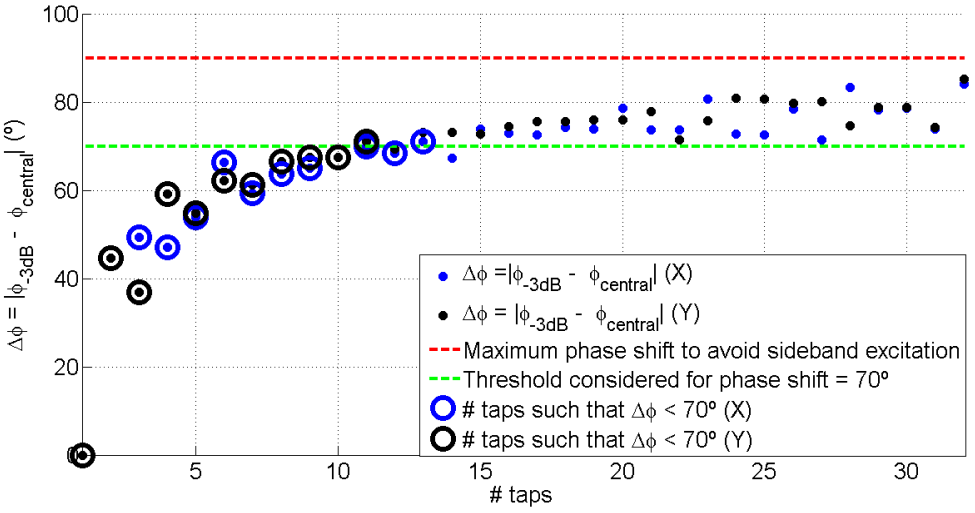

Figure 4.8.: Phase shift introduced by the FIR filter (phase advance at its bandwidth in respect of the phase at its central frequency) as a function of the number of taps. The theoretical maximum phase shift allowed in order to avoid exciting the synchrotron sidebands is indicated with a red, dashed line; the maximum phase shift allowed considered in the presented algorithm corresponds to the green, dashed line

Figure 4.9 shows the filter bandwidth as a function of the number of taps, using the same filter coefficients for Figure 4.8. Horizontal and vertical cases are superimposed and the biggest circles indicate which numbers of taps provide a phase shift between the bandwidth and the central frequency below the maximum of 70° allowed.
To illustrate that synchrotron sidebands are comprised within the filter bandwidth, as it has been mentioned before, the red, dashed line indicates the usual position of these sidebands during energy ramping, i.e. the distance between the sideband and the fractional betatron tune. This distance, as presented in section 3.2, corresponds to the synchrotron fractional tune, which is in the order of 36 kHz during energy ramping.
Among the candidate number of taps, the value providing the narrowest bandwidth is selected as the optimal configuration.

To summarize, criteria to dimension the filter configurable parameters using the automatic tuning algorithm are the following:

- Central frequency is set to the betatron fractional tune in the corresponding level of energy during ramping.
- Central gain and shift gain are dimensioned at the beginning of the ramping to be as big as possible, without provoking the instability of the feedback loop.
- Number of taps is such, that it provides a maximum phase shift between the central frequency and the bandwidth of $\pm 70°$; and the narrowest possible bandwidth.

In the next section, the algorithm to achieve the optimal dimension of FIR parameters in an automatic way following the aforementioned criteria is presented.

4.3.2. Algorithm for automatic FIR filter tuning

Due to the variation of betatron tune during energy ramping, an algorithm for the automatic tuning of the FIR filter in the BBB transverse control is required in order to readjust the

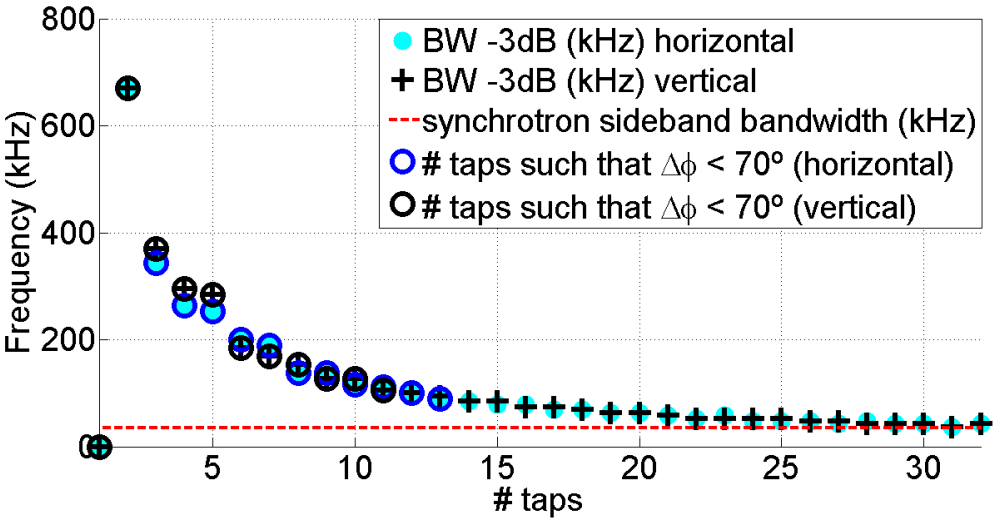

Figure 4.9.: Bandwidth of the FIR filter and as a function of the number of taps. The distance between the synchrotron sidebands and the betatron fractional tune, which corresponds to the synchrotron fractional tune, is indicated with a red, dashed line

feedback accordingly to the change in the tune. By doing so, the control action is locked to the tune and the appropriate performance of the transverse BBB can be guaranteed during energy ramping.
This algorithm is composed of two parts:

- On the one hand, the filter shift gain and central gain are configured before the beginning of the energy ramp. They are set to the maximum value which does not provoke the instability of the feedback loop, since this will provide the maximum strength of the feedback to damp CBI.
  The procedure followed for their dimension is explained next.

- On the other hand, the filter central frequency and number of taps are updated periodically during the energy ramp in order to track the change in the betatron fractional tune with energy. This update is performed at a maximum frequency of 5Hz, which is the highest rate allowed by the BRAM acquisition module (from which the spectra used by the algorithm are obtained), but it might be lower depending on the settings of the BBB control system.
  The procedure use to set these parameters is depicted at Figure 4.10. First, the betatron fractional tune corresponding to a given level of energy is detected by means of the method explained in section 4.1. The central frequency of the filter is set to this value by modifying the corresponding signal or PV of the EPICS interface.
  Second, the number of taps is set to its optimal value for that level of energy by modifying the corresponding signal or PV of the EPICS interface. The procedure followed to determine the optimal number of taps is explained next.

Configuration of shift gain and central gain of the FIR filter before the energy ramp

The shift gain, which provides a coarse tuning of total filter gain at its central frequency, is adjusted first. Starting from its minimum value (0), it is progressively incremented until its maximum value is achieved (7) or until feedback instability is provoked. This instability can be detected in two ways:

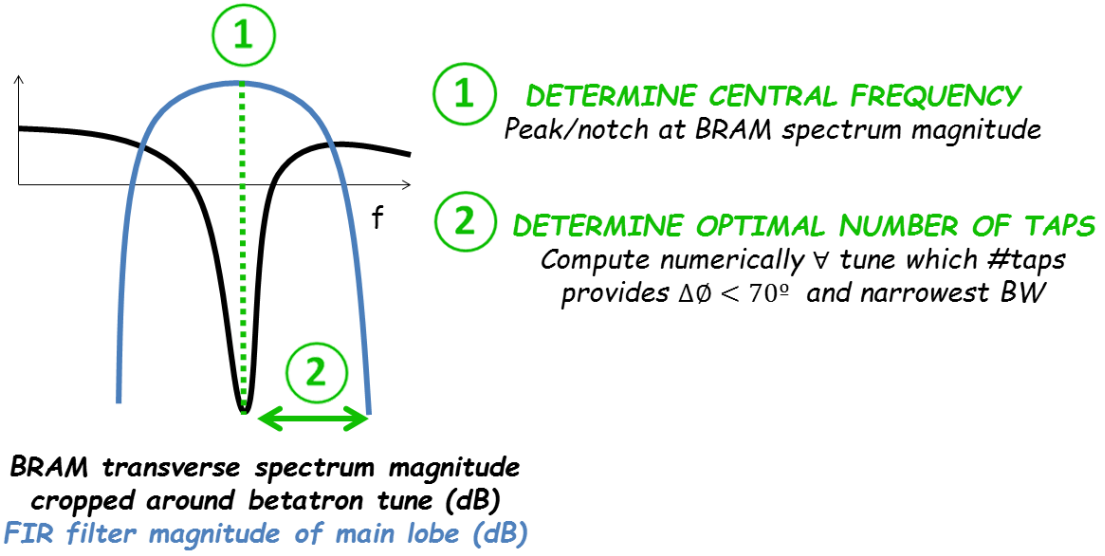

Figure 4.10.: Steps of the algorithm for automatic FIR filter tuning which are executed periodically during energy ramping

- Betatron tune is detected in a peak instead of a dip in the magnitude of the corresponding spectrum. This means that instabilities are excited instead of being attenuated.
- Beamloss is produced, which is detected as a drop in the beam current below a minimum threshold (0.1 mA is considered).

If either of above conditions are matched, shift gain is set to the value immediately lower than that provoking instability. Finally, the signal or PV of the EPICS interface corresponding to the FIR filter's shift gain is set to the obtained value.
With the achieved shift gain value, the central gain is iterated in the same way, starting from the minimum value (0) and increasing until its maximum value is achieved (1) or until feedback instability is provoked, which is detected analogously as for the shift gain. If either of the two conditions are matched, the central gain is set to the value immediately below that provoking instability. Finally, the signal or PV of EPICS interface corresponding to the FIR filter's central gain is set to the obtained value.
At this point, shift gain and central gain are configured to the maximum allowed value which does not provoke feedback instability.

Dimension of the optimal number of taps of the FIR filter for a given level of energy during ramping

Regarding the criteria defined in section 4.3.1, the optimal number of taps for a given level of energy during ramping is such, that the phase shift between the central frequency and the bandwidth of the filter is lower than $\pm 70°$ and it provides the narrowest possible bandwidth.
The phase at the central frequency, shift gain and central gain have a fix value during the energy ramp. Therefore, the optimal number of taps will only vary with the central frequency of the filter, which tracks de evolution of the betatron tune.
As a consequence, the optimal number of taps can be computed for all the expected values

of the fractional betatron tune (its range of variation can be seen in Figure 4.1) and stored as a lookup table: instead of recomputing the optimal number of taps for every value of energy during ramping, the detected betatron fractional tune is matched to the stored optimal number of taps and the signal or PV of EPICS interface corresponding to the FIR filter's number of taps is set to this value.

The computation of the optimal number of taps is performed as follows: the filter coefficients are calculated regarding expression 3.10, for the phase at central frequency defined in Table A.2 and a constant value for shift and central gains (both equal to 1).
The value of these gains does not affect the obtained optimal number of taps: the total gain at the central frequency ($2^g G$ regarding expression 3.10) will introduce a scaling in the amplitude response of the filter, but it will not change the slope of its phase response, which is used to determine the optimal number of taps.
To compute the filter coefficients, a sweep is performed in respect of the number of taps, which leads to a pair of curves as those depicted at Figure 4.8 and Figure 4.9. The criteria to dimension the optimal number of taps is applied: regarding Figure 4.8, a subset is determined with those numbers of taps that provide a phase shift between the bandwidth and the central frequency below 70°. Out of them, that providing the narrowest bandwidth is selected using Figure 4.9.
This procedure is implemented with Matlab as indicated in Appendix C. The obtained optimal number of taps for the betatron fractional tunes in the range of variation observed in Figures 4.1a and 4.1b is depicted at Figure 4.11.

The algorithm for automatic tuning of the FIR filter in the transverse BBB control system has been implemented in C++ (code is provided in Appendix B) and it is to be integrated as an additional feature in the EPICS interface. It has been tested in ANKA and the evaluation of the obtained results is presented next.

4.4. Discussion on results obtained with automatic FIR filter tuning

Several energy rampings were performed in the ANKA storage ring in order to assess the enhancement of performance of the transverse BBB control system with the automatic FIR filter tuning. Performance of the rampings in which this algorithm was disabled will be compared to those rampings in which it was applied.
This section presents the results obtained in terms of issues and methods presented in sections 4.2 and 4.3, namely: the excitation of betatron CBI and synchrotron sidebands, the asymmetry of the dip in the spectrum magnitude at betatron fractional tune and the partial beamloss observed during energy ramping.

4.4.1. Effect of the automatic FIR filter tuning on the damping of betatron CBI and synchrotron sidebands

Measurement of the magnitude at the at betatron fractional tune in the spectrum corresponding to the temporal changes of a single bunch's positions reflects the strength of the transverse BBB feedback when damping the CBI in this plane: the lower this magnitude, that is, the deeper the dip in the spectrum, the better the attenuation ([Sch15], Kapitel 7 and Kapitel 8).
Another effect of CBI are the synchrotron sidebands that appear due to the coupling of the

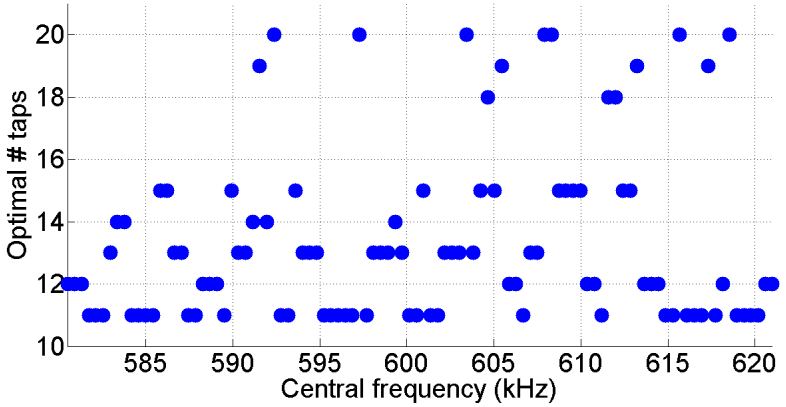

(a) Optimal number of taps for horizontal axis as a function of horizontal fractional tune

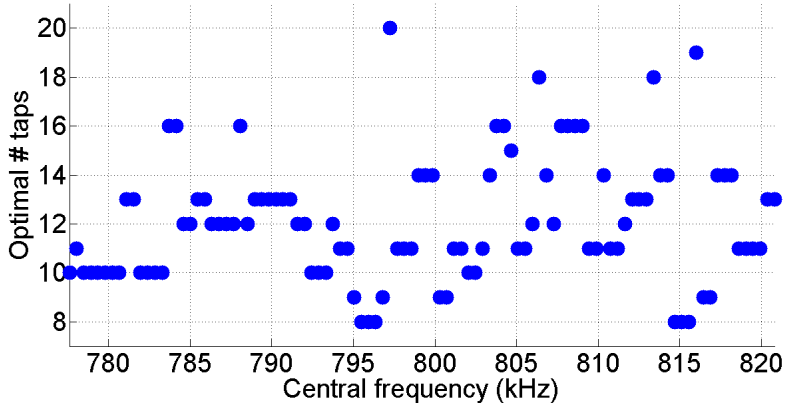

(b) Optimal number of taps for vertical axis as a function of vertical fractional tune

Figure 4.11.: Optimal number of taps as a function of the FIR central frequency (betatron fractional tune expressed in kHz) for central gain = shift gain = 1

longitudinal to the transverse plane, as explained in section 3.4.1. The lower the magnitude of the spectrum at the synchrotron sidebands, the more robust will be the transverse feedback against the synchrotron instabilities.

Regarding the damping at the betatron fractional tune, Figure 4.12a and 4.12b show the magnitude of horizontal and vertical spectra respectively, measured at the corresponding betatron fractional tune. As for synchrotron sidebands, Figure 4.12c and 4.12d show the magnitude of horizontal and vertical spectra respectively, measured at the synchrotron sideband frequency.
Three rampings are superimposed in each case: in one of them, automatic FIR filter tuning was disabled and ramping was performed with the coefficients of the FIR filter in Table A.2; for the other two, automatic tuning was applied in the axis to be evaluated.
The results are cropped to those levels of energy in which the most significant effect achieved with the automatic tuning is observed.

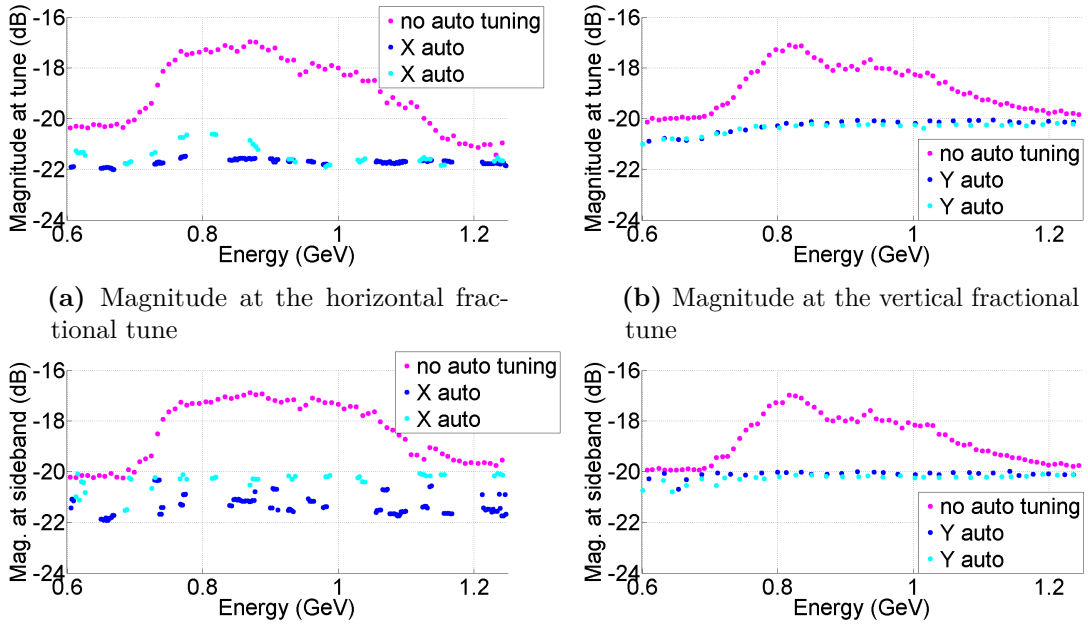

(a) Magnitude at the horizontal fractional tune

(b) Magnitude at the vertical fractional tune

(c) Magnitude at the synchrotron sideband in the horizontal spectrum

(d) Magnitude at the synchrotron sideband in the vertical spectrum

Figure 4.12.: Evolution of the magnitude of the transverse spectrum (obtained from the BRAM acquisition module) at the synchrotron sideband and at the betatron fractional tune frequencies as a function of energy during ramping. The range of energy displayed is that in which the effect of the automatic FIR filter tuning algorithm is most significant

At first glance, it can be seen that the magnitude at the fractional tune and also at the synchrotron sideband have a lower variability when ramping with the automatic FIR filter tuning enabled. This means that the system has a more constant performance during the ramp, with the benefit that fewer adjusments are required in the optics of the accelerator, amongst others ([Kei03], p.11).
Automatic tuning also shows a significant enhancement in terms of damping of CBI: horizontal oscillations are more attenuated than in the case of the fix-parameter filter, with a maximum improvement of 5 dB (that is, the magnitude at this frequency is 5dB lower than in the case of the fix-parameter filter) located at a 0.9 GeV energy level. A maximum improvement of 3 dB in respect of the fix-parameter filter is observed in the vertical axis, located at 0.8 GeV.

Damping of synchrotron sideband is improved as well: in the horizontal axis, the magnitude at this frequency is a maximum of 4 dB lower than in the case of the fix-parameter filter at 0.87 GeV; and a maximum improvement of 3 dB is measured at 0.82 GeV for the vertical axis.
The maximum enhancement is thus achieved at low levels of energy. It can be explained as follows:

- At the higher energy levels of the ramp, more power is required by the kicker to deflect the beam, that is, the control action is not as effective as with lower energies. This occurs because a high-energy electron beam is stiff and largely confined by its own magnetic fields ([Hum86], p.346). In addition, the effect of CBI is not as significant as for the lower energies, because the natural or radiation damping is more intense (radiated power is proportional to the fourth power of energy), so the action of the BBB control system is not as strong as in the lower energy levels.

- For the lower energies of the ramp, CBI are stronger because the natural damping is more limited. On the other hand, a lower power is required by the kicker to deflect the beam, which makes the feedback more effective at these energies.

The convergence of these two factors, a lower natural damping (which means the beam is more unstable) and a larger effect of the kicker with lower powers, provides the most significant enhancement achieved with automatic FIR filter tuning at the lower energies of the ramp.

4.4.2. Effect of the automatic FIR filter tuning on the asymmetry of the dip at the betatron fractional tune

As presented in section 4.2, the assymetry of the dip in the magnitude of the transverse spectrum corresponding to the temporal changes of a single bunch's positions reveals the detuning of the BBB control, which can lead to the excitation (instead of damping) of CBI. The asymmetry is evaluated as the mean value of the difference in the spectrum magnitude at frequencies located above and below the betatron fractional tune in the range delimited by the synchrotron sidebands.
Figure 4.13a shows the evolution of the average dip asymmetry with energy corresponding to the horizontal axis, and so does Figure 4.13b for the vertical axis. Three rampings are superimposed in each case: in one of them, automatic FIR filter tuning was disabled and the ramp was performed with the filter coefficients in Table A.2; for the other two, it was applied in the axis to be evaluated. Results are cropped to the same levels of energy as in section 4.4.1 in order to compare the performance with that observed in terms of damping of CBI and synchrotron sidebands.

A very similar average asymmetry is observed when the automatic tuning is applied and when it is disabled, which should mean that the presented algorithm does not provide the required readjustment of the transverse BBB feedback during the ramp. However, the enhancement of performance associated to the proper retuning has been observed in section 4.4.1, which indicates that the betatron fractional tune is correctly tracked during the ramp.
The divergence of results might be due to the low resolution of the spectrum from which the asymmetry is computed. In the present measurement, the BRAM acquisition module was used, which provides an acquisition window up to 0.57 ms. In order to achieve a better resolution and thus verify the consistency of the computed mean asymmetry, further measurements can be performed using the SRAM acquisition module, which provides an acquisition window up to 25.2 ms.

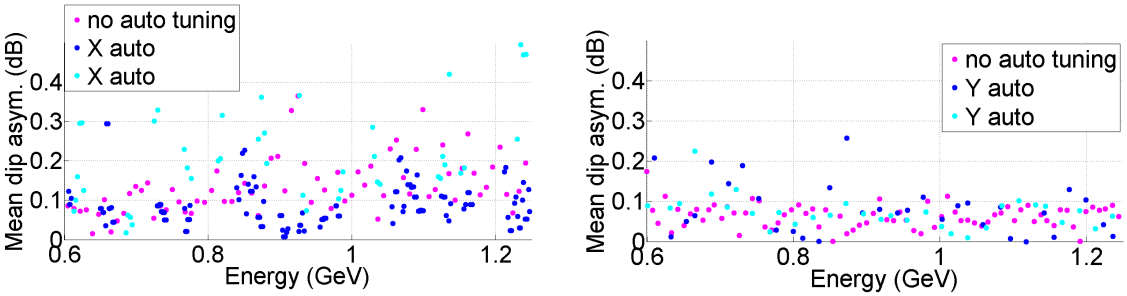

(a) Evolution of the mean asymmetry of the dip in the horizontal spectrum magnitude. One case when automatic FIR filter tuning was disabled and two in which it was applied in the horizontal axis are superimposed

(b) Evolution of the mean asymmetry of the dip in the vertical spectrum magnitude. One case when automatic FIR filter tuning was disabled and two in which it was applied in the vertical axis are superimposed

Figure 4.13.: Evolution of the mean asymmetry of the dip in the betatron spectrum magnitude with energy during ramping. The range of energy displayed is that in which the effect of the automatic tuning algorithm is most significant

4.4.3. Effect of the automatic FIR filter tuning on the partial beamloss during energy ramping

Partial or total beamloss can occur during energy ramping due to the effect of CBI. As an example of the partial beamloss, Figure 3 in [LCC+] shows the current decay with energy during rampig in the case of the SRRC storage ring.
Figure 4.14 shows the decay in the beam current recorded during several energy rampings in the case of ANKA. In subfigure 4.14a, three rampings are superimposed in which the automatic FIR filter tuning was disabled. Two rampings with automatic tuning applied in the horizontal axis are superposed in subfigure 4.14b, and two rampings with automatic tuning in the vertical axis are shown in subfigure 4.14c. Beam current has been measured once for every energy level during the ramp.
Two numbers are displayed in the legend for each of the cases: the first stands for partial beamloss computed regarding expression 4.1. The second is the absolute value of the slope of beam current decay, if it were fitted with a linear approximation (computed as initial minus final beam currents, divided over total energy variation).
In subfigures 4.14b and 4.14c, a very steep initial beam decay is observed. This can be due to the settings of optics ([Kei03], p.11) and possible timing shifts between the power supplies ([BFH+08], p.93), a mismatch which could be intensified due to the poor vacuum conditions under which the measurements were performed. As these effects are not related to the BBB control system, this initial, steep decay is skipped for the computation of partial beamloss and beamloss slope, which are calculated from the energy level marked with the red, dashed line.

At first glance, no clear improvement in terms of partial beamloss is observed with automatic tuning. The case depicted in light blue in subfigures 4.14b and 4.14c is deceitful: a lower loss is obtained; however, this ramping was performed at a different initial current as the rest of rampings, so the observed loss is not strictly comparable.

The actual benefit of automatic FIR filter tuning is achieved in terms of the slope of partial beamloss: when it is enabled, this slope is reduced up to a factor of 3 in respect of the case with the fix-parameters filter. This means that the system has a more constant performance during the ramp, with the benefit that fewer adjustments are required in the optics of the accelerator, amongst others ([Kei03], p.11).

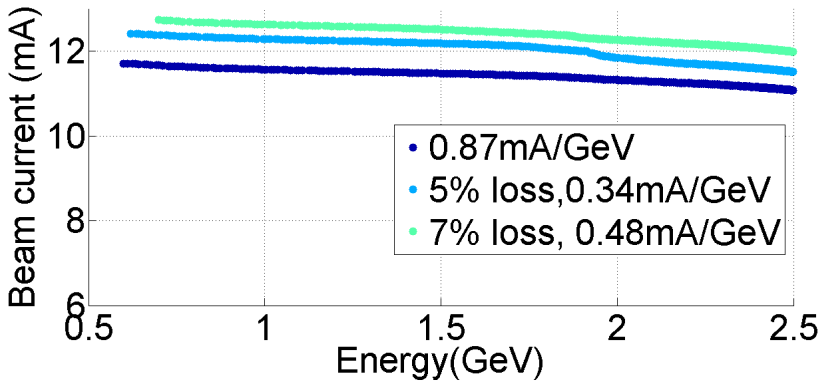

(a) Decay of the beam current with energy without automatic FIR filter tuning

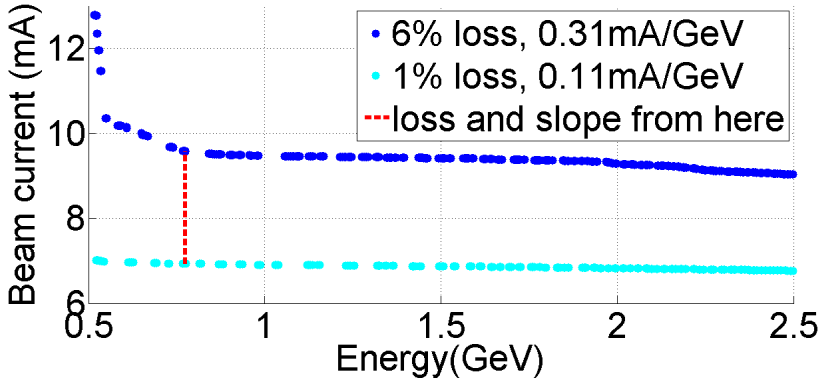

(b) Decay of the beam current with energy when automatic FIR filter tuning is applied in the horizontal axis

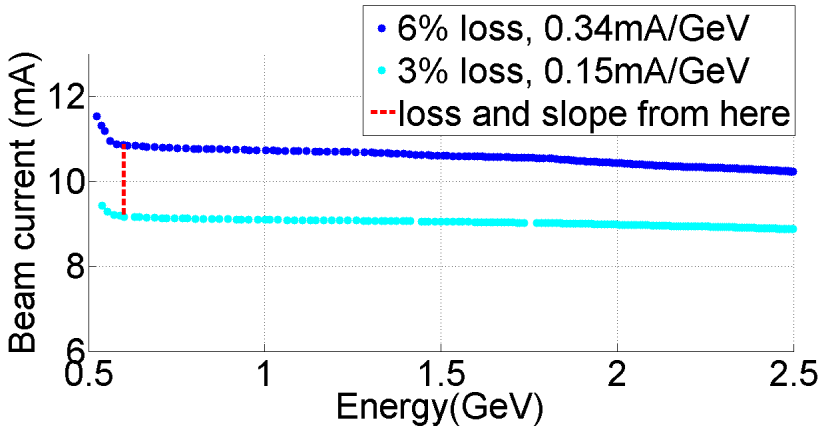

(c) Decay of the beam current with energy when automatic FIR filter tuning is applied in the vertical axis

Figure 4.14.: Beam current decay during energy ramping; three rampings without automatic FIR filter tuning, two with automatic tuning applied in the horizontal axis and two with automatic tuning applied in the vertical axis are shown. In the cases when automatic FIR filter tuning is applied, the partial beamloss and the slope of beam current decay are computed from the red, dashed line (the steep initial decay is not considered because is not related to the BBB control system)

It has been seen that the performance of the transverse BBB control system can be enhanced with an automatic FIR filter tuning algorithm that readjusts the FIR filter parameters during energy ramping. A higher damping of CBI and synchrotron sidebands and a lower slope of partial beamloss (beam current decay) during energy ramping have been achieved. In the next chapter, a solution to enhance the peformance of longitudinal BBB control is presented, which will be applied at injection energy.

5. Algorithm for the automatic tuning of the DAC Drive arbitrary signal generator in the longitudinal feedback

As presented in section 2.5, the beam lifetime can be limited by several factors, such as the gas scattering effects, the intrabeam scattering or Touschek effect, the quantum effects or as a result of CBI. When CBI are not limiting and vacuum pressure is below the residual gas pressure, the Touschek effect becomes the dominant factor. These are the conditions that apply for the contribution presented in this chapter.

A short bunch length in the longitudinal axis is required for the proper operation of the undulators. These are periodic structures of dipole magnets that stimulate the emission of highly brilliant synchrotron radiation.
Usual values for bunch length are a few hundreds of μm (compare [KPPL08], [MTH+07], [KKJ+16]). However, for too short a bunch length, the Touschek effect, i.e. the intrabeam scattering or collisions among particles inside the bunch when they perform oscillations revolving about the ring, decreases the beam lifetime and can lead to particle loss, thus deteriorating the performance of the storage ring [Wol09b].
Since a long lifetime is critical for the proper performance of the ring ([SIM+00], p.690), a correction method is required to increase the bunch length, for this will reduce the particle density. With this, the probability of intrabeam scattering will be reduced and the beam lifetime will be enhanced ([WN13], p.25; [Wie07], p.573). Effects of intrabeam scattering derived from the betatron and longitudinal motion are projected into the longitudinal plane ([Piw98], p.2); in addition, intrabeam scattering is most significant at low energies (below 1.0 GeV regarding [Boc03], p.7). Therefore, the correction action presented in this chapter to increase the bunch length will be applied on the longitudinal axis at injection energy (0.505 GeV for ANKA).

A method for increasing the bunch length and thus enhancing the beam lifetime was introduced in section 2.5. In ANKA, an analogous solution using the longitudinal BBB control system is implemented: by exciting the quadrupole eigenfrequency of the beam in the longitudinal axis, the bunch length in this axis is incremented and thus the beam lifetime is enhanced. The quadrupole resonance is excited by adding a sinusoid of this very frequency to the longitudinal feedback signal generated by the BBB control system.
This is achieved by means of the DAC Drive arbitrary signal generator, which is located in the BBB control loop (see Figure 3.3). This module provides an analog waveform of configurable frequency and amplitude (amongst other parameters) which is superimposed to the control action and sent to the RF power amplifer and later to the kicker, reaching

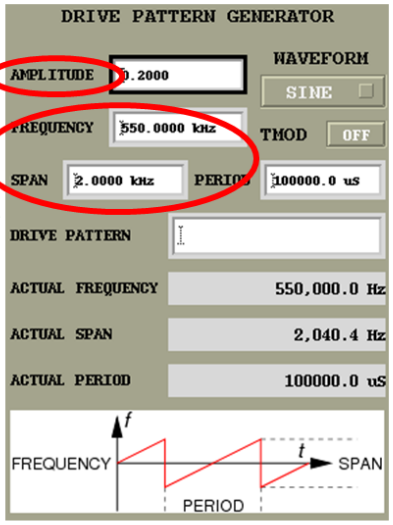

Figure 5.1.: Panel of the EPICS graphic interface corresponding to the DAC Drive arbitrary signal generator. Fields marked in red are modified by the automatic tuning algorithm

the beam to excite its quadrupole motion in the longitudina laxis.

DAC Drive generator parameters are accessible by means of a control panel in the EPICS interface and its associated signals or PVs, as explained in chapter 3.2. This panel is depicted at Figure 5.1 and the parameters which are relevant for this work are the following:

- $AMPLITUDE$: a magnitude between 0 and 1 which is related to the amplitude of the generated signal.
- $SPAN$ (kHz), $FREQUENCY$ (kHz) and $PERIOD$ (μs): this module can generate a signal at a fix frequency (specified by $FREQUENCY$ when either $SPAN$ or $PERIOD$ are set to 0); or a sweep in the range $[FREQUENCY - SPAN/2, FREQUENCY + SPAN/2]$, with such an update rate that all the generated frequencies are evaluated within $PERIOD$. Both options are used in the present project, as it will be seen in the next section.

The implementation with the longitudinal BBB control system offers the following advantages over the LLRF alternative: the frequency of modulation (which is approximately twice the synchrotron frequency) is safely comprised within the bandwidth of the control; it can benefit from the existing signal readouts in the BBB architecture (such as beam current, spectra of BPM readouts, etc.) and there is no need to implement any additional electronics. In addition, automatic tuning of the DAC Drive generator parameters is easily implementable with the existing EPICS platform.

As indicated in [SIMT], the quadrupole eigenfrequency is expected to be located at about twice the synchrotron frequency. Driving the beam at exactly the quadrupole resonance is required to maximize the benefits of this modulation.
In ANKA, the parameters of the DAC Drive generator are manually selected so far: the frequency of the modulating signal is set to twice the observed synchrotron frequency and the amplitude of the generator is set to the maximum available (that is, to 1). These might not match neither the actual quadrupole resonance nor the optimal amplitude, and thus the maximum improvement achievable with this solution might not be obtained.

The contribution of the present project to the longitudinal BBB control system is an algorithm for the automatic tuning of the DAC Drive generator parameters to ensure that the modulating sinewave is located at the quadrupole motion resonance and its amplitude is the optimal one.
In this section, the aforementioned algorithm is explained; then the methods used for evaluating its performance and the obtained results are presented.

5.1. Algorithm for the automatic tuning of the DAC Drive generator parameters to enhance beam lifetime

The algorithm for the automatic tuning of the DAC Drive generator, which determines the signal to be applied in order to modulate the quadrupole resonance of the beam in the longitudinal axis, is executed before the injection. Then the injection is performed with the aforementioned signal superimposed to the longitudinal BBB control signal. With this, the quadrupole resonance of the beam in this axis is excited, which will increase the corresponding bunch length; this, in turn, will reduce the probability of intrabeam scattering and thus will provide an enhancement in the Touschek lifetime ([SIMT], p.11).
The algorithm is composed of two main steps, as depicted at Figure 5.2, which are explained next.

Step 1: Dimension of the frequency of the DAC Drive generator

The frequency of the DAC Drive generator is set to the quadrupole resonance of the beam in the longitudinal axis. Its value is determined as follows: first, the same method explained in section 4.1 is applied to determine the synchroton fractional tune using the magnitude of the longitudinal spectrum in Figure 3.8c, which corresponds to the temporal changes in a single bunch's positions in the longitudinal axis. Then a sweep in frequency with $SPAN = 0.4kHz$ (this value has been determined experimentally, it provides the desired functionality) around twice the synchrotron fractional tune ($FREQUENCY = 2Q_s f_o$) is performed, since the quadrupole resonance is expected in this range [SIMT]. $PERIOD$ is set to 1/10 times the acquisition time of the BRAM module, from which the spectra are obtained, to ensure that the whole sweep is covered within the acquisition window of the module.
The magnitude of the longitudinal spectrum is evaluated again: in the range determined by $SPAN$ around the configured $FREQUENCY$, a peak is detected for every frequency provided by the DAC Drive generator. The peak with the largest amplitude corresponds to the quadrupole resonance (in the longitudinal axis) because it is an eigenfrequency of the beam.
At this point, $FREQUENCY$ is set to the detected quadrupole resonance and $SPAN$ is set to 0 in order to force the generation of a signal at this fix frequency.

Step 2: Dimension of the amplitude of the DAC Drive generator

The $AMPLITUDE$ parameter is a field ranging from 0 to 1 (with 1 providing the highest amplitude of the generated signal). It is expected that the higher the amplitude, the more intense the modulation, and thus the greater the increment in the bunch length. As a consequence of this, a higher possible beam current is also expected [Iei00]. Higher currents provoke stronger wakefields, which means CBI become stronger and this can lead to beamloss ([Ues], p.77).
Therefore, the strategy to determine the optimal amplitude of the generator proceeds as follows: starting with its minimum value (0), the amplitude is incremented until a) the

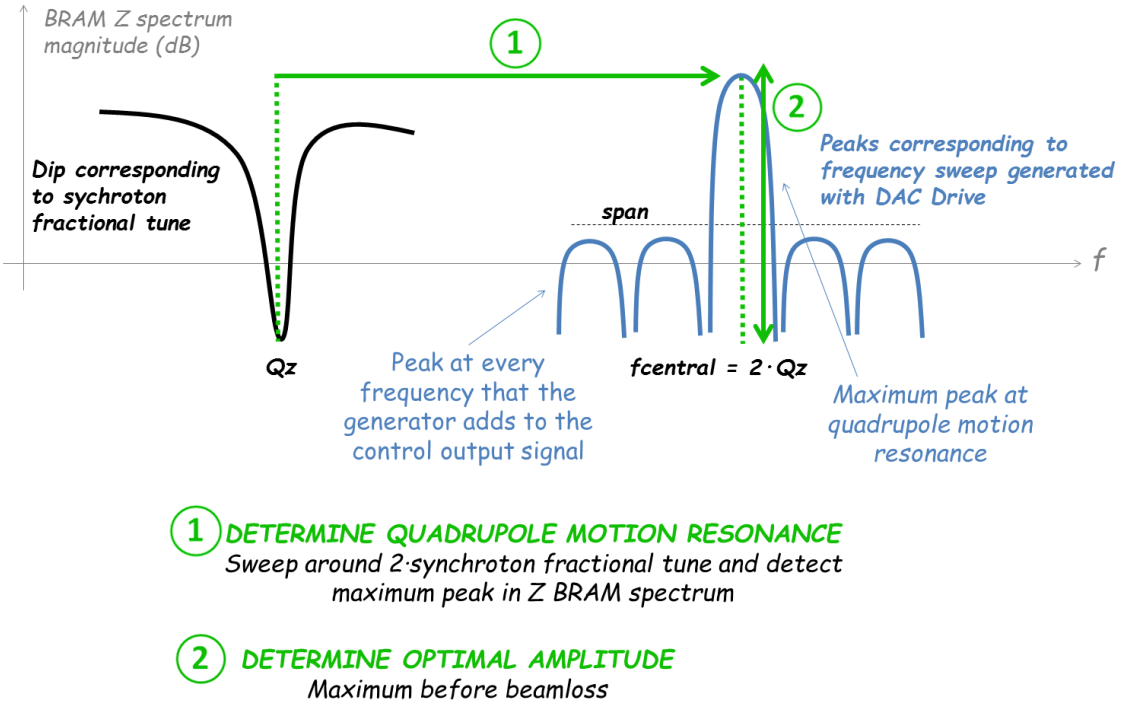

Figure 5.2.: Algorithm for phase modulation using the DAC Drive generator in the longitudinal BBB control system

beam is lost because the current limit imposed by CBI is reached, which is detected with a drop in the beam current below a given threshold (0.1 mA in the present configuration); or b) the maximum available value (1) is reached and the beam is not lost due to strong CBI. If the first situation occurs, the amplitude is decremented to the immediate value below that provoking the beamloss due to strong CBI.

The algorithm for automatic configuration of the DAC Drive generator is implemented in C++ (its code is provided in Appendix B) and is to be integrated as an additional feature in the EPICS interface. The methods used to evaluate its performance and the obtained results are discussed next.

5.2. Methods to evaluate the performance of the automatic DAC Drive generator tuning algorithm and discussion on the obtained results

Phase modulation (modulation of the longitudinal motion) at the quadrupole resonance of the beam aims to enhance the beam lifetime by incrementing the bunch length in the longitudinal axis, because this reduces the Touschek effect. As explained in section 2.5, the Touschek lifetime is proportional to the bunch length in the longitudinal axis, so the first should be elongated in the same amount as the second ([SIMT], p.11).
Therefore, the effectiveness of the presented algorithm can be measured in terms of Touschek lifetime. Its value can be obtained from the corresponding signal or PV in the EPICS interface, and the procedure used for the measurement is the following: first, the algorithm is applied to determine the frequency and optimal amplitude of the signal generated to modulate the quadrupole resonance of beam in the longitudinal axis. Then the current is injected into the storage ring. Injection is stopped and, for a fix level of current (otherwise the lifetime would vary),the lifetime PV is read.

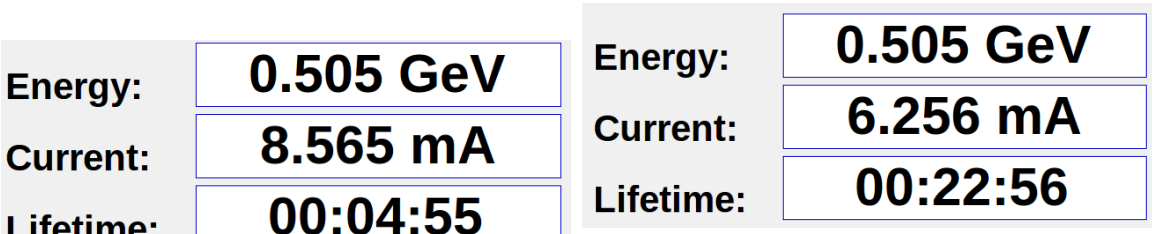

(a) Lifetime measured when the phase modulation is disabled

(b) Lifetime measured when phase modulation at the quadrupole resonance is applied with automatic tuning of the DAC Drive generator parameters

Figure 5.3.: Effect of the phase modulation at the quadrupole resonance of the beam on the beam lifetime

Figure 5.3 shows the beam lifetime provided by this PV for the case when phase modulation was applied with the automatic tuning of DAC Drive parameters and when the modulation was not applied. At first glance, it might seem that the algorithm provides a radical benefit, for it increases the beam lifetime by a factor of five. However, there are strong limitations on the validity and reproduciblity of this result, for the following reasons:

- Measurements were performed right after a shutdown of the accelerator, which was forced by the replacement of a damaged component. Linked to this, there was a poor vacuum pressure, which influenced the result: the motivation to apply the phase modulation is that lifetime is dominated by the Touschek effect, and thus it could be enhanced by increasing the bunch length. However, in such vacuum conditions, beam lifetime was most probably limited by the gas scattering effect, as presented in section 2.5. This would mean that the obtained results are not relevant to assess the enhancement in lifetime achieved with the automatic tuning algorithm.
- Only one measurement was performed for each of the cases (phase modulation disabled and automatic tuning of DAC Drive generator parameters with phase modulation enabled).
- Current levels are slightly different in each of the cases.
- Measurement performed when the phase modulation was applied was performed with the automatic tuning of DAC Drive generator parameters enabled. Therefore, it can be useful to illustrate the benefits of having this modulation in respect of when it is disabled; but it does not show if the automatic tuning achieves a better performance in respect of manual tuning, as it has been performed so far in ANKA.

In light of the achieved results and indicated limitations, further measurements are required.

At this point, the two main contributions of this work to the BBB control system in the ANKA storage ring have been presented: on the one hand, an algorithm for the automatic tuning of the FIR filter parameters in the transverse feedback, which aims to improve its performance during energy ramping and thus increase the storable beam current; on the other hand, an automatic tuning algorithm to adjust the DAC Drive generator parameters in the longitudinal feedback, which aims to enhance the beam lifetime at injection energy. In the next section, the achieved results are revisited and discussed.

6. Summary

In this work, two main contributions have been presented which enhance the performance of the BBB control system in the ANKA storage ring: one the one hand, the storable beam current is increased by improving the damping of CBI during the energy ramp. So is achieved by means of an algorithm for the automatic tuning of the FIR filter in the transverse BBB control system, which tracks the evolution of the betatron tunes with energy and readjusts the controller in the tranverse BBB feedback accordingly. In addition to improving the performance of the transverse BBB control system, this automatic tuning opens the door to custom optics settings, e.g. for the generation of THz radiation in the so-called low-alpha mode.
On the other hand, Touschek beam lifetime is enhanced by modulating the beam at its quadrupole resonance in the longitudinal axis, which increases the longitudinal bunch length and thus reduces the Touschek effect. The quadrupole resonance in the longitudinal axis and the optimal amplitude of the modulating signal are determined by means of an automatic tuning algorithm.

The algorithm for the automatic tuning of the FIR filter in the transverse BBB feedback matches its central frequency to the betatron fractional tune as it changes during energy ramping, thus retuning the BBB control system so that the phase advance introduced by the filter at its central frequency provides the required correction action to damp the betatron oscillations. In addition, this algorithm searches the optimal configuration for the FIR filter's gain at its central frequency, which maximizes the damping of betatron oscillations; and the number of coefficients, which avoids exciting the synchrotron sidebands (observed in the transverse spectrum corresponding to the temporal changes of a single bunch's positions) while providing the narrowest possible bandwidth.
It has been seen that this algorithm can improve the damping of betatron oscillations (up to 5 dB a more intense damping in the horizontal axis and 3 dB in the vertical axis) and the synchrotron sidebands observed in the aforementioned transverse spectrum (up to 4 dB a more intense damping in the horizontal axis and 3 dB in the vertical axis). This enhancement takes place at low levels of energy (around 0.8 GeV), at which the feedback action is most effective.

An additional benefit obtained with the automatic tuning is that the system has a more constant performance during the ramp, which means that fewer adjusments are required in the optics of the accelerator, amongst others ([Kei03], p.11). This benefit is observed in terms of the variability of the magnitude at the betatron fractional tunes and at the synchrotron sidebands observed in the aforementioned transverse spectrum; this variability is reduced.
The more constant performance is also observed in terms of beam current: results show that the slope of the beam current decay during the ramp is reduced up to a factor of 3 in

respect of the case with the fix-parameters filter.

Another figure to evaluate the performance of the automatic FIR filter tuning algorithm is the average value of the assymetry of the dip in the magnitude of the aforementioned transverse spectrum. This value reveals the detuning of the BBB control, which can lead to the excitation (instead of damping) of CBI. The performed measurements show a very similar average value of the dip asymmetry when the automatic tuning is applied and when it is disabled during the energy ramp, which might not reflect the effect of the algorithm: the similarity of results when the automatic tuning was applied and when it was disabled might be due to the low resolution of the spectrum from which the asymmetry is computed. The BRAM acquisition module was used for these measurements, so the SRAM acquisition module can be used in further tests to achieve a higher resolution and thus be able to corroborate the enhancement of performance observed in terms of damping of CBI and synchrotron sidebands.

On the other hand, the algorithm for the automatic tuning of the DAC Drive generator in the longitudinal axis provides the frequency (the quadrupole resonance of the beam) and the optimal amplitude of the signal which modulates the longitudinal motion of the beam at its quadrupole resonance, with the aim of enhancing beam lifetime. It has been measured an increase in lifetime by a factor of 5 when the algorithm is applied in respect of the case when the phase modulation is disabled.

In spite of the enhancement observed in performance during the energy ramp and at injection energy with the presented algorithms, the validity and reproducibility of these results should be assessed with further measurements. The presented values were obtained right after a shutdown forced by the replacement of a damaged component, and the measurement conditions were not the nominal ones, so this might have influenced the obtained results.
On the one hand, the level of current (in the order of a dozen of mA) was lower than the nominal one (around 150 mA [ANKc]). As a consequence, the effect of CBI might not have limited the storable beam current, which was the motivation to apply the automatic FIR filter tuning algorithm in the transverse BBB feedback during energy ramping.
On the other hand, the poor vacuum conditions might have provoked that the factor which limited the beam lifetime was the gas scattering effect instead of the Touschek effect, while the second was the motivation to apply the automatic tuning algorithm in the longitudinal BBB control system in order to configure the signal which modulates the beam at its quadrupole resonance.
Therefore, further measurements under nominal conditions of operation should be performed in order to verify the functionality of the presented algorithms.

Appendix

A. Figures of ANKA storage ring

B. C++ source code corresponding to algorithms presented in this thesis

EPICS interface Code to handle access to PVs using the API implemented by Manuel Schedler

`Code: /cplusplus/nep_epicsInterface_20160503.cpp`

Generic functionality General purpose code (vector handling, reading EPICS PVs, calculation of eigenfrequencies from the BRAM spectrum magnitude, etc.) invoked by B and B

`Code: /cplusplus/nep_general_20160503.cpp`

Automatic FIR filter tuning Implementation of the algorithm for automatic FIR filter tuning in the transverse feedback during energy ramping

`Code: /cplusplus/nep_autofir_20160503.cpp`

Automatic configuration of DAC Drive Implementation of the algorithm for automatic configuration of the DAC Drive signal generator in the longitudinal feedback at injection energy

`Code: /cplusplus/nep_phmod_20160503.cpp`

Output log Code to generate a text file or print to console the variables acquired from EPICS interface

`Code: /cplusplus/nep_outputtxt_20160503.cpp`

C. Matlab code for processing of signals acquired from EPICS interface

Mean asymmetry of dip Computation of the mean value of asymmetry of the notch at betatron fractional tune in BRAM spectrum magnitude

`Code: /matlab/nep_averageasymmetry.m`

Detection of synchroton sidebands Detection of synchroton sidebands around betatron fractional tune in the magnitude of transverse BRAM spectrum

`Code: /matlab/nep_detectsideband.m`

Computation of optimal number of taps Computation of the optimal number of taps of FIR filter in transverse feedback as a function of betatron tune, for a fix central gain, shift gain and central phase

`Code: /matlab/nep_optimaltaps.cpp`

Table A.1.: Compilation of parameters of the ANKA storage ring

Parameter	**Value**
Harmonic number	184
theoretical maximum bunch repetition frequency	500MHz
RF frequency	500MHz
Revolution frequency	500/184MHz ≈ 2.7MHz
ADC sampling frequency	500MHz
ADC sampling frequency (for 1 single bunch)	500/184MHz ≈ 2.7MHz

Table A.2.: Predetermined FIR filter parameters for the transverse BBB feedback (horizontal/vertical/longitudinal)

FIR filter parameter	**Value of the parameter (X/Y/Z)**
Central frequency normalized to revolution frequency	0.22/0.3/0.03
Central phase (º)	79 / 130 / -30
Central gain	0.9 / 1 / 1
Number of taps	14 / 3 / 25

Bibliography

[AL97] Ahamed, Syed V. und Victor B. Lawrence: *Design and Engineering of Intelligent Communication Systems*. Springer - Science+Business Media, 1997, ISBN 978-1-4613-7888-4.

[ANKa] *Accelerator*. https://www.anka.kit.edu/965.php. Accessed: 2016-06-04.

[ANKb] *ANKA*. http://www.anka.kit.edu/28.php. Accessed: 2016-06-04.

[ANKc] *ANKA Accelerator*. http://www.anka.kit.edu/964.php. Accessed: 2016-06-04.

[Bar94] Barbalat, O.: *APPLICATIONS OF PARTICLE ACCELERATORS*. In: *ICFA Panel om Spin—Off from Particle Physics*, Nummer SW9412, Seiten 841–853, 1994. Accessed: 2016-05-16.

[BFH+08] Balling, A., F. Frommberger, W. Hillert, J. Dedic, M. Kobal und R. Stefanic: *Machine-mode aware beam loss monitor*. In: *Proceedings of PCaPAC08, Ljubljana, Slovenia*, Nummer TUP007, Seiten 93–95, 2008.

[Boc03] Bocchetta, Carlo J.: *Intra Beam Scattering*. In: *CERN Accelerator School: Synchrotron Radiation and Free Electron Lasers, Brunnen, Switzerland*, 2003.

[Bru66] Bruck, H.: *Accelerateurs Circulaires de Particules*. Presses Universitaires de France, 1966.

[CVCMa] Cid Vidal, Xabier und Ramon Cid Manzano: *BEAM LIFETIME, Taking a closer look at LHC*. http://www.lhc-closer.es/taking_a_closer_look_at_lhc/0.beam_lifetime. Accessed: 2016-06-04.

[CVCMb] Cid Vidal, Xabier und Ramon Cid Manzano: *Measurement of Beam Current*. http://www.lhc-closer.es/taking_a_closer_look_at_lhc/0.beam_current. Accessed: 2016-06-04.

[DBH+] Decker, G., M. Borland, D. Horan, A. Lumpkin, N. Sereno und B. Yang: *Transient bunch compression using pulsed phase modulation in high-energy electron storage rings*. 9:120702–1–120702–12.

[DCH+03] Decker, G., J. Carwardine, R. Hettel, N. Sereno und J. Sebek: *Introduction to Multibunch Instabilities and Feedback*. In: *Beam Stability at Light Sources / USPAS 2003, Santa Barbara, CA, USA*, 2003. Accessed: 2016-05-16.

[DES16] *Storage Rings as Synchrotron Radiation Sources*. http://photon-science.desy.de/research/studentsteaching/primers/storage_rings___beamlines/index_eng.html, 2016. Accessed: 2016-05-16.

[DGG+03] Drago, A., A. Gallo, A. Ghigo, M. Zobov, J. D. Fox und D. Teytelman: *Longitudinal quadrupole instability and control in the Frascati DAFNE electron ring*. In: *Submitted to Physical Review Special Topics - Accelerators and Beams*, Nummer SLAC–PUB–9829, 2003.

[Dia14] *About Synchrotrons.* http://www.diamond.ac.uk/Home/About/FAQs/About-Synchrotrons.html, 2014. Accessed: 2016-05-16.

[dim] *Introducing Low-Level RF Control Solution.* http://www.dimtel.com/. Accessed: 2016-06-04.

[epi] *Experimental Physics and Industrial Control System.* http://www.aps.anl.gov/epics/. Accessed: 2016-06-04.

[FCM+] Fox, J., J. Cesaratto, T. Mastorides, C. Rivetta, D. Van Winkle, O. Turgut, A. Young, S. Uemura und A. Drago: *Feedback Control of Particle Beam Instabilties.* http://uspas.fnal.gov/materials/12MSU/CT_Feedback_Control.pdf. Accessed: 2016-05-16.

[FEH+93] Fox, J. D., N. Eisen, H. Hindi, I. Linscott, G. Oxoby und L. Sapozhnikov: *Feedback Control of Coupled-Bunch Instabilities.* In: *Proceedings of PAC93, Washington, DC, USA*, Nummer SLAC-PUB-6180, Seiten 2076–2080, 1993.

[Fox16] Fox, J. D.: *Understanding Signals from Beams - part II.* https://events.synchrotron.org.au/event/6/contribution/11/material/slides/0.pdf, 2016. Accessed: 2016-06-11.

[Fun] *Fundamentals of rf systems.* http://physics.indiana.edu/~shylee/p570/iu12/P570_04a.pdf. Accessed: 2016-05-16.

[HEF+93] Hindi, H., N. Eisen, J. Fox, I. Linscott, G. Oxoby und L. Sapozhnikov: *Analysis of DSP-Based Longitudinal Feedback System: Trials at SPEAR and ALS.* In: *Proceedings of PAC93, Washington, DC, USA*, Nummer SLAC-PUB-6151, Seiten 2352–23554, 1993.

[Her13] Hertle, Edmund: *Studies of Beam Losses at the ANKA Storage Ring.* Diplomarbeit, Karlsruher Institut für Technologie, 2013.

[Hol12] Holzer, B.J.: *Introduction to Longitudinal Beam Dynamics.* In: *CAS-CERN Accelerator School: Ion Sources, Senec, Slovakia*, Seiten 47–61, 2012.

[Hum86] Humphries, Stanley: *Principles of Charged Particle Acceleration.* Dover Publications, Inc., 1986, ISBN 978-0-486-49818-8.

[Iei00] Ieiri, Takao: *MEASUREMENT OF BUNCH LENGTH BASED ON BEAM SPECTRUM IN THE KEKB.* In: *Proceedings of EPAC 2000, Vienna, Austria*, Seiten 1735–1737, 2000.

[JHKM14] Jebramcik, M. A., H. Huck, S. Khan und R. Molo: *Study of the beam lifetime at the synchrotron light source DELTA.* In: *Proceedings of IPAC2014, Dresden, Germany*, Nummer MOPRO061, Seiten 222–224, 2014.

[JYA+] Jena, S., S. Yadav, R. K. Agrawal, A.D. Ghodke, P. Fatnani und T.A. Puntambekar: *Stabilization of betatron tune in Indus-2 storage ring.* https://arxiv.org/ftp/arxiv/papers/1307/1307.4512.pdf. Accessed: 2016-06-11.

[Kei03] Keil, Boris: *A Unified Distributed DSP-Based Beam Diagnostics and Global Feedback System for Ramped Electron Storage Rings: Development, Construction and Applications.* Dissertation, Universität Dortmund, 2003.

[KFH+10] Khan, S., J. Fursch, P. Hartmann, T. Weis und D. Teytelman: *Studies and Control of Coupled-Bunch Instabilities at DELTA.* In: *Proceedings of IPAC'10, Kyoto, Japan*, Nummer WEPEB032, Seiten 2755–2757, 2010.

[KHK+] Kang, H. S., W. H. Hwang, D. T. Kim, Y. J. Kim, M. K. Park und J. Y. Huang: *Suppression of longitudinal coupled bunch instabilities by LFS in PLS storage ring*. Seiten 112–125.

[KHP+03] Kang, H.S., W.H. Hwang, H.J. Park, J.S. Yang, M.H. Chun, Y.J. Kim, M.K. Park, J.Y. Huang, S.H. Nam, Y. M. Koo, M. Kwon, J. Fox und D. Teytelman: *Cure of Coupled-Bunch Instabilities in PLS Storage Ring*. In: *Proceedings of EPAC 2000, Vienna, Austria*, Nummer SLAC-PUB-9718, Seiten 1130–1132, 2003.

[KHY01] Kim, Eun San, Il Moon Hwang und Moohyun Yoon: *Longitudinal Coupled-Bunch Instabilities in the PLS Storage Ring*. In: *Proceedings of the Second Asian Particle Accelerator Conference, Beijing, China*, Nummer THP077, Seiten 389–391, 2001.

[KKJ+16] Ko, J. H., I. S. Ko, S. H. Jung, J. H. Park und S. H. Kang: *Electron Bunch Length Measurement Using Coherent Radiation Source of fs-THz Accelerator at POHANG Accelerator Laboratory*. In: *Proceedings of IPAC2016, Busan, Korea*, Nummer MOPMR003, Seiten 235–237, 2016.

[KPPL08] Karantzoulis, E., G. Penco, A. Perucchi und S. Lupi: *Coherent THz Radiation at ELETTRA*. In: *Proceedings of EPAC08, Genoa, Italy*, Nummer WEPC027, Seiten 2043–2045, 2008.

[Lac92] Laclare, J.L.: *Coasting beam transverse coherent instabilities*. In: *CERN Accelerator School: 5th General Accelerator Physics Course, Jyväskylä, Finland*, Seiten 317–359, 1992.

[LCC+] Luo, Gwo Huei, L.H. Chang, Y. Cheng, K.T. Hsu, C.C. Kuo, W.C. Lau, Ch. Wang, P.K. Tseng und Y.C. Liu: *Asynchronized Energy Ramping at SRRC Storage Ring*. Seiten 201–203.

[Lon08] Lonza, M.: *Multi-bunch feedback systems*. In: *CERN Accelerator School: Beam Diagnostics,Dourdan, France*, Seiten 285–330, 2008.

[Lor98] Lorenz, R.: *Cavity Beam Position Monitor*. In: *AIP Conf. Proc., Stanford, CA, USA*, 1998. Accessed: 2016-05-16.

[lso16] *Synchrotron*. http://www.lightsources.org/regions/europe, 2016. Accessed: 2016-05-16.

[Mar09] Marsching, Sebastian: *Implementierung eines Mess- und Analysesystems für Beschleunigeroptiken*. Diplomarbeit, Karlsruher Institut für Technologie, 2009.

[Mat] *R2016a Documentation / Analyzing Control Systems with Delays*. http://es.mathworks.com/help/control/examples/analyzing-control-systems-with-delays.html. Accessed: 2016-05-16.

[Mat16] *Practical Introduction to Digital Filtering*. http://de.mathworks.com/help/signal/examples/practical-introduction-to-digital-filtering.html?prodcode=ML, 2016. Accessed: 2016-07-18.

[ME15] *Butterworth Filter Design*. http://www.electronics-tutorials.ws/filter/filter_8.html, 2015. Accessed: 2016-07-18.

[Mit01] Mitra, Sanjit K.: *Digital Signal Processing - A Computer-Based Approach*. McGraw Hill, 2. Auflage, 2001, ISBN 978-0072321050.

[Mos] Mosnier, A.: *Limiting Instabilities in Multibunch: Review and Cures*. http://www.esrf.fr/machine/conferences/BIW/PROC/BIW_multi.ppt. Accessed: 2016-05-16.

[Mos99] Mosnier, A.: *Cures Of Coupled Bunch Instabilities*. In: *Proceedings of PAC 1999, New York, USA*, Seiten 628–632, 1999.

[MTH+07] Muto, T., T. Tanaka, F. Hinode, M. Kawai und K. Nanbu: *Coherent THz Light Source Using Very Short Electron Bunches From A Thermionic RF Gun*. In: *Proceedings of FEL 2007, Novosibirsk, Russia*, Nummer WEPPH054, Seiten 476–479, 2007.

[N+] Nakazato, T. *et al.*: *Coherent Synchroton Radiation*. 33:141–146.

[Nak] Nakamura, Takeshi: *Possible Methods for Cure of Multi-Bunch Instabilities in the SPring-8 Storage Ring*. http://www.spring8.or.jp/pdf/en/ann_rep/96/P172-174.pdf. Accessed: 2016-06-04.

[NDKO04] Nakamura, T., S. Daté, K. Kobayashi und T. Ohshima: *Transverse Bunch-By-Bunch Feedback System for the SPRING-8 Storage Ring*. In: *Proceedings of EPAC 2004, Lucerne, Switzerland*, Nummer THPLT068, Seiten 2649–2651, 2004.

[Ng15] Ng, K.Y.: *Coupling Impedances and Beam Instabilities in Accelerator Rings*. http://physics.indiana.edu/~shylee/p571/AAP_part_4.pdf, 2015. Accessed: 2016-06-04.

[NJ98] Naumann, O. und J. Jacob: *Landau Damping of Longitudinal Instabilities for the Operation of the ESRF Storage Ring*. In: *6th European Particle Accelerator Conference, Stockholm, Sweden*, Nummer THP04G, Seiten 987–989, 1998.

[NSR10] *Synchroton radiation*. http://www.nsrrc.org.tw/english/lightsource.aspx, 2010. Accessed: 2016-05-16.

[Oct] *Extra packages for GNU Octave (FIR filters)*. http://octave.sourceforge.net/signal/function/fir1.html. Accessed: 2016-07-18.

[Pea12] Peake, David: *Diagnostics and Control of Transverse Coupled-Bunch Instabilities in Third Generation Electron Storage Rings*. Dissertation, The University of Melbourne, 2012.

[Pir09] Pircher, T.: *Digital Filters with GNU Octave*. https://tty1.net/blog/2009/filters-with-gnu-octave_en.html, 2009. Accessed: 2016-07-18.

[Piw98] Piwinski, A.: *The Touschek effect in strong focusing storage rings*. https://arxiv.org/pdf/physics/9903034.pdf, 1998. Accessed: 2016-06-04.

[San79] Sands, M.: *The Physics Of Electron Storage Rings: An Introduction*. In: *SLAC Report*, Nummer SLAC- 121, 1979. Accessed: 2016-05-16.

[SCG+] Song, J.J., A. Cours, A. Grelick, K. Harkay, D. Horan und Y.W. Kang: *Review of the APS SR RF systems*. Accessed: 2016-06-04.

[Sch15] Schedler, Manuel: *Intensitäts- und Energieerhöhung an ELSA*. Dissertation, Universität Bonn, 2015.

[SES] *Radio Frequency System*. http://www.sesame.org.jo/sesame/images/sesame-publications/yellow/8RF.pdf. Accessed: 2016-06-04.

[SHL+98] Senichev, Yu., N. Hertel, S. Lunt, S.P. Moeller und J.S. Nielsen: *Increasing the Life Time of SR Sources by RF Phase Modulation*. In: *Proceedings of EPAC 1998, Stockholm, Sweden*, Nummer THP23F, Seiten 1339–1341, 1998.

[SIM+00] Sakanaka, S., M. Izawa, T. Mitsuhashi, M. Tadano und T. Takahashi: *Improvement in the Beam Performance by an RF Phase Modulation at the KEK Photon Factory Storage Ring.* In: *Proceedings of EPAC 2000, Vienna, Austria*, Nummer WEP1A08, Seiten 690–692, 2000.

[SIMT] Sakanaka, Shogo, Masaaki Izawa, Toshiyuki Mitsuhashi und Takeshi Takahashi: *Improvement in the beam lifetime by means of an rf phase modulation at the KEK Photon Factory storage ring.* 3:050701–1–050701–14.

[Ste08] Steinhagen, R.J.: *Tune and chromaticity diagnostics.* In: *CERN Accelerator School: Beam Diagnostics,Dourdan, France*, Seiten 317–359, 2008.

[Tey03] Teytelman, D.: *Survey of Digital Feedback Systems in High Current Storage Rings.* In: *Proceedings of PAC03, Portland, Oregon, USA*, Nummer SLAC–PUB–9932, Seiten 318–322, 2003.

[Tey04] Teytelman, Dmitry: *Architectures and Algorithms for Control and Diagnostics of Coupled-Bunch Instabilities in Circular Accelerators.* Dissertation, Stanford University, 2004.

[THH] Thomas, Jeff, Tom Holmes und Terri Hightower: *Learn RF Spectrum Analysis Basics.* http://www.keysight.com/upload/cmc_upload/All/02-18-03-B2B-RF-SpectrumAnalysis-Thomas-Holmes-Hightower-839.pdf?&cc=DE&lc=ger. Accessed: 2016-05-16.

[Tia] *Types of accelerators.* http://www.accelerators-for-society.org/about-accelerators/index.php?id=21#synchrotron. Accessed: 2016-05-16.

[Ues] Uesaka, Mitsuru: *Femtosecond Beam Science.* Imperial College Press, ISBN 1-86094-343-8.

[USP01] *USPAS Lecture 18: Beam loss and beam emittance growth.* http://www.lns.cornell.edu/~dugan/USPAS/Lect18.pdf, 2001. Accessed: 2016-05-16.

[uWo01] *RF System.* http://www2.lbl.gov/MicroWorlds/ALSTool/ALS_Components/RFSystem/, 2001. Accessed: 2016-05-16.

[VB] Verghese, G. und H. Balakrishnan: *Lecture notes: Modulation and Demodulation.* http://web.mit.edu/6.02/www/s2012/handouts/14.pdf. Accessed: 2016-06-04.

[Ver93] Verdier, A.: *Chromaticity.* In: *CERN Accelerator School: 5th Advanced Accelerator Physics Course, Rhodes, Greece*, Seiten 77–100, 1993.

[VKK+95] Veshcherevich, V., S. Krutikhin, I. Kuptsov, S. Nosyrev, A. Novikov und I. Sedlyarov: *RF Measurements and Control of Higher Order Modes in Accelerating Cavities.* In: *Proceedings of PAC 1995, Dallas, Texas, USA*, Nummer WPP10, Seiten 1678–1680, 1995.

[Wal92] Walker, R.P.: *Quantum excitation and equilibrium beam properties.* In: *CERN Accelerator School: 5th General Accelerator Physics Course, Jyväskylä, Finland*, Seiten 481–498, 1992.

[WBX] Wu, Qiong, Sergey Belomestnykh und Wencan Xu: *RF for Mechanical Engineers, Part I.* http://www.c-ad.bnl.gov/ardd/docs/RF4ME_v2.pdf. Accessed: 2016-06-23.

[WCC+99] Wang, M.H., P. Chang, P.J. Chou, K.T. Hsu, C.C. Kuo, J.C. Lee und W.K. Lau: *EXPERIMENT OF RF VOLTAGE MODULATION AT SRRC.*

In: *Proceedings of the 1999 Particle Accelerator Conference, New York, USA*, Nummer THA106, Seiten 2837–2839, 1999.

[Wei03] Weis, Thomas: *Multibunch Instabilities in Electron Storage Rings*. http://www.delta.tu-dortmund.de/cms/de/Studium/Homepage_Weis/Vortraege/Vortrag_Coupled_Bunch_Instabilities.pdf, 2003. Accessed: 2016-05-16.

[Wie03] Wiedemann, Helmut: *Synchroton radiation*. Springer Berlin Heidelberg New York, 2003, ISBN 978-3-642-07777-7.

[Wie07] Wiedemann, Helmut: *Particle Accelerator Physics*. Springer Berlin Heidelberg New York, 3. Auflage, 2007, ISBN 978-3-540-49043-2.

[WN13] Wolski, Andy und David Newton: *Design of Electron Storage and Damping Rings, Part 9: Synchrotron Light Sources*. In: *US Particle Accelerator School Fort Collins, Colorado, USA*, 2013. Accessed: 2016-06-04.

[Wol09a] Wolski, Andy: *Course A4: Damping Ring Design and Physics Issues; Lecture 6: Classical Coupled-Bunch Instabilities*. In: *Fourth International Accelerator School for Linear Colliders, Beijing, China*, 2009. Accessed: 2016-05-16.

[Wol09b] Wolski, Andy: *Course A4: Damping Ring Design and Physics Issues; Lecture 7: Space Charge, Intrabeam Scattering and Touschek Effects*. In: *Fourth International Accelerator School for Linear Colliders, Beijing, China*, 2009. Accessed: 2016-06-04.

[Wu12] Wu, Wenzhong: *Feedback Systems for Control of Coupled-bunch Instabilities in the Duke Storage Ring*. Dissertation, Duke University, 2012.

[Zum] Zumbahlen, Hank (Herausgeber): *BASIC LINEAR DESIGN*, Kapitel 4. Analog Devices, Inc. Accessed: 2016-06-04.